Expression and regulation of efflux transporters in chemoresistant breast, colon and ovarian cancer cells in Bangladeshi patients

A dissertation submitted to the Department of Genetic Engineering and Biotechnology, University of Dhaka for the partial fulfillment of the requirement for the degree of Master of Philosophy (MPhil) in Genetic Engineering and Biotechnology

Roll no: 01

Registration no: 34/2020-2021

Session: 2020-2021

Date of Submission: October 2024

Department of Genetic Engineering and Biotechnology
University of Dhaka

Certificate

This is to certify that the thesis entitled “Expression and regulation of efflux transporters in chemoresistant breast, colon and ovarian cancer cells in Bangladeshi patients” submitted by Sudipta Deb Nath, roll No. 01 of Jagannath Hall, carried out his research under our supervision. This is further to certify that it is an original work and suitable for partial fulfillment of the degree of Master of Philosophy in Genetic Engineering and Biotechnology, University of Dhaka.

…….

(Supervisor)

Name: Dr. Abu Ashfaqur Sajib

Designation: Professor

Address: Department of Genetic Engineering and Biotechnology, University of Dhaka, Dhaka-1000, Bangladesh

…….

(Joint-supervisor)

Name: Dr. S.M. Mahbubur Rashid

Designation: Associate Professor

Address: Department of Genetic Engineering and Biotechnology, University of Dhaka, Dhaka-1000, Bangladesh

Dedication

This work is dedicated to my mother (Ratna Nath) and my grandmother (Niva Rani Nath).

Acknowledgements

I would like to express my deepest gratitude to my supervisor, Prof. Dr. Abu Ashfaqur Sajib, from the Department of Genetic Engineering and Biotechnology at the University of Dhaka, for his unfathomable guidance throughout this journey. I am especially thankful for the creative freedom he granted me and for his unwavering trust upon me. His support and encouragement have greatly expanded my knowledge and nurtured my aspirations as a researcher. His continual motivation helped me think innovatively and make significant scientific decisions. I feel incredibly fortunate to have been supervised by my greatest teacher.

My sincere thanks also go to Prof. Dr. Mohammad Golam Mostafa of Anowara Medical Services for his tremendous support in providing tissue specimens and data and for teaching me the practical aspects of tissue sample processing. I am immensely grateful to Md. Mahmudul Hasan Akash, Lecturer in the Department of Genetic Engineering and Biotechnology at the University of Dhaka, for his support with both wet-lab and dry-lab procedures. Additionally, I am thankful to Assc. Prof. Dr. S M Mahbubur Rashid for his motivational support throughout this process.

I cannot adequately express my gratitude to my family for their unending faith in me and the dreams I saw. They have given me the strength to pursue my passions. Special thanks to my father (Sajal Kumar Nath) and my brother (Tanmoy Debnath) for their support through all the ups and downs of this journey. Finally, I would like to thank my friends for always championing my dreams.

Abstract

Chemotherapy is a cornerstone in cancer treatment, but multidrug resistance (MDR) poses a substantial challenge. Hyperactivity of efflux pumps is one of the vital reasons to confer MDR. P-GP, MRP1 and ABCG2- these key ABC efflux pumps collectively transport a spectrum of chemotherapeutic drugs out of cells. HIF1A, a master regulator, is also associated with cancer biology, influencing cellular invasion, angiogenesis and metabolism. HuR regulates the expression of various carcinogenic molecules by mRNA trafficking, stabilization and enhancement of protein translation as well. Thereby this study addresses a crucial research gap in Bangladeshi population by inspecting the expression patterns of P-GP, MRP1 and ABCG2 in chemoresistant breast, colorectal and ovarian tissues. This study also aimed to delve into the mechanisms of drug resistance, focusing on HIF1A and HuR driven overexpression of ABC transporters, thus leading to chemoresistance. In this prospective study, 57 (chemoresistant) and 57 (paired control) tissue samples from Bangladeshi cancer patients were processed for immunofluorescence staining. The data showed the consistent co-expression of P-GP, MRP1 and ABCG2 across all cases, suggesting a potential synergistic function of transporter proteins in chemoresistance. The observations from this study also revealed that HIF1A and HuR overexpress in chemoresistant tissues, suggesting their pivotal role in chemoresistance mechanisms across malignancies and potential as therapeutic targets in Bangladeshi population. This study also suggests a direct regulation of *P-GP*, *MRP1* and *ABCG2* transcription by HIF1A that binds to the 'CGTG' sequence in the promoter regions. Besides, HuR might facilitate posttranscriptional mRNA stabilization by interacting with AU-rich elements (AREs) in the 3'UTR regions of the ABC transporters. Inhibition of these interactions of HIF1A and HuR appears as a promising approach to reverse chemoresistance. Thus, this study offers constructive insights for designing more efficient treatment strategies.

Table of Contents

List of Figures

List of Tables

Chapter 1

Introduction

1.1. Chemoresistance

Cancer has been a substantial worldwide health concern for decades, leading to the invention of numerous remedial interventions. Amid the array of current cancer treatment techniques, chemotherapy stands out as the most potent and efficient approach for those with limited or unsatisfactory responses to surgery or radiation therapy [1,2]. Anthracyclines, taxanes, antimetabolites like antifolates and nucleoside analogs, cyclin-dependent kinase inhibitors (CDKIs), tyrosine kinase inhibitors (TKIs), platinum-derived compounds and vinca alkaloids are the extensively utilized chemotherapeutic agents across various cancer types [3]. Although the creation of novel antineoplastic drugs has enhanced the efficacy of cancer treatment, the issue of multidrug resistance remains particularly formidable, especially in addressing metastatic cancers [4–6].

Chemoresistance refers to the phenomenon of tumors developing resistance against chemotherapeutics, thereby diminishing the effectiveness and contributing to relapse and metastasis [7]. Multidrug resistance effects a broad spectrum of drugs which include Vinka alkaloids (*e.g.* vinblastine and vincristine), Anthracyclines (*e.g.* doxorubicin and daunorubicin), the RNA transcription inhibitor actinomycin-D and the microtubule-stabilizing agent paclitaxel [8].

1.1.1. Mechanisms of Chemoresistance

When subjected to chemotherapy, cancer cells can exhibit multiple mechanisms of multidrug resistance [4]. This can be categorized into two groups: 1) inherent resistance, which stems from the genetic attributes of the tumor cells that serves as a protective mechanism and 2) acquired resistance, result from the exposure of cells to drugs over time [9–13]. Moreover, chemoresistance mechanisms include the reduction of water-soluble drugs uptake in the cells, the promotion of DNA damage repair, the suppression of apoptosis, the increase in the efflux of hydrophobic drugs, as well as alterations in drug metabolism and the cell cycle [14].

Elevated expression of drug transporters leads to a decrease in the levels of chemotherapeutic agents within the cancerous intracellular environment [4]. Numerous anticancer drugs target the intracellular components and so the involvement of cell-membrane transporters becomes crucial in the context of multidrug resistance [15]. In cases where the drugs are unable to traverse the cell membrane, their potential to exert any effect is nullified [15]. This mechanism falls in the ‘inherent resistance’ category.

Resistance through the mechanism of diminished drug uptake occurs particularly with water-soluble drugs relying on transporters and carriers responsible for transferring nutrients into the cell, even if there is no noticeable rise in efflux. Notable examples contain methotrexate, an antifolate, nucleotide analogs like 5-fluorouracil and 8-azaguanine, as well as cisplatin [4]. Multidrug resistance through the activation of synchronized detoxification systems, such as DNA repair and Cytochrome P450 mixed-function oxidases can be prompted by exposure to different drugs [4]. Finally, malignant transformation of apoptotic pathways, such as in cases of cancers exhibiting mutated or non-functional p53 leads to resistance to chemotherapy drugs [16].

1.1.2. Global Status of Chemoresistance

The worldwide prevalence of chemoresistance is quite high. Drug resistance mechanisms have been contributing to over 90% of treatment failures in metastatic malignancies [17–20]. Approximately 30% of women diagnosed with early-stage breast cancer encounter relapse, along with drug resistance in at least 25% of diagnosed cases and this is playing a pivotal role in the elevated mortality rate associated with breast cancer [21]. Nearly half of the patients experiencing recurrent disease indicate that multidrug resistance is a predominant trait for colorectal cancer [22]. Around 50% to 70% of cases with ovarian adenocarcinomas experience recurrence within the initial year following surgical intervention and chemotherapy [23]. Another research revealed that 20% to 30% of individuals diagnosed with ovarian cancer show chemoresistance and a notable portion of primary responders to chemotherapy eventually experience disease relapse within 12 to 24 months [24]. Non-small cell lung cancer (NSCLC) recur in 30%-50% of the cases, which ultimately leads to mortality [25]. Out of those who undergo surgical resection for pancreatic adenocarcinoma, merely 19% to 22% manage to survive up to five years, as a result of either local or distant recurrence [26,27]. Furthermore, pancreatic cancer has a possibility of relapse even during adjuvant chemotherapy [28]. Pattison *et al.* stated that more than 50% of diffuse gastric cancer patients can face relapse within the first year of surgery and adjuvant chemotherapy [29]. In addition, the ineffectiveness of drugs resulting from chemoresistance contributes to as much as 90% of cancer-associated deaths [23]. While there are about 1.3 to 1.5 million cancer patients with an approximation of 0.2 million annual new diagnoses in Bangladesh, the realm of cancer chemoresistance lacks empirical investigation, aside from a few *in silico* studies conducted thus far [30,31].

1.2. Current Landscape of Breast, Colorectal and Ovarian Cancer

1.2.1. Breast Cancer

On a global scale, breast cancer ranks as the most prevailing form of cancer among women [21,32]. In the year 2020 alone, over 2 million patients were diagnosed with breast cancer, constituting 11.7% of all cancer incidence and resulting in 684,996 deaths [33]. Especially, the mortality rates for breast cancer exhibit evident differences between transitioning and transitioned countries, with transitioning nations suffering a heavier burden [34]. The year 2020 witnessed nearly 1 million new breast cancer cases in Asia and 346,009 related fatalities [33]. South Asia, in particular, struggles with an increasing breast cancer crisis [35]. Breast cancer has ascended to the top five leading cancers for females in Bangladesh, where in 2020, the recorded incidence was 2,753 cases, with 1,772 mortalities [33,36].

1.2.2. Colorectal Cancer

Colorectal cancer (CRC) also appears as a prevalent malignancy globally. Despite surgical procedures and chemotherapy, it upholds its position as a significant contributor to cancer-related mortality [22,37–39]. In the year 2020, the worldwide landscape saw a devastating incidence of around 1.2 million cases of CRC followed by 576,858 deaths [33]. The Asian region encounters its own share of this formidable disease. With 569,186 newly diagnosed cases and 296,236 reported mortalities during 2020, the impact of CRC remains as a concern in Asia [33]. Bangladesh, particularly, faces the impact of this malignancy, reporting a number of 2,753 incidents and 1,772 deaths in the same year [33].

1.2.3. Ovarian Cancer

Ovarian cancer stands as one of the most frequent gynecologic malignancy, comprising nearly 4% of all gynecologic cancers [40,41]. Moreover, it possesses high mortality rate within the reproductive system cancers [41,42]. Oftentimes, ovarian cancer is diagnosed at an advanced stage, contributing to the death of the patients within five years [43]. From the worldwide view, the year 2020 saw an incidence of 313,959 ovarian cancer cases accompanied by 207,252 deaths [33]. This pattern similarly echoed in Asia during 2020, where 170,759 cases were detected and 112,936 lives were lost [33]. As ovarian cancer also took a place in the top five female cancers in Bangladesh, this nation is confronting its own burdens in battling this disease [36]. In 2020, a report from Global Cancer

Observatory by World Health Organization (WHO) showed that there were 3,122 ovarian cancer incidents and 2,096 related deaths in Bangladesh [33].

1.3. ATP-binding Cassette (ABC) Transporters

The ATP-binding Cassette (ABC) transporter superfamily is recognized as one of the largest and most widely expressed protein superfamilies in the context of size and expression diversity [44]. The human genome has revealed the existence of 49 distinct ABC transporters, grouped into seven classes (A–G) according to sequence resemblances [45,46]. These transporters innately exist in various tissues as membrane proteins [15,46]. They are distributed within tissues, such as the blood-brain barrier, kidneys, liver and gastrointestinal tract, which reinforces their role not only in defense, but also other functions as well [17,47–49]. Notably, all eukaryotic ABC proteins function as efflux pumps that transport toxins, drugs, metabolites, ions, etc [50].

1.3.1. Structure of ABC Transporters

The fundamental structure of a typical ABC transporter consists of two conserved nucleotide-binding domains (NBDs), denoted as NBD1 and NBD2 and two transmembrane domains (TMDs), designated as TMD1 and TMD2 [51] (Figure 1.1). On all ABC transporters, NBDs display a uniform composition by three highly conserved amino acid (AA) sequences: Walker A, Walker B and Walker C [52]. The functional roles of Walker A and Walker B motifs are vital for ATP binding and hydrolysis activities, respectively and these are located approximately 100 to 200 AAs apart [52]. These two motifs are universally found in all ATP-binding proteins [52]. While the Walker A motif interacts with alpha- and gamma-phosphates of di- or trinucleotides, Walker B motif coordinates to magnesium ions [51]. Remarkably, the Walker C (LSGGQ) motif is exclusive to ABC transporters and proposed to play a significant role in dimerization of NBD1 and NBD2 [53].

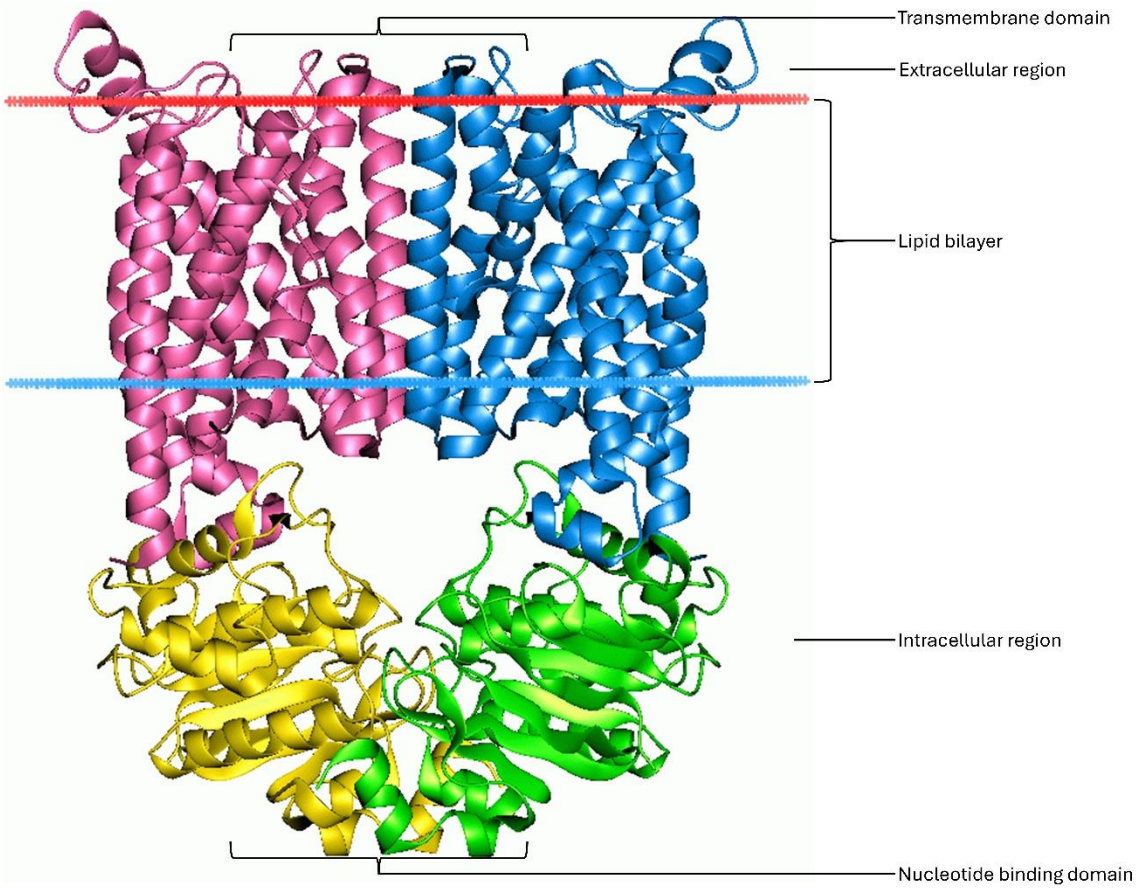

Figure 1.1: Basic structure of ABC transporters (adopted from [54])**.**

1.3.2. Mechanism of ABC Transportation

In the case of most ABC transporters, the transportation process involves the binding and subsequent hydrolysis of ATP at their NBDs, serving as the crucial energy source to transport substrates across membranes [52]. The TMDs collaborate to generate a permeable channel, enabling the selective and energy-driven movement of substrates from the cytoplasm to the extracellular space [55].

1.3.3. Function of ABC Transporters

Functioning as a superfamily of transport systems, the predominant role of most members within this superfamily involves active transportation of a broad spectrum of compounds across biological membranes [7,56]. This includes substances like phospholipids, ions, peptides, steroids, polysaccharides, AAs, organic anions, bile acids, drugs, xenobiotics and other foreign elements [7,56].

1.3.4. ABC Transporters in Cancer Chemoresistance

In order to establish the connection of ABC transporters in conferring resistance to antineoplastic drugs, some criteria need to be fulfilled: 1) cancer cells exhibit transporter expression against specific medications. This implies that the transporters need to be expressed at levels sufficient to contribute to resistance. 2) the level of transporter expression should correlate with the degree of chemoresistance observed. 3) over the treatment course, the development of drug resistance should align with the expression of the transporter. 4) when the transporter is expressed and no other resistance mechanisms are evident, the use of transporter inhibitors should effectively reverse the condition. 5) incorporating transporter inhibitors in chemoresistant cases should yield a remarkable survival advantage [45].

Four members of the ABC superfamily (A, B, C and G) have been proven to bestow drug resistance on cancer cells [45]. The transporters participating in multidrug resistance include ABCA2, ABCA3, ABCB1 (MDR1/P-GP), ABCB4 (MDR2/MDR3), ABCB5, ABCC1 (MRP1), ABCC2 (MRP2/cMOAT), ABCC3 (MRP3), ABCC10 (MRP7) and ABCG2 (BCRP/MXR/ABC-P) [57–66]. Their behavior in chemoresistance, however, varies exclusively for each transporter. Among these, P-GP, MRP1 and ABCG2 play a collective role in transporting 80% of all drugs out of cells [23,32,38,39,67–71].

1.4. P-GP, ABCG2 and MRP1: Key Players in Drug Transport and Resistance

1.4.1. P-GP/MDR1/ABCB1

Discovered by Biedler *et al.* in 1970, the 170 kDa phosphoglycoprotein, also known as the ‘permeability’ glycoprotein (P-GP), was detected as a cell surface protein in mammalian cell lines responsible for progressing multidrug resistance [72–75]. This protein belongs to the subfamily B within ABC gene family that is found universally across all life forms and serves a vital role in cellular homeostasis [76–78]. With 12 transmembrane segments and two ATP-binding regions / NBDs, it operates as a broad-spectrum multidrug efflux pump (Figure 1.2) [79]. P-GP efficiently effluxes cytotoxic orally administered drugs and a wide array of common pharmaceuticals from the lipid bilayer by first-pass elimination [4,80]. This protein operates within systems such as the intestinal epithelium, liver cells, renal proximal tubule and capillary endothelial cells [7].

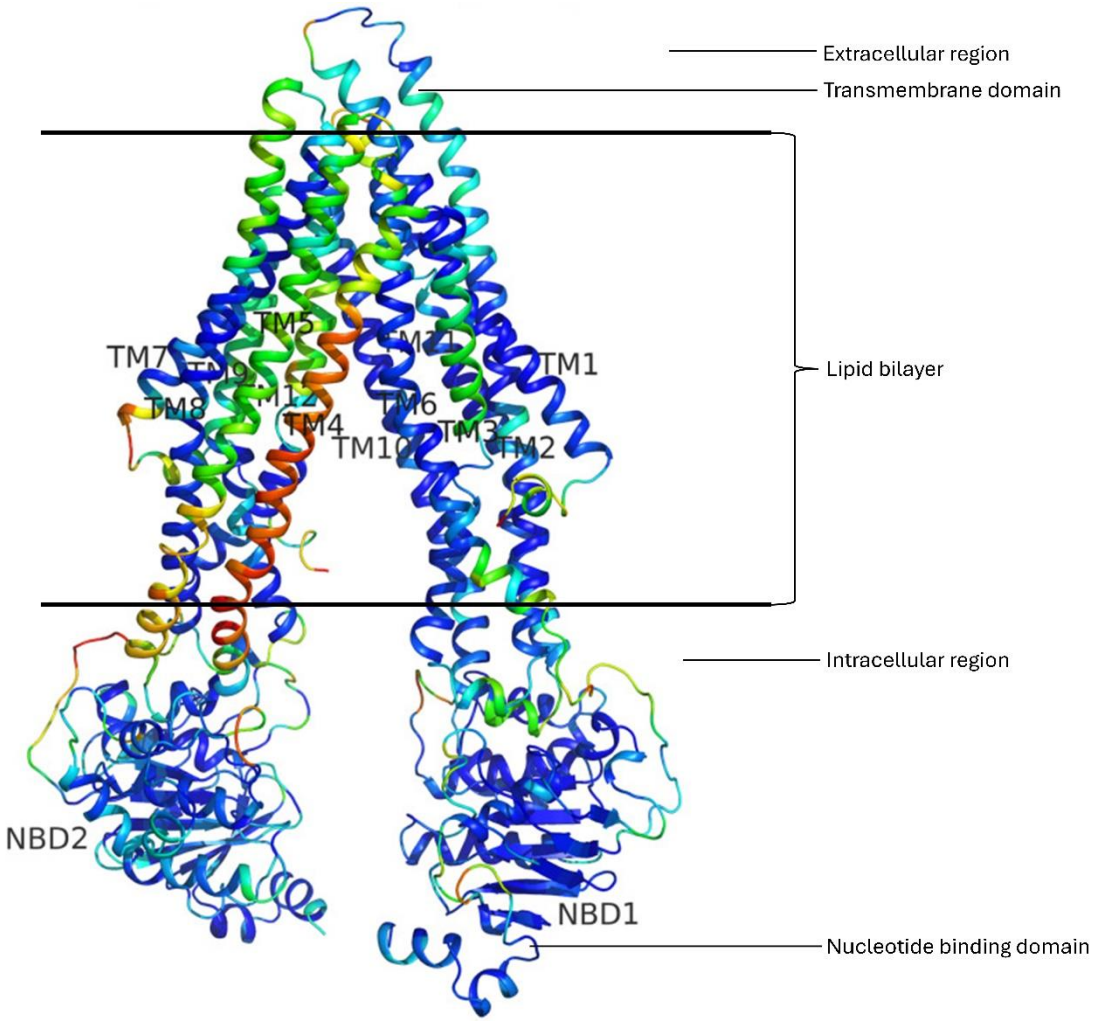

Figure 1.2: Structure of P-GP (adopted from [81])**.** *NBD = Nucleotide binding domain; TM = Transmembrane domain*

To transfer a single drug molecule outside the cell, two discrete ATP hydrolysis events are required, which occurs consecutively rather than concurrently [82]. ATPase activity of P-GP is prompted with the binding of a substrate to the transmembrane regions, inducing a structural shift that discharges the substrate either into the extracellular space or the outer leaflet of the membrane [83]. Hydrolysis at the second ATP site is essential for resetting the transporter, enabling it to bind with a new substrate, thereby fulfilling a catalytic cycle [84]. P-GP can facilitate the transportation of a broad spectrum of agents, including actinomycin D, colchicine, puromycin, tacrolimus, daunorubicin, bisantrene, quinidine, mithramycin, etoposide, vincristine, paclitaxel, docetaxel, doxorubicin, vinblastine, mitomycin C, lipids, steroids, bilirubin, digoxin, teniposide and dexamethasone [7,74,80,85–89].

P-GP is identified to be responsible for detoxifying cancer cells by effluxing cytotoxic drugs and simultaneously leading to its overexpression in cancer-transformed tissues [80,90]. This elevation of P-GP expression is regulated through two distinct mechanisms: Firstly, inherent expression, where malignancies originating from epithelial tissues (e.g., colon, kidney, brain and liver) innately exhibit P-GP. Secondly, inducible expression, whereby cancers induce P-GP expression over the chemotherapy course [15,18,80]. The correlation between the drug-triggered increase in P-GP levels and the lack of response to chemotherapeutic agents is also addressed by Takara *et al* [91]. Significantly, overexpression of this protein and contribution to drug nonresponse have been documented across various hematological and solid tumors, including leukemia, neuroblastomas, ovarian, colorectal and breast cancers [92–101].

1.4.2. MRP1/ABCC1

In 1992, Cole et al. cloned the 190 kDa multidrug resistance-associated protein-1 (MRP1), which is a member of the C subfamily of the ABC superfamily [46,92]. The chromosomal location of MRP1 encoding gene is at 16p13.1 and this gene results in a 1531-AA protein product [102]. MRP1 is structurally similar to P-Glycoprotein (P-GP), featuring an exclusive amino-terminal extension that includes five membrane-spanning domains, incorporated into a core alike of P-GP. The current structure of MRP1 is characterized by three TMDs (TMD0, TMD1, TMD2) along with two NBDs (NBD1, NBD2) (Figure 1.3) [46,103]. With a prevalent presence in normal tissues and cellular organelles, MRP1 specifically expresses in locations, such as the testes, kidneys, placenta and various pharmacological barriers [44].

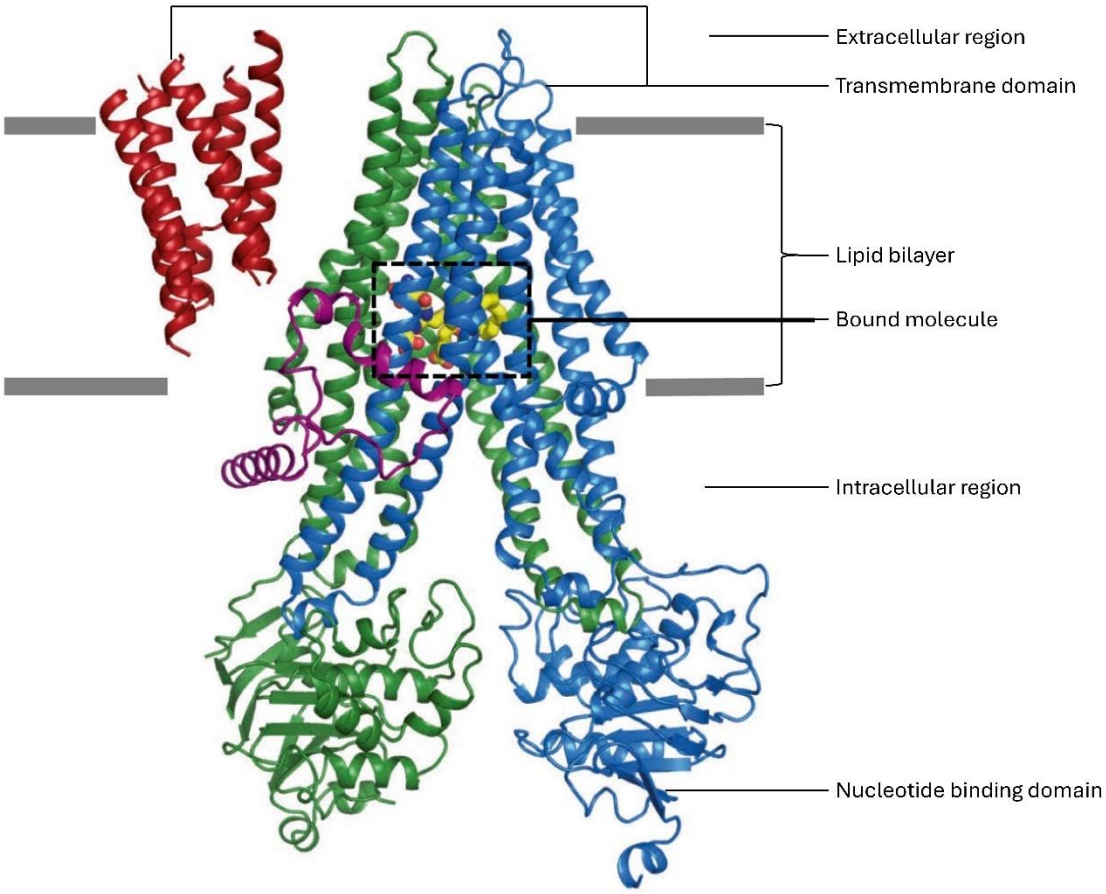

Figure 1.3: Structure of MRP1 (adopted from [104])**.**

The transport cycle of this protein is outlined as follows [53,103,105,106]: Initially, the substrate, either conjugated with glutathione (GSH) or GSH itself, docks onto the high-affinity site of MRP1. This interaction initiates a series of conformational changes, directing to ATP engagement with NBD1. This, in turn, results in additional structural adjustments and the interaction of NBD1 with the Walker C signature of NBD2, recruiting a second ATP molecule to NBD2. The NBDs are aligned in a head-to-tail position, enclosing the ATP molecules in-between. The ATP binds to the Walker A and B motifs of one NBD and the C signature of the other NBD [53]. Conformational shifts in the TMD are prompted by the dimerization of the two NBDs. This "closure" of the NBD regions plays the pivotal role for the unidirectional movement of substrates across the membrane. The closure also begins a shift in the TMDs, transitioning from a "right-side out" to an "inside-out" configuration. In this conformation, the substrate changes into a low-affinity state and is subsequently emitted into the surrounding environment [107]. The transport cycle terminates with ATP hydrolysis, releasing ADP. This destabilizes the NBD dimer, restoring the resting state, prepared for the recruitment of new substrates for

export. MRP1 plays a crucial role in identifying and expelling an array of varied hydrophobic and hydrophilic antineoplastic agents, thereby steering diminished drug accumulation and contributing to the progression of chemoresistance within tumor cells [108–110]. In certain instances, MRP1 can target such anticancer agents, which is designed to modify components of different signaling pathways regulating tumor growth, proliferation and metastasis [46]. This protein also demonstrates recognition capabilities for neutral and anionic natural products [111–113]. These anticancer compounds include anthracyclines, camptothecins, antimetabolites, epipodophyllotoxins and vinca alkaloids [15,51].

The involvement of MRP1 in conferring drug resistance has been frequently observed in solid tumors such as NSCLC, prostate cancer and certain subtypes of breast cancer [114]. Additionally, other research suggests that MRP1 has a substantial contribution to the multidrug resistance in CRC, where it inhibits the apoptosis of cancer cells [115]. This emphasizes its potential as a therapeutic target to enhance the effectiveness of other chemotherapeutic drugs used in CRC treatment [115]. Moreover, within ovarian cancer, heightened representation of MRP1 in cell membranes is stated to be playing a crucial role in both cancer prognosis and drug resistance of the disease [116].

1.4.3. ABCG2/BCRP/MXR1

First cloned in 1998 by Doyle *et al.*, ABCG2 stands as the breast cancer resistance protein (BCRP) encoded by the ABCG2 gene [117,118]. Primarily, it was discovered from a multidrug-resistant breast cancer cell line co-selected with doxorubicin and verapamil while scientists were aiming to unveil non-P-GP mechanisms of chemoresistance [117]. ABCG2 is the second member of subfamily G within the vast ABC transporter superfamily and it appears as a 72 kDa polytopic transmembrane protein with a composition of 655 AAs [119,120]. Notably, it distinguishes itself from most other ABC transporters, like P-GP and MRP1, through two exclusive characteristics: First, this protein functions as a half ABC transporter, featuring a single N-terminal NBD and one C-terminal TMD (Figure 1.4) [65,110,120]. Secondly its NBD precedes the TMD, exhibiting an opposing structural organization compared to P-GP and MRP1 [65,110]. Like P-GP, the ABCG2 gene also displays high conservation [120]. ABCG2 expression is detected not only in drug-resistant cancer cells but also in normal tissues (that includes the placenta, colon, small intestine, liver and biliary canaliculi, blood-testis or -brain barrier, breast and hematopoietic stem cells), where it heightens the efflux of cytotoxic

drugs [90,121]. Specifically, when scrutinizing the expression of ABCG2 across the human gastrointestinal tract (GIT), the highest levels are found in the duodenum, followed by a gradual reduction along the tract from terminal ileum to the rectum [122]. The prevalence of ABCG2 expression in the GI tract indicates its contribution to restraining the oral absorption of drugs [120]. Encompassing 16 exons and 15 introns, the human ABCG2 gene is situated on chromosome 4 at the 4q21–4q22 band and spans 66 kb [123]. The exons are variable in size, ranging from 60 to 532 bp [123]. The second exon accommodates the translation initiation site, while the Walker A region lies within exon 3 and exon 6 houses the ABC signature motif [123].

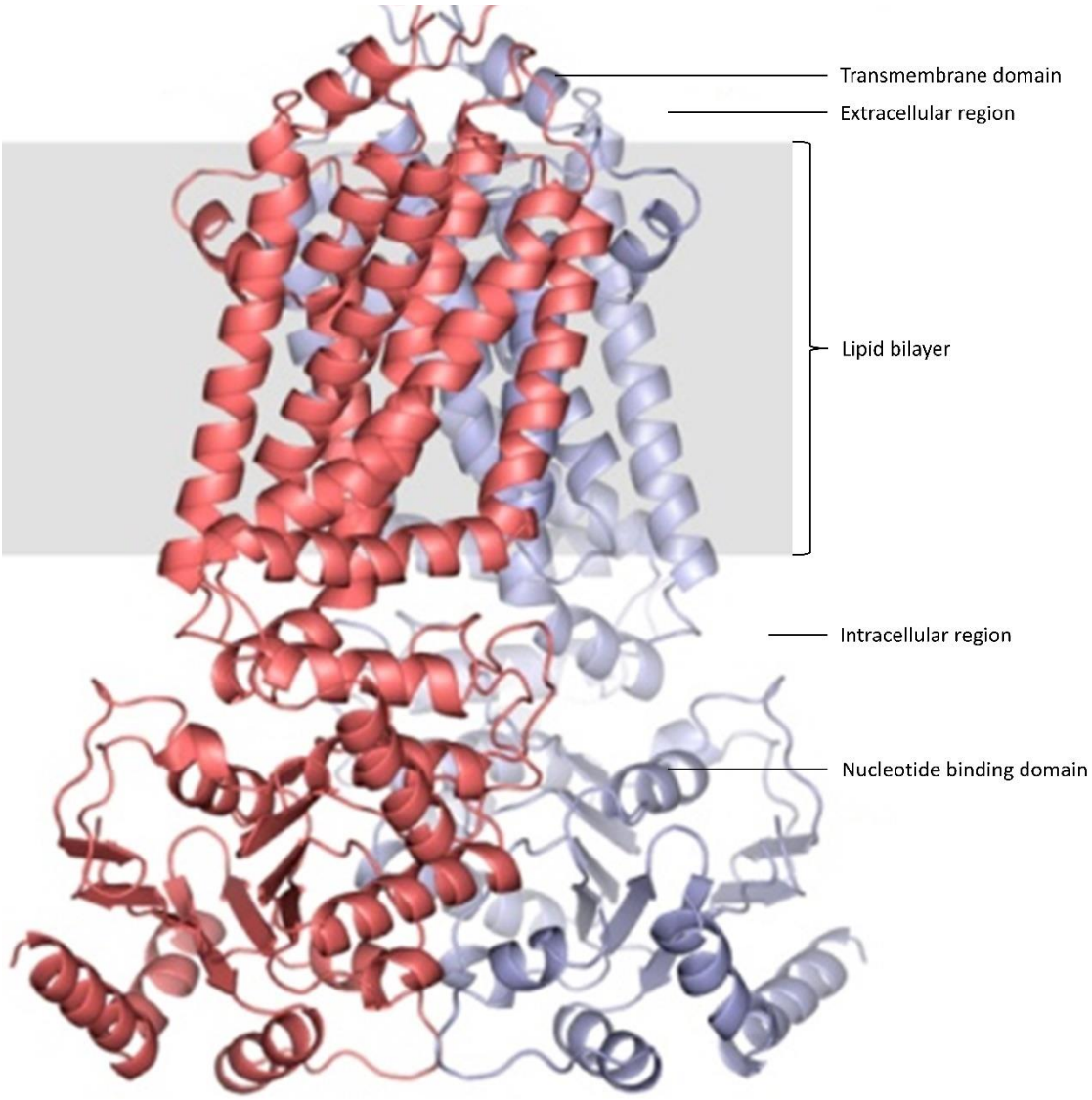

Figure 1.4: Structure of ABCG2 (adopted from [124])**.**

Besides the upregulation of ABCG2 had been examined on transcriptional level. Notably, functional cis elements in the ABCG2 promoter, such as estrogen and hypoxia response elements and a peroxisome proliferator-activated receptor gamma (PPARγ) response element, located upstream of the ABCG2 gene, were found to be regulating ABCG2 expression [125–127]. Nakanishi *et al.* identified another mechanism for ABCG2 upregulation which includes the utilization of alternative 5' promoters due to differential expression of splice variants within 5'-untranslated region (5'UTR) of the gene [128].

Though the complete transport cycle of ABCG2 is yet to be understood, its unique structural features indicate the prospect of distinct differences in its transport mechanism when compared to other prominent ABC transporters like P-GP and MRP1. From the study by Khunweeraphong et al., the transport mechanism is summarized as below [129]: During the ATP-free state, ABCG2 adopts an inward-facing conformation of the central cavity, to recognize and attract both structurally and chemically diverse drug substrates from the intracellular region. Besides, E446, located within the TMD-TMD interface, plays a pivotal role in substrate recognition. On the other hand, by either pairing ATP hydrolysis to substrate translocation or by regulating substrate binding, residue E451 undertakes a crucial position in drug transportation. Along with other loops, the extracellular re-entry helix forms and regulates a polar roof that might serve as a barrier for substrate discharge or the switch for an outward-open state. Speculatively, intracellular loop 1 (ICL1), functioning as a molecular spring in the transmission interface, facilitates the conformational switch. This switch involves the elbow helix, NBD dimerization triggered by ATP binding and an upward movement of ICL1. That eventually directs to the opening of the polar roof within the extracellular loop (ECL) for controlled substrate release. In the context of multidrug resistance, the role of ABCG2 becomes substantially evident as it effectively transports a broad-spectrum of chemotherapeutic agents. The efflux of mitoxantrone explicitly characterizes the cells expressing ABCG2 [130]. Other anticancer substrates transported by this protein encompass flavopiridol; topoisomerase inhibitors (9-aminocamptothecin, topotecan, irinotecan and SN-38); indolocarbazoles (J-107088, NB-506, compound A and UCN-01); antimetabolites (methotrexate); porphyrins (2-(1-hexyloxethyl)-2-devinylpyropheophorbide a (HPPH), pyropheophorbide and chlorin e6); anthracyclines (daunorubicin and doxorubicin); and tyrosine kinase inhibitors (imatinib, gefitinib and erlotinib) [44,130–136].

ABCG2 protein overexpression within stem-like cells (in both cell lines and primary tumor samples) has been a significant discovery in the realm of cancer research. These cells have been identified in diverse types of solid tumors, including head and neck carcinoma, breast cancer, gastrointestinal cancers (such as colon cancer), pancreatic cancer, ovarian carcinoma, osteosarcoma, prostate cancer, transitional cell carcinoma of the bladder and neuroblastoma [137,138,147–150,139–146].

1.5. Transcription Factor

In the realm of molecular biology, transcription factors (TFs), also known as DNA-binding factors (DBFs), can be defined as proteins that govern the transcription rate (thus converting genetic information from DNA to messenger RNA) of a gene by selectively binding to specific DNA sequences [151,152]. Therefore, TFs show two important features: (1) Ability to bind with DNA in a sequence-specific manner. (2) Regulation of transcription processes [153–155]. Moreover, the human genome contains a range of 1500 to 1600 TFs, making them the largest family of human proteins [156].

Notably, the same TF can control a diverse array of genes across various cell types, even within a single organism [157]. This special feature highlights the regulatory dynamic nature of the TFs. Functioning both independently and collaboratively is also one of the vital characteristics of these proteins. Their exclusive expression within specific tissues and cells proves the precision in their physiological functionality [155]. Interestingly, almost half (49%) of all TFs present cell- and tissue-specific expression [155]. The importance of this protein family extends to the underlying sources of several human diseases. Mutated TFs and their associated binding sites can mediate aberrant gene expression thus contributing to a range of disorders such as cancer [155].

1.5.1. Structure of TF

TFs exhibit a modular structure with distinct domains [152]. DNA-binding domain (DBD), that binds to specific DNA sequences of target genes, is named as enhancers or promoters or alternatively, response elements. Activation domain (AD), containing binding sites (also referred to as activation function, AF or transactivation domain, TAD) for additional proteins like transcription coregulators [158]. Optionally, a signal-sensing domain (SSD) (e.g., ligand-binding domain) may be present to perceive external signals and subsequently conveying those signals to the transcription complex. As a result,

targeted gene expression is either up-regulated or down-regulated. On top of that, DBD and SSD can potentially belong to separate protein entities.

1.5.2. Mechanism of Transcription

While decoding the DNA sequence, TFs role in initial interpretation of genome is the fundamental first step [155]. Hence, this protein superfamily exhibits a remarkable selectivity (a thousandfold or higher) to specific sequences [159,160]. In their mission to control the expression of a particular gene, TFs deploy a vast array of mechanisms [161]. First, enhancing or inhibiting the bond of RNA polymerase with DNA. Second, catalyzing acetylation or deacetylation of histone proteins [162]. Such catalytic reactions can be implemented directly by the TF or facilitated through the recruitment of other proteins with these enzymatic functions [162]. Third, involving coactivator or corepressor proteins to the TF-DNA complex [163].

1.5.3. Function of TF

One of the most important functions of the TFs is to operate as "master regulators" and "selector genes," to control the process of defining cell types and embryonic developmental patterns precisely [164,165]. These proteins showcase the capability of not only driving cellular differentiation but also accelerating de-differentiation and trans-differentiation events [166]. Another core function of TFs is in their capacity to regulate gene expression (either initiating or silencing). This ensures appropriate manifestation of genes within specific cells of the organism. TFs can also function in a synchronized pattern to govern cell division, growth, migration and apoptosis [167–170].

1.6. HIF1A as a TF and its Implications in Cancer

Hypoxia is referred to as lower level of oxygenation is cells, inducing cellular apoptosis [171]. It is a critical factor associated with the pathogenesis of numerous human diseases, such as cancer, diabetes and stroke [172]. To adapt to conditions like hypoxia and to govern cellular responses to oxygen levels within mammals, hypoxia-inducible factor 1 (HIF1) functions as a master regulator of many genes at the transcriptional level [173–176]. It presents a heterodimeric architecture, comprised of: 1) Alpha subunit, HIF1A, the protein (encoded by HIF1A gene) and 2) Beta subunit, aryl hydrocarbon receptor nuclear translocator (ARNT) [177–179].

1.6.1. Structure of HIF1A

The HIF1A protein encompasses 826 AAs and is capable of triggering the transcription of more than 40 genes [180]. It features a fundamental helix-loop-helix structure located near the C-terminal [181]. The helix-loop-helix organization is followed by two unique sets of domains: (1) PAS (PER-ARNT-SIM) domains and (2) PAC (PAS-associated C-terminal) domain (Figure 1.5) [178]. Notably, the HIF1A polypeptide includes a signal motif for nuclear localization, along with two transactivating domains, named C-terminal transactivating domain (CTAD) and N-terminal transactivating domain (NTAD) [182]. Additionally, an intervening inhibitory domain (ID) is also present, the purpose of which is to suppress the transcriptional activities of CTAD and NTAD [182].

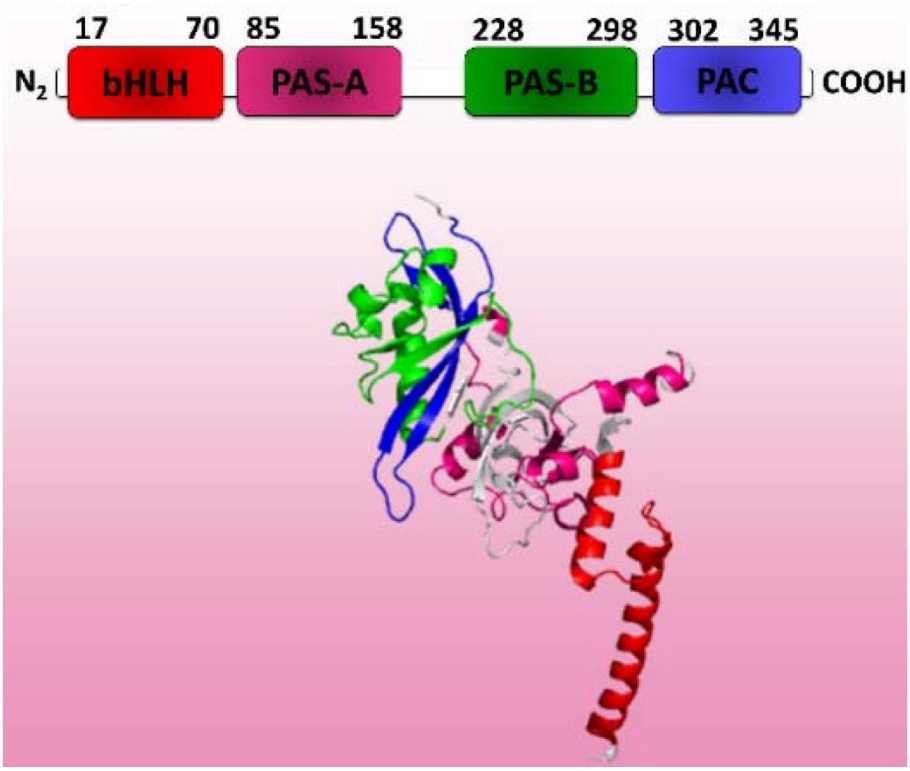

Figure 1.5: Structure of HIF1A. Helix loop structures followed by PAS and PAC regions are shown (adopted from [183])**.** *HLH = helix-loop-helix; PAS = PER-ARNT-SIM; PAC = PAS-associated C-terminal*

1.6.2. Role of HIF1A in Cancer

The impact of hypoxia on malignant growth of cells has been acknowledged well since the work from 1955 by Thomlinson and Gray, revealing the existence of hypoxic cells around the necrotic tumor-core [184]. Hence dysregulated expression of HIF1A has a noteworthy role in cancer biology [185]. This involves biological processes like tumor angiogenesis and invasion, energy metabolism and cell survival [185,186]. In 2003, Bos

et al. also proved the close link between HIF1A and tumor growth along with metastasis [187].

Both hypoxic tumor microenvironments and genetic alterations cause HIF1A overexpression [185]. Moreover, decreased oxygen in cells radically influences the activation of signaling pathways related to chemoresistance mechanisms [155]. This results in elevated expression of HIF1A mRNA in drug resistant tumors [188]. Numerous experimental studies found heightened HIF1A levels in various types of malignant tumors, including NSCLC, breast cancer (both ER-positive and -negative), oligodendroglioma, oropharyngeal cancer, pancreatic carcinoma, renal cancer, ovarian cancer, uterine cancer, cervical carcinoma, endometrial cancer, esophageal cancer, head and neck carcinoma, colon cancer, gastric cancer, prostate cancer and bladder cancer [185,189–196]. As a result, HIF1A has emerged as a potential therapeutic target to eradicate aforementioned solid tumors and it has become a predictive and prognostic marker for resistance to chemotherapy and increased mortality as well [172].

1.7. Association of HIF1A and ABC transporters

Two HIFs (HIF1 and HIF2) control the regulation of more than 1000 genes [197]. But the precise connection between HIF1A and ABC drug transporters is largely elusive yet. In mammalian cells, the primary processes of glycolytic ATP generation need oxygen [198]. Interestingly, malignant cells often activate glycolysis which increases ATP production [198,199]. These insights suggest that reducing glycolysis might counteract chemoresistance by disabling the ATP-dependent ABC transporter activity [200]. Meanwhile, under hypoxia, HIF1A increases oxygen availability by angiogenesis. On the other hand, interlinks between HIF1A and P-GP in the progression of drug resistance have been stated in previous studies [201–203]. So, overexpression of HIF1A and ABC transporters might be interlinked.

1.8. RNA-Binding Protein

RNA-binding proteins (RBPs), are a class of proteins interacting with double- or single-stranded RNA molecules in cells, therefore aiding the formation of ribonucleoprotein complexes. Their localization can be both cytoplasmic and nuclear. More than 1500 RBPs have already been found in the human genome [204]. Additionally, remarkable dysregulation of RBPs in different human cancers underscore their contribution to tumorigenesis [205].

1.8.1. Structure of RBP

RBPs usually show a modular structure comprised of diverse distinct motifs which influence the multifaceted nature of interacting with mRNAs [206,207]. Some of them are: (1) RNA recognition motifs (RRMs); bind with around four nucleotides of single-stranded RNA (ssRNA) via stacking interactions, electrostatic bonds and hydrogen bonds, (2) Double-stranded RNA binding domain (dsRBD); identifies the minor-major-minor groove pattern of double-stranded RNA (dsRNA) by interacting with the sugar-phosphate backbone, (3) Zinc finger (ZnF)-CCHH; establishes interactions between protein side chain with bulged bases in loops and forms electrostatic bonding among the RNA backbone and protein side chains and (4) PAZ; recognizes single-stranded 3′ extensions of small interfering RNA (siRNA) through stacking and hydrogen bonds.

1.8.2. Function of RBP

Particularly, RBPs possess significant impacts on post-transcriptional modifications of mRNAs, including editing, alternate splicing, polyadenylation, localization, stabilization and translation [208].

1.9. HuR as a RBP and its Implications in Cancer

Human antigen R (HuR) or embryonic lethal abnormal vision (ELAV)-like protein 1 (ELAVL1), a ~36kDa protein, belongs to the ELAV family of RBPs [209,210]. It was primarily identified in Drosophila and first cloned in 1996 by Ma *et al* [209,211]. The chromosomal location of the encoding gene, *ELAVL1*, is 19p13.2 elevating their stability [212]. Specifically, HuR protein binds to poly-U elements and AU-rich elements (AREs) in the 3'- untranslated region (3'-UTR) of target mRNAs to elevate their stability [211,213–216]. Interaction of this proteins with the cis-acting regulatory elements of the 5'-UTR of unstable mRNAs had also been observed [217]. Naturally, subcellular localization of HuR is in the nucleus of quiescent cells [217]. Upon encountering external stimuli and forming complexes with mRNA, it can translocate to the cytoplasm [217]. Therefore, it prevents mRNAs from swift degradation by exonucleases [217]. After completing this process, HuR returns to the nucleus again [217]. An essential fact about HuR is it needs to homodimerize to gain physiological functionality [216].

1.9.1. Structure of HuR

Comprising 326 AAs, the HuR protein contains three RNA recognition motifs (RRMs) [180,210,218,219]: (1) RRM1, (2) RRM2 and (3) RRM3 (Figure 1.6). RRM1 and RRM2

(two N-terminal RRM domains) identify hairpin-loops of AREs in target mRNAs. The third RRM domain, RRM3, help HuR interact with the poly-A tail of unstable mRNAs. Additionally, RRM3 contributes to stabilize mRNAs through adenosyltransferase activity [220]. Furthermore, HuR nucleo-cytoplasmic shuttling sequence (HNS) (located between the second and third RRMs) empowers HuR translocation from the nucleus to the cytoplasm during the stabilization process of the mRNA [221].

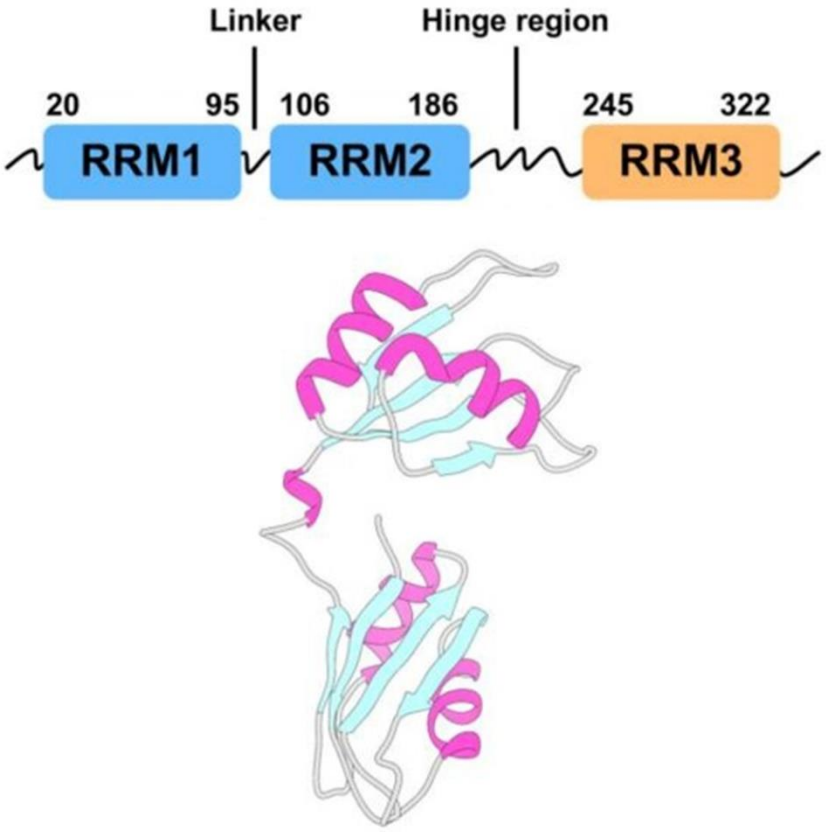

Figure 1.6: Structure of HuR. 3D structure of HuR and Region-ranges of RRM1, RRM2 and RRM3 are shown (adopted from [222])**.** *RRM1 = RNA recognition motif-1; RRM2 = RNA recognition motif-2; RRM3 = RNA recognition motif-3*

1.9.2. Role of HuR in Cancer

By mRNA trafficking, stabilization and enhancement of protein translation, HuR stands a unique position in governing the expression of numerous cancer-associated molecules thus leading to carcinogenesis [217,223–225]. Clinical insights already shed light on HuR overexpression (both nuclear and cytoplasmic) in many cancers such as breast-, lung-, ovarian-, colon-, oral-, gastric-, renal- and skin- cancer along with mesothelioma [24,226,235–240,227–234]. Previous research data also suggest that HuR overexpression is significantly correlated with some clinicopathological features like advanced stages in

cancer, lymph node metastasis and poor survival rates [217]. On top of that, multiple studies have underscored the connection between the cytoplasmic localization of HuR and the progression of multidrug resistance in cancer cells following chemotherapy [225,241,242]. Association of this protein with urinary cancer chemoresistance has also been shown in a recent study by Zhang *et al*. signifying its potential as a novel therapeutic target [223].

1.10. Association of HuR and ABC transporters

Recently, several investigations have highlighted the concomitant overexpression of HuR and ABC efflux transporters. In the context of NSCLC, HuR has been observed to interact with the mRNA of P-GP, resulting in the enhancement of its stability [243]. Furthermore, upregulated expression of cytoplasmic HuR have been stated to coincide with P-GP overexpression among patients with breast and ovarian cancer [40,225]. On the other hand, To *et al.* pointed out the potential interaction between ABCG2 mRNA and HuR protein in colorectal chemoresistance [244]. Still, more comprehensive research is necessary to find out the exact relationship between these two types of proteins.

1.11. Aims and Objectives

In Bangladesh, the emergence of cancer, metastasis and chemoresistance have been contributing to unfavorable outcomes for the patients. Despite these challenges, there is a conspicuous lack of experimental research on cancer chemoresistance. With this multifaceted study, our focus is to address this research gap and shed light on:

(1) The expression patterns of P-GP, MRP1, ABCG2, HIF1A and HuR in chemoresistant breast, colorectal and ovarian tissue samples (both tumor and corresponding control) obtained from Bangladeshi cancer patients.

(2) The co-expression profiles of ABC transporter proteins (P-GP, MRP1 and ABCG2) and HIF1A, as well as HuR by means of experimental and computational methods.

(3) The correlations between the expression and co-expression patterns of these proteins (P-GP, MRP1, ABCG2, HIF1A and HuR) with patient-specific information.

Ultimately, the insights gathered from this study will contribute significantly to the conceptions of the underlying mechanisms leading to chemoresistance irrespective of the treatment regimen. Thus, this research will help reveal potential determinants to treat cancer chemoresistance.

Chapter 2

Materials and Methods

2.1. Study design

The investigation is structured into three different but interconnected parts: (1) Immunofluorescence microscopy and imaging, (2) Statistical analyses and (3) Bioinformatic analyses

2.1.1. Tissue processing, immunofluorescence staining, microscopy and imaging

This portion of this study was prospective. For this experimental part, paired control and chemoresistant breast, colorectal and ovarian tissue samples, along with relevant patient data, were sourced from Anowara Medical Services in Dhaka, Bangladesh, where tissue collection, formalin fixation, paraffin embedment, sectioning and fixation on slides were also carried out. After collecting slides from there, the immunofluorescence staining, microscopy and imaging was undertaken at the Molecular Biotechnology Laboratory in the Department of Genetic Engineering and Biotechnology, University of Dhaka.

2.1.2. Statistical analyses

The data generated through immunofluorescence imaging underwent rigorous statistical analyses to detect trends, patterns and statistically significant associations. By utilizing robust statistical methods, our aim was to draw meaningful conclusions concerning the expression patterns of ABC transporters, HIF1A and HuR, along with the role of HIF1A and HuR in the regulation of the particular drug transporters (P-GP, MRP1 and ABCG2) in chemoresistance.

2.1.3. Bioinformatic analyses

This part was done with the computational facility in the Molecular Biotechnology Laboratory at the Department of Genetic Engineering and Biotechnology, University of Dhaka. 3D structures of HIF1A and HuR proteins were predicted and validated using multiple bioinformatic online and offline tools. Subsequently, molecular docking was executed involving HIF1A and the ‘CGTG’ sequences within the promoter regions of pivotal ABC transporters— *P-GP*, *MRP1* and *ABCG2* genes. Likewise, molecular docking was conducted with HuR protein and the ARE sequences positioned in the 3'UTR regions of the mRNA of the respective drug transporters. These dry-lab experiments provided a computational framework to figure out the potential interactions

between regulatory proteins like HIF1A/HuR and gene promoters/3'UTRs of ABC efflux pumps.

2.2. Inclusion and exclusion criteria for experimental samples

This study enrolled individuals based on some inclusion and exclusion criteria. To be eligible for participation, patients had to meet the inclusion criteria stated below: (1) participants must be Bangladeshi by ethnicity, (2) breast, colorectal and ovarian cancer patients with the previous history of non-responsiveness to chemotherapeutic drugs and (3) individuals who willingly wanted to participate in the study and provided informed consent.

On the contrary, individuals were excluded from the study based on the following exclusion criteria: (1) individuals who had been diagnosed with any psychiatric illnesses and were suffering at the time of sample and data collection.

2.3. Development of the questionnaire

A questionnaire was developed to collect the sociodemographic and clinical information from the participants. The questionnaire had seven variables comprising of address, age, sex, diagnosis, differentiation, grade and stage. The address was collected to ensure the geographic diversity of samples around Bangladesh.

2.4. Sample size and data collection

A total of 57 paired tissue samples (57 control and 57 chemoresistant) were collected containing 28 breast cancer, 21 CRC and 8 ovarian cancers. For controls, we collected paired non-cancerous adjacent tissues for each sample. The samples were collected from Anowara Medical Services, which is an oncopathology center that receives and diagnoses cancer tissues from all regions of Bangladesh. An experienced histopathologist determined the non-cancerous and cancerous tissue by observing the morphology of the specimens, using hematoxylin and eosin (H&E) staining. The corresponding data for each patient were documented after the experimental work to reduce the cancer-specific biasness. During data collection, the participants were provided with a clear insight into the aims and objectives of this research. Additionally, strict measures such as private interviews were implemented to conserve the anonymity of the patients.

2.5. Patient consent and ethical approval

This study was approved by the Ethical Review Committee of the Faculty of Biological Sciences at the University of Dhaka (117/Biol.Scs). Consent was also taken from all the patients.

2.6. Collection, processing, staining, microscopy and imaging of samples

2.6.1. Sample collection from patients

Specific invasive surgical procedures, implemented by skilled surgeons, were conducted to collect the tissue samples. Following extraction, the tissues were kept in cassettes and immediately immersed in 10% formalin solution protective measure to maintain quality of the samples.

2.6.2. Preparation of formalin-fixed, paraffin-embedded (FFPE) tissue

At this phase, to prepare FFPE tissue, the tissue cassettes were processed using the ASP6025 - Automated Vacuum Tissue Processor (Leica Biosystems), following a 12-hour protocol outlined below: the tissues in cassettes were incubated in 10% Formalin for 1.5 hours, followed by sequential rinsing in 70% Isopropanol (for 30 minutes), 90% Isopropanol (for 30 minutes), 100% Isopropanol (for 1 hour), 100% Isopropanol (for 30 minutes), 100% Isopropanol (for 1.5 hours), 100% Isopropanol (for 30 minutes) and Xylene (twice for 45 minutes each and once for 1.5 hours). All these steps were conducted in different chambers in the processor at 37ºC. The tissues then underwent paraffin bath three times for 1 hour each at 65ºC. Following paraffin bath, the tissues were inserted in a cube-shaped mold filled with melted paraffin to form tissue blocks.

2.6.3. Fixation of the tissue sections onto glass slides

The tissue blocks were sectioned into slices measuring 3-4 µm using the Leica RM2235 Manual Rotary Microtome (Leica Biosystems). Following this step, the freshly cut sections were immediately transferred into a hot water bath (HHS4 Digital Thermostatic Water Bath) with a temperature of 45ºC. Then the uncoiled sections were delicately positioned onto positively charged (electrostatic) glass slides (10010-882; VWR) followed by the slides drying out entirely.

2.6.4. Specimen labeling

Each slide containing tissue specimens (both control and chemoresistant) was labeled for future identification. Following the labeling, the glass slides were shifted to the designated slide rack for subsequent stages of experimentation.

2.6.5. Deparaffinization

At the initial stage of deparaffinization, slides carrying the specimen sections underwent a controlled heating process with 60ºC for a duration of 15 minutes within a dry block heater LBH-T01 (Daihan Labtech co., ltd). This application of heat aided in the removal of the paraffin in the latter steps. Then the rack with slides were submerged into Xylene thrice in three distinct glass chambers with 8 minutes duration each. During this process, the slides were manually agitated in Xylene to facilitate deparaffinization.

2.6.6. Rehydration of cells in the tissue

In order to fully remove any residual Xylene, the slides were immersed in 100% ethanol (100983; Merck; absolute for analysis EMSURE® ACS,ISO,Reag. Ph Eur) twice in separate glass chambers for 3 minutes each. Afterwards, the rack containing the slides were sequentially submerged into 95% ethanol, followed by 70% ethanol and finally 50% ethanol to rehydrate the cells across the tissue sections. Each of these rehydration steps involved a 3-minute immersion individually. The slides were then briefly washed with distilled water for 1 minute. To prevent the tissues from drying out, the slides were carefully maintained in water from this step onward.

2.6.7. Antigen retrieval

Following rehydration, the slide rack was transferred into an incubation chamber containing a Tri-Sodium Citrate buffer with Tween20 (10mM Sodium Citrate, 0.05% Tween® 20 (0777; VWR life science), pH 6.0). To reactivate the antigens, this process also involved heating the slides at P80 until boiling started, which took approximately 3.5 minutes, followed by heating at P50 for an additional 20 minutes. This heating step was conducted in a WMWO-25ETX microwave oven (WALTON). The samples still immersed in the Citrate buffer underwent a cooling step to reach room temperature and this duration was 30 minutes. Post-cooling, the slides were briefly rinsed with flowing distilled water for 5 minutes. The boundaries around the tissue sections were then marked by a hydrophobic-liquid blocker super PAP pen (008899; ThermoFisher Scientific).

2.6.8. Permeabilization

After removing water from the slides by thorough shaking, the slides were transferred into another chamber. Then the tissue sections on the slides were immersed with Phosphate buffer saline (PBS) with 0.1% Triton X-100 for 20 minutes. The PBS solution consisted of 137mM NaCl, 2.7mM KCl, 10mM Na_2HPO_4, 1.8mM KH_2PO_4 and distilled water with a pH level adjusted to 7.4. Following the immersion step, the tissue sections underwent three sequential washes with PBS, each taking 10 minutes.

2.6.9. Blockage of nonspecific binding

In an effort to minimize background fluorescence of antibody (Ab)-related nonspecific binding, the tissue sections underwent two different steps. At first, the slides were incubated with PBS containing 0.3M Glycine (194825; MP Biomedicals). This took place for 20 minutes within an incubation chamber. Subsequently, the slides were thoroughly washed thrice in PBS for 10 minutes each. After that, the specimens entered the second step of blocking. This time, they were incubated for another 30 minutes with 5% (w/v) normal goat serum (NGS) (ab7481; Abcam) in PBS. A brief one-minute wash with distilled water was done following the previous incubation.

2.6.10. Incubation with Primary Ab

Subsequently, the tissue sections were treated with primary Abs in a solution of 3% NGS in PBS. The list of primary Abs is given in Table 2.1. The following primary Abs were used: rabbit Anti-P-GP polyclonal Ab (ab235954; Abcam; diluted 1:1000); rabbit Anti-MRP1 recombinant monoclonal Ab (ab233383; Abcam; diluted 1:200); rabbit Anti-ABCG2 recombinant monoclonal Ab (ab229193; Abcam; diluted 1:200); mouse Anti-HIF1A monoclonal Ab (ab8366; Abcam; diluted 1:200); and mouse Anti-HuR monoclonal Ab (ab136542; Abcam; diluted 1:200). Moreover, tissue quality assessment involved incubation of one section for each sample with rabbit Anti-Pan-Cadherin polyclonal Ab (4068; Cell Signaling Technology®; diluted 1:200) (Supplementary figure 1). To ascertain high cell proliferation across the cancerous tissues, mouse Anti-Ki-67 monoclonal Ab (ab238020; Abcam; diluted 1:500) was used (Supplementary figure 2). To ensure the specific binding ability of primary Abs for ABC transporters, non-specific rabbit (DA1E) monoclonal Ab IgG XP® isotype control (3900; Cell Signaling Technology®; diluted 1:1500) was applied on an individual section (Supplementary figures 3, 4, 5). This incubation lasted overnight at 4°C. After incubation, the slides

containing tissue sections underwent four eight-minute washes with PBS containing 0.1% Tween-20 (PBS-T). All the washes were done on a Rockymax™ - 4080 shaker (Tarsons).

2.6.11. Incubation with labelled Secondary Ab and DAPI

After primary Ab incubation, all the succeeding procedures were conducted in a dark environment. The tissue sections were treated with secondary Abs diluted in 3% NGS in PBS at room temperature within a dark incubation chamber for 1 hour. The list of secondary Abs is given in Table 2.1. The secondary Abs were Alexa Fluor® 488-labeled Goat Anti-Rabbit IgG H&L polyclonal Ab (ab150077; Abcam) and Alexa Fluor® 555-labeled Goat Anti-Mouse IgG H&L polyclonal Ab (ab150114; Abcam). For anti-ABC transporters, -HIF1A, -HuR and -IgG primary Ab, secondary Abs were diluted at a ratio of 1:2000, whereas in case of Anti-Pan-Cadherin and Anti-Ki-67, the dilution was 1:1000. Moreover, to assess the of fluorescence of Alexa Fluor® 555, separate sections from all samples were treated with Anti-HIF1A and Anti-HuR along with goat Anti-Mouse IgG, (H+L) horseradish peroxidase (HRP) conjugated polyclonal Ab (another secondary Ab without fluorophore) (31430; Invitrogen; ThermoFisher Scientific; diluted 1:1500) (Supplementary figures 6, 7). On the other hand, to evaluate the binding specificity of secondary Abs, another section was treated only with NGS (without primary Abs) and secondary Abs (Supplementary figures 8, 9, 10, 11, 12). The tissue sections then underwent four eight-minute washes with PBS-T in a dark box on an orbital shaker. Subsequently, mounting medium with 4',6-diamidino-2-phenylindole (DAPI) (ab104139; Abcam) was used. Then the stained sections were covered with glass coverslips and were stored in non-transparent sealed boxes at 4°C until examined under microscope.

Table 2.1: List of primary and secondary Abs

#	Ab name	Primary/ Secondary Ab	Host sepcies	Target species	Cat. No	Manufacturer
1	Anti-P-GP polyclonal Ab	Primary	Rabbit	Human	ab235954	Abcam
2	Anti-MRP1 recombinant monoclonal Ab	Primary	Rabbit	Human	ab233383	Abcam
3	Anti-ABCG2 recombinant monoclonal Ab	Primary	Rabbit	Human	ab229193	Abcam
4	Anti-HIF1A monoclonal Ab	Primary	Mouse	Human	ab8366	Abcam
5	Anti-HuR monoclonal Ab	Primary	Mouse	Human	ab136542	Abcam
6	Anti-Pan-Cadherin polyclonal Ab	Primary	Rabbit	Human	4068	Cell signaling
7	Anti-Ki-67 monoclonal Ab	Primary	Mouse	Human	ab238020	Abcam
8	non-specific rabbit (DA1E) monoclonal Ab IgG XP® isotype control	Primary	Rabbit	Non-specific	3900	Cell signaling
9	Alexa Fluor® 488-labeled (IgG H&L polyclonal Ab)	Secondary	Goat	Rabbit	ab150077	Abcam
10	Alexa Fluor® 555-labeled (IgG H&L polyclonal Ab)	Secondary	Goat	Mouse	ab150114	Abcam
11	IgG, (H+L) horseradish peroxidase (HRP) conjugated polyclonal Ab	Secondary	Goat	Mouse	31430	ThermoFisher Scientific

2.6.12. Fluorescence microscopy and imaging

The stained tissue specimens were finally examined using a widefield fluorescence microscope (EVOS FL Core upright) utilizing objective lenses with various magnifications, such as 10x, 20x and 40x, combined with a 10x eyepiece lens. To facilitate the visualization of different protein expressions, specific band pass filter sets like Red Fluorescent Protein (RFP) and Green Fluorescent Protein (GFP) were used, while the DAPI filter was for nuclear staining. In the imaging process, we captured three randomly selected images from each section.

2.6.13. Cell and protein expression counting

Cell quantification was conducted through a manual process with the help of ImageJ software [245]. The initial step involved the enumeration of nuclei, individual red and individual green expressions within the captured images. Afterwards, to quantify the co-expression among the cell population, a comprehensive cell count was carried out with the colors merged in the ImageJ software. In order to minimize potential biasness during the counting process, two independent individuals counted the cells and protein expressions separately. Any substantial gap of 10% between two counts led to recounting

of the same images. This dual-counting strategy was undertaken to ensure a more accurate representation of our data.

2.7. Statistical analysis

Data analysis was conducted using GraphPad Prism 9.5.0 and IBM SPSS Statistics v25. Sociodemographic and clinical data of the patients were presented with frequencies, percentages, mean and standard deviation (sd) (Table 3.1, 3.2, 3.3). To standardize the evaluation of protein expressions, relative expression in percentage (%) was calculated. Relative expression in cells (%) = Relative ratio of expression in cells * 100. Relative ratio of expression in cells = Protein expression count / Total cell count. For individual ABC efflux transporter expressions, two technical replicates were measured and for HIF1A and HuR expressions, three technical replicates were considered. The ratios from technical replicates were averaged to avoid counting biases. Co-expression counts, such as ABC transporter-HIF1A/HuR in the same cells, were similarly transformed into relative co-expression in percentage (%) {Relative co-expression in cells (%) = (Cell number of co-expression / Cell number of specific ABC transporter expression) * 100}. To examine the Gaussian distribution of the ratios, normality tests were performed using D'Agostino & Pearson anderson-Darling, Shapiro-Wilk and Kolmogorov-Smirnov tests (Supplementary table 1, 2, 3, 4, 5, 6, 7, 8, 9, 11, 12, 13, 19, 20, 21). A P value of > 0.05 indicated normal distribution. If any of these tests failed to demonstrate normal distribution, the data was considered as non-normal data. For the non-normally distributed data, the Wilcoxon signed-rank test for paired samples was applied, while the paired samples T-test was performed for the normally distributed data. In these cases, P values < 0.05 were considered statistically significant. To visualize expression level variations of the transporters in chemoresistant tissues, heatmaps were generated. Moreover, the link between independent expression of ABC transporters and HIF1A/HuR was evaluated through simple linear regression analysis. Regarding the relationship between patient data and expression of proteins in chemoresistant tissues, Pearson's correlation coefficient (for normally distributed numerical data), Spearman correlation (for non-normally distributed numerical data), independent samples T-test (for variables with two categories and normally distributed numerical data), Mann–Whitney U test (for variables with two categories and non-normally distributed numerical data), ANOVA (for variables with more than two categories and normally distributed numerical data) and Kruskal–Wallis test (for variables with more than two categories and non-normally

distributed numerical data) were used. All the figures were crafted using GraphPad Prism 9.5.0.

2.8. Bioinformatic analyses to identify the interplay between HIF1A and ABC transporters

2.8.1. HIF1A structure prediction

The AA sequence of HIF1A was sourced from UniProt and the 3D model was predicted using GalaxyTBM option within the GalaxyWEB online platform [180,246]. The protein model validation involved the generation of a Ramachandran plot utilizing the PROCHECK function within the SAVES v6.0 web-platform [247]. Qualitative Model Energy ANalysis (QMEAN) tool in SWISS-MODEL was also used to assess the Q-mean score for the predicted protein model [248]. Lastly, the structural integrity was further inspected by determining the Z-score with ProSA-web [249]. Following model validation, five specific AA regions (238-348, 395-411, 549-582, 717-757 and 775-826) within HIF1A were nominated from RCSB PDB for subsequent docking [250]. These five regions were selected because the structures of these portions were determined by X-ray crystallography.

2.8.2. Identification of 'CGTG' sequence within the promoter regions of respective transporter genes and 3D modelling of DNA

Directional orientation of the transporter genes within the genome directed our search for their promoters in NCBI Gene [251]. The 'CGTG' sequence was identified prior to the 5' end, promoter area, of the genes, particularly in four regions for *P-GP* (-1000 to -1003, -1592 to -1595, -1625 to -1628 and -1630 to -1633), two regions for *MRP1* (-1516 to -1520 and -1742 to -1745) and one region for *ABCG2* (-6111 to -6114). Then, we selected -1630 to -1633 for *P-GP*, -1516 to -1520 for *MRP1* and -6111 to -6114 for *ABCG2* for further 3D DNA modeling and molecular docking. The 3D modeling of DNA involved 50 nucleotide bases preceding and following the 'CGTG' region and the modeling was accomplished using the 'DNA Sequence to Structure' tool in the Supercomputing Facility for Bioinformatics & Computational Biology, IIT Delhi web-based platform [252].

2.8.3. Molecular docking of selected regions inside HIF1A and 'CGTG' sequences in the promoters of ABC transporter genes

To evaluate the binding ability, the 3D structures of HIF1A from 2.2.1 and DNAs from 2.2.2 were subjected to molecular docking analyses by HADDOCK 2.4 [253]. In total, 15 docking simulations were performed, comprising five runs for each transporter gene (P-GP, MRP1 and ABCG2) with five AA ranges of HIF1A from 2.2.1. All the docking parameters were set as default and the scores provided by HADDOCK 2.4 were collected for further assessment. Docking outcomes with negative Z-scores were considered indicative of effective binding. Docking results were visualized by PyMOL 2.5.4 and ChimeraX [254,255].

2.9. Bioinformatic analyses to identify the interplay between HuR and ABC transporters

2.9.1. HuR structure prediction

After the AA sequence retrieval from UniProt, 3D structure of HuR protein was predicted through 'Ab initio' modeling using the Robetta platform [180,256]. Validation of the structure involved inspections using the Ramachandran plot from PROCHECK within SAVES v6.0, the Qualitative Model Energy Analysis (QMEAN) score through SWISS-MODEL and the Z-score computed by ProSA-web online-based platforms [247–249]. Then the specific AA regions for RRM1 (18-99) inside HuR were identified from RCSB PDB [250].

2.9.2. Identification and 3D modeling of ARE region in the 3'UTR of respective transporters mRNA

For *P-GP*, *MRP1* and *ABCG2* mRNA, variant sequences were obtained from NCBI Gene, revealing several transcript variants (TVs) within different isoforms [251]. *P-GP* mRNA has four TVs within two isoforms; *MRP1* has two TVs within two isoforms; and *ABCG2* has seven TVs within three isoforms. Utilizing Clustal Omega as a multiple sequence alignment tool for each transporter separately, specific TVs (TV1_isoform1 for *P-GP*, TV1_isoform1 for *MRP1*, TV1_isoform1 for *ABCG2*, TV2_isoform2 for *ABCG2* and TV3_isoform1 for *ABCG2*) were considered for further evaluations [257]. Then we focused on the 3'UTR of these chosen mRNAs. Consequently, secondary structures were generated using the RNAfold WebServer in ViennaRNA Web Services and the linear 3D RNA structures of five 3'UTRs were modeled by the 3dRNA/DNA service in 3dRNA by

Xiao lab [258,259]. Optimization procedure was applied for 3D RNA structure prediction to get a highly validated model. Meanwhile, ARE sites within 3'UTR regions of ABC transporters were identified by means of AREsite2, which ended with the extraction of 17 ARE sites for *P-GP*, 26 for *MRP1* and 39 for *ABCG2* [260]. The ARE regions were then selectively taken out from the 3D structures of their respective mRNA TVs, that were generated previously.

2.9.3. Molecular docking of RRM1 and RRM3 inside HuR and ARE sequences in the 3'UTRs of ABC transporter mRNAs

To assess binding capabilities, the 3D structures of HuR from 2.3.1 and AREs from 2.3.2 were analyzed with molecular docking simulations using HADDOCK 2.4 [253]. Employing default parameters, dockings were simulated between all the ARE regions and RRM1 of HuR. Post-docking analysis included collecting all the scores from HADDOCK 2.4 with successful docking acknowledged by negative Z-scores. For visual representation, PyMOL 2.5.4 and ChimeraX were used [254,255].

Chapter 3

Results

3.1. Information of Chemoresistant Breast, Colorectal and Ovarian Cancer Patients

The information for 28 chemoresistant breast cancer patients is shown in Table 3.1. The mean age of the patients was 50.29 ± 13.35 years. Notably, 92.86% of these patients were diagnosed with infiltrating ductal carcinoma. Most of the breast cancer cases (88.89%) showed moderate cell differentiation and were classified as grade II. With each accounting for 39.29% of the patients, tumor staging revealed an equal distribution between T1 and T2 stages. Besides, 57.69% were classified as stage N0.

Table 3.1: Chemoresistant breast cancer patient information

Variables (n = 28)	**Frequency (%)**
Age (mean ± sd)	50.29 ± 13.35
Diagnosis	
Infiltrating ductal carcinoma	26 (92.86%)
Ductal carcinoma in situ	1 (3.57%)
Infiltrating ductal and lobular carcinoma	1 (3.57%)
Differentiation	
Moderate	24 (88.89%)
Poor	3 (11.11%)
Grade	
II	24 (88.89%)
III	3 (11.11%)
T staging	
1	11 (39.29%)
2	11 (39.29%)
3	2 (7.14%)
4	3 (10.71%)
Tis	1 (3.57%)
N staging	
0	15 (57.69%)
1	2 (7.69%)
2	5 (19.23%)
3	4 (15.38%)

Table 3.2 presents data pertaining to 21 CRC patients who also exhibited resistance to chemotherapy. The mean age was 35.24 ± 11.56 years and 61.90% were male patients. All the individuals had a diagnosis of colorectal adenocarcinoma. While half of the patients exhibited well-differentiated cells, 40.00% demonstrated moderate differentiation. These numbers are also mirrored in tumor grading. Most patients (55.00%) were under T3 staging, followed by the second-highest percentage (35.00%) in T2 staging. Stage N0 was found in 52.63% of the patients.

Table 3.2: Chemoresistant CRC patient information

Variables (n = 21)	**Frequency (%)**
Age (mean ± sd)	35.24 ± 11.56
Sex	
Male	13 (61.90%)
Female	8 (38.10%)
Diagnosis	
Adenocarcinoma	21 (100.00%)
Differentiation	
Well	10 (50.00%)
Moderate	8 (40.00%)
Poor	2 (10.00%)
Grade	
I	10 (50.00%)
II	8 (40.00%)
III	2 (10.00%)
T staging	
1	1 (5.00%)
2	7 (35.00%)
3	11 (55.00%)
4	1 (5.00%)
N staging	
0	10 (52.63%)
1	4 (21.05%)
2	5 (26.32%)

Information for chemoresistant ovarian cancer patients is shown in Table 3.3. There were eight ovarian cancer patients in this study with 87.50% having papillary serous carcinoma and 12.50% having squamous cell carcinoma. The average ± standard deviation of age was 53.13 ± 11.52 years. Unlike the previous cancers, 87.50% presented poor differentiation of tumor cells and was graded as III. Moreover, 83.33% and 66.67% of the patients were categorized under T3 and N1 staging, respectively.

Table 3.3: Chemoresistant ovarian cancer patient information

Variables (n = 8)	**Frequency (%)**
Age (mean ± sd)	53.13 ± 11.52
Diagnosis	
Papillary serous carcinoma	7 (87.50%)
Squamous cell carcinoma	1 (12.50%)
Differentiation	
Moderate	1 (12.50%)
Poor	7 (87.50%)
Grade	
II	1 (12.50%)
III	7 (87.50%)
T staging	
1	1 (16.67%)
3	5 (83.33%)
N staging	
0	1 (33.33%)
1	2 (66.67%)

3.2. Expression of ABC Transporters in Chemoresistant Breast, Colorectal and Ovarian Cancer

The immunofluorescence image of ABC transporters shows the expressions of P-GP, MRP1 and ABCG2 around the nucleus (blue) in chemoresistant tissues with a scale of 25 µm (Figure 3.1).

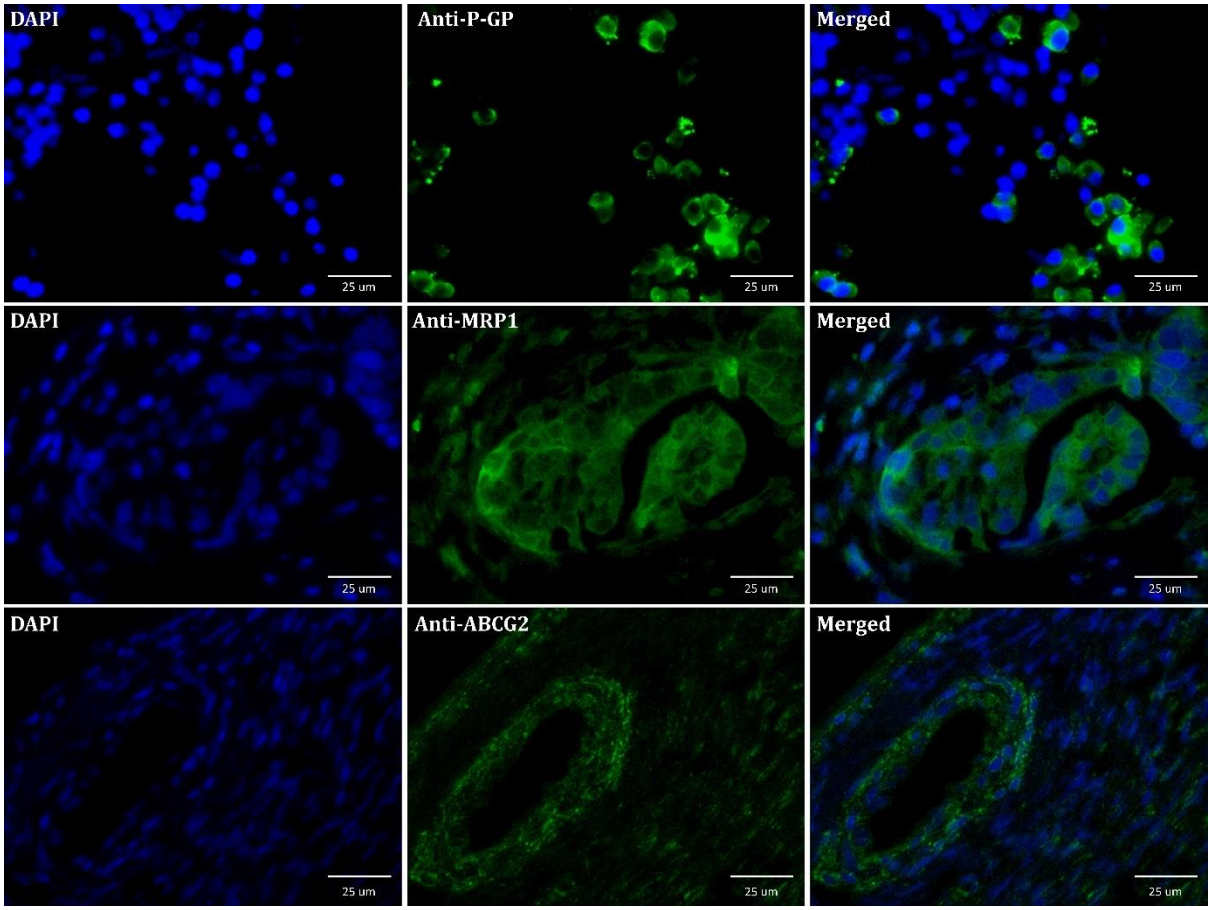

Figure 3.1: Immunofluorescence image of ABC transporter expression. The image shows DAPI staining (blue) and the expressions of P-GP, MRP1 and ABCG2 (all in green) in chemoresistant cancer tissues. The scale bar is 25 µm.

3.2.1. ABC Transporter in Chemoresistant Breast Cancer

Differences in ABC transporter expression between chemoresistant and adjacent control tissues obtained from breast cancer patients are illustrated in Figure 3.2. Average relative expression of P-GP in chemoresistant tissues was 11.14%, significantly (P value < 0.0001) higher from the control tissues (1.09%). Similarly, the mean percentage of MRP1 expression in chemoresistant breast tissues was about 16.67%, while in control tissues, the percentage was 1.78%. This distinction was also observed to be highly significant (P value < 0.0001). In the case of ABCG2 expression, the mean percentage in chemoresistant tissues (27.25%) was more than two-fold higher than the control (12.36%) (P value < 0.0001). Notably, ABCG2 expression was the highest among chemoresistant breast cancer patients from Bangladesh, whereas the expression of P-GP transporter was detected to be the lowest.

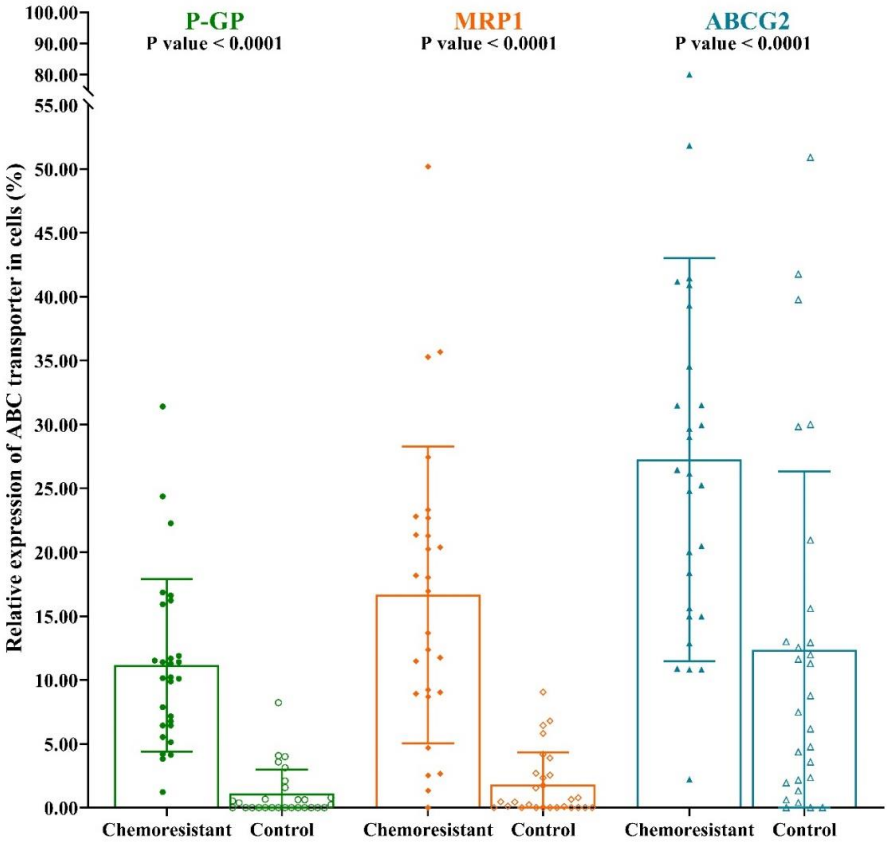

Figure 3.2: Comparison of ABC transporter expression between chemoresistant and adjacent control breast tissues. X-axis represents P-GP (green), MRP1 (orange) and ABCG2 (blue) transporters. Y-axis denotes the relative expression of ABC transporter to total cells in percentage. Wilcoxon signed rank test for paired samples was conducted to validate the significance of differences for P-GP, MRP1 and ABCG2 expression in both type of tissues.

The relatively overexpression of one efflux transporter leads to a reduction in the expression of the others (Figure 3.3). For most chemoresistant tissue samples, ABCG2 exhibited a higher expression than the other two ABC transporters. Conversely, some samples (2 and 5) displayed more P-GP expression and less MRP1 and ABCG2 expression. None of the samples were observed to have an equal expression of transporters in case of chemoresistant breast cancer tissues. However, there was no significant correlation between ABC transporters expression and patient data concerning breast cancer (Table 3.4).

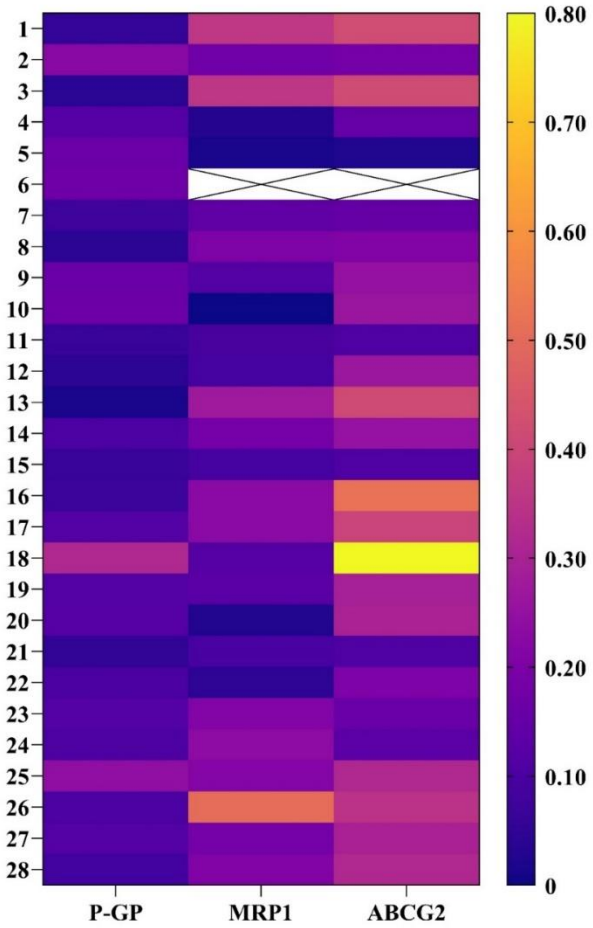

Figure 3.3: Heatmap illustrating the comparative levels of P-GP, MRP1 and ABCG2 in chemoresistant breast cancer tissues. Each row denotes a tissue sample and the color intensity bar reflects the relative expression levels. (For sample 6, we could not stain the tissue sections with MRP1 and ABCG2, thus we did not get expression result.)

Table 3.4: Association between ABC transporter expression and clinical features of chemoresistant breast cancer patients

Variables	P-GP		MRP1		ABCG2	
	mean ± sd	**P value**	**mean ± sd**	**P value**	**mean ± sd**	**P value**
Age (correlation coefficient)	-0.32	0.0922	-0.15	0.4428	-0.03	0.8796
Diagnosis						
Infiltrating ductal carcinoma	0.11 ± 0.07	0.9090	0.16 ± 0.28	0.4390	0.28 ± 0.16	0.3940
Ductal carcinoma in situ	0.10 ± 0.00		0.23 ± 0.00		0.13 ± 0.00	
Infiltrating ductal and lobular carcinoma	0.08 ± 0.00		0.20 ± 0.00		0.31 ± 0.00	
Differentiation						
Moderate	0.11 ± 0.07	0.4370	0.15 ± 0.11	0.4900	0.27 ± 0.16	0.1340
Poor	0.09 ± 0.07		0.24 ± 0.20		0.36 ± 0.09	
Grade						
II	0.11 ± 0.07	0.4370	0.15 ± 0.11	0.4900	0.27 ± 0.16	0.1340
III	0.09 ± 0.07		0.24 ± 0.20		0.36 ± 0.09	
T staging						
1	0.15 ± 0.08	0.2360	0.18 ± 0.13	0.1500	0.33 ± 0.20	0.2000
2	0.08 ± 0.04		0.15 ± 0.10		0.23 ± 0.11	
3	0.12 ± 0.07		0.04 ± 0.06		0.19 ± 0.11	
4	0.10 ± 0.07		0.28 ± 0.11		0.36 ± 0.07	
Tis	0.10 ± 0.00		0.23 ± 0.00		0.13 ± 0.00	
N staging						
0	0.13 ± 0.08	0.5710	0.17 ± 0.12	0.5610	0.28 ± 0.19	0.7740
1	0.11 ± 0.07		0.24 ± 0.17		0.33 ± 0.12	
2	0.07 ± 0.05		0.12 ± 0.09		0.24 ± 0.12	
3	0.10 ± 0.06		0.22 ± 0.13		0.23 ± 0.16	

** Spearman correlation, Mann–Whitney U test, Kruskal–Wallis test were conducted.*

3.2.2. ABC Transporter in Chemoresistant CRC

Variations in the expression of ABC transporters between colorectal chemoresistant tissues and corresponding control tissues are shown in Figure 3.4. Relative P-GP expression in chemoresistant cells was approximately 22.35%, whereas in controls, the percentage was much lower (5.09%) (P value = 0.0003). In case of MRP1 relative expression, the average percentage in chemoresistant tissues was 30.46%, which was almost 11.5 times less in controls (2.65%), with a highly significant P value of < 0.0001. Besides, the mean percentage of ABCG2 expression in chemoresistant tissues was around 42.15%, while the percentage was 27.73% in control tissues (P value = 0.0096). Noteworthy is the observation that like breast cancer samples, overall ABCG2 expression was remarkably higher than the other two efflux transporters among Bangladeshi chemoresistant CRC patients.

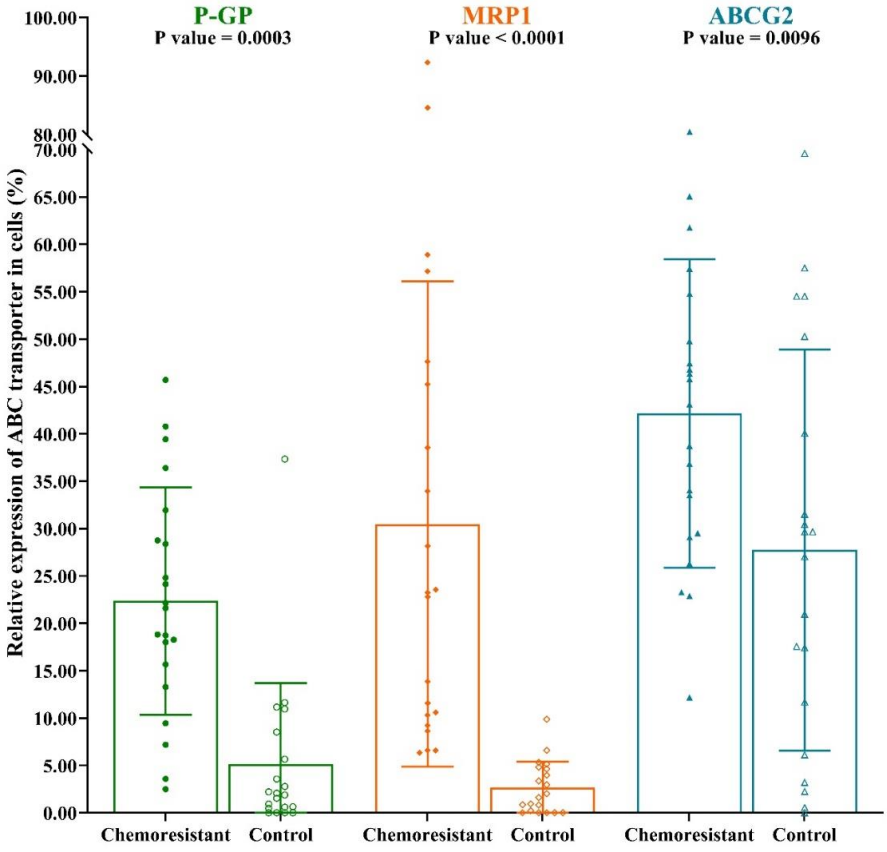

Figure 3.4: Comparison of ABC transporter expression between chemoresistant and adjacent control colorectal tissues. X-axis represents P-GP (green), MRP1 (orange) and ABCG2 (blue) transporters. Y-axis denotes the relative expression of ABC transporter to total cells in percentage. Wilcoxon signed rank test for paired samples was conducted to validate the significance of differences for P-GP and MRP1 expression in both type of tissues and paired samples T-test was run for ABCG2 expression.

Similar to Figure 3.3, Figure 3.5 also shows that relative overexpression of one efflux transporter reduced the expression of the others. For most of the chemoresistant CRC cases, ABCG2 showcased a higher expression than P-GP and MRP1. On the contrary, some samples, such as sample- 2, 4, 6, 7, 9, 10 and 14, displayed more MRP1 expression and sample- 11 and 19 had higher P-GP expression than the others. None but sample 5 and 21 were found to have similar expression level of transporters. The associations between CRC patient data and drug transporters (P-GP, MRP1 and ABCG2) expression reveals that the age of CRC patients was significantly correlated with the expression of MRP1 (Table 3.5).

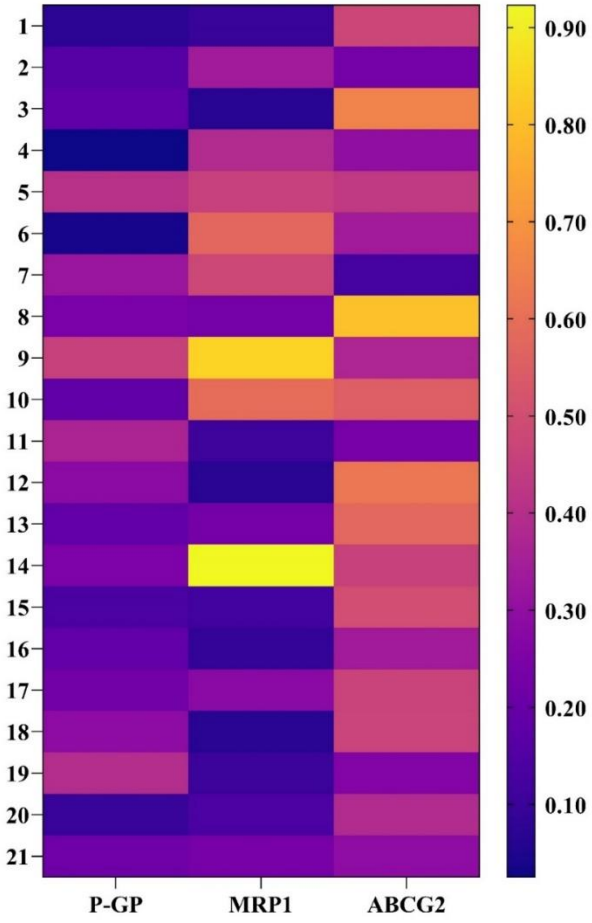

Figure 3.5: Heatmap illustrating the comparative levels of P-GP, MRP1 and ABCG2 in chemoresistant CRC tissues. Each row indicates a tissue sample and the color intensity bar reflects the relative expression levels.

Table 3.5: Association between ABC transporter expression and clinical features of chemoresistant CRC patients

Variables	P-GP		MRP1		ABCG2	
	mean ± sd	**P value**	**mean ± sd**	**P value**	**mean ± sd**	**P value**
Age (correlation coefficient)	0.17	0.459	0.56	**0.008**	-0.28	0.22
Sex						
Male	0.24 ± 0.13	0.549	0.34 ± 0.29	0.595	0.40 ± 0.16	0.415
Female	0.20 ± 0.11		0.25 ± 0.19		0.46 ± 0.17	
Diagnosis						
Adenocarcinoma	0.22 ± 0.12	NA	0.30 ± 0.26	NA	0.42 ± 0.16	NA
Differentiation						
Well	0.25 ± 0.13	0.599	0.26 ± 0.18	0.525	0.42 ± 0.19	0.51
Moderate	0.20 ± 0.13		0.41 ± 0.34		0.43 ± 0.12	
Poor	0.17 ± 0.02		0.21 ± 0.18		0.28 ± 08	
Grade						
I	0.25 ± 0.13	0.599	0.26 ± 0.18	0.525	0.42 ± 0.19	0.51
II	0.20 ± 0.13		0.41 ± 0.34		0.43 ± 0.12	
III	0.17 ± 0.02		0.21 ± 0.18		0.28 ± 08	
T staging						
1	0.46 ± 0.00	0.166	0.85 ± 0.00	0.479	0.37 ± 0.00	0.38
2	0.20 ± 0.13		0.26 ± 0.19		0.50 ± 0.15	
3	0.23 ± 0.10		0.32 ± 0.26		0.36 ± 0.16	
4	0.09 ± 0.00		0.14 ± 0.00		0.39 ± 0.00	
N staging						
0	0.23 ± 0.14	0.684	0.33 ± 0.27	0.601	0.39 ± 0.11	0.23
1	0.17 ± 0.09		0.22 ± 0.25		0.53 ± 0.06	
2	0.22 ± 0.06		0.27 ± 0.15		0.36 ± 0.26	

** Pearson's correlation coefficient, Spearman correlation, independent samples T-test, Mann–Whitney U test, ANOVA, Kruskal–Wallis test were conducted.*

3.2.3. ABC Transporter in Chemoresistant Ovarian Cancer

Differences in ABC transporter expression between ovarian cancer chemoresistant and adjacent control tissues are displayed in Figure 3.6. The relative P-GP expression in chemoresistant tissues was approximately 19.67%, which is 7.7 times higher than controls (2.55%) (P value = 0.0005). Similarly, MRP1 expression in chemoresistant tissues was much higher (28.83%), compared to the control tissues (1.85%). This difference was also highly significant (P value = 0.0078). Regarding ABCG2 expression, the average percentage in chemoresistant tissues was about 41.35%, contrasting to the control tissues, where the percentage is around four times less (10.42%) (P value = 0.0078). Like chemoresistant breast cancer and CRC, ABCG2 expression was noticed to be the highest and P-GP expression was the lowest.

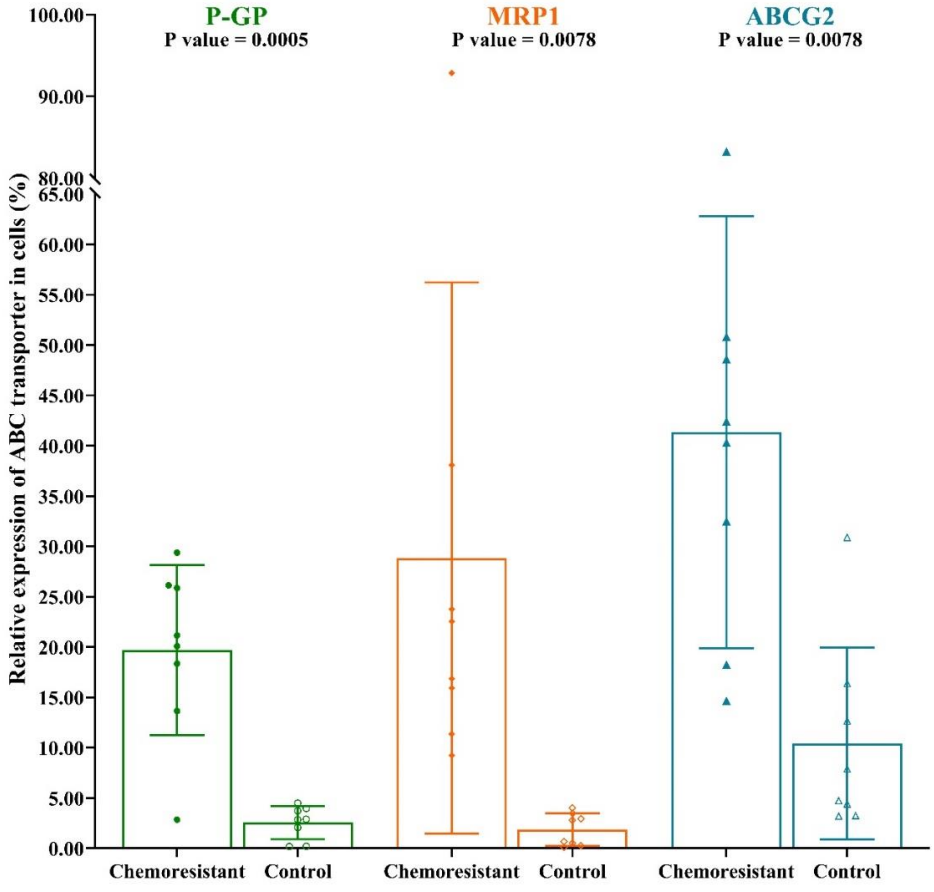

Figure 3.6: Comparison of ABC transporter expression between chemoresistant and adjacent control ovarian tissues. X-axis represents P-GP (green), MRP1 (orange) and ABCG2 (blue) transporters. Y-axis denotes the relative expression of ABC transporter to total cells in percentage. Paired samples T-test was conducted to validate the significance of differences for P-GP expression in both type of tissues and Wilcoxon signed rank test for paired samples was run for MRP1 and ABCG2.

Alike Figures 3.3 and 3.5, observations from Figure 3.7 also implies that overexpression of a specific efflux transporter corresponds to a drop in the expression of other two. Remarkably, ABCG2 protein manifested higher expression in most of the chemoresistant tissues (sample- 3, 4, 5, 6 and 8), while the expression of other ABC transporters was relatively lower. On the other hand, some samples (1 and 2) displayed more P-GP expression and MRP1 expression was predominant in sample 7. None of the ovarian cancer samples was noticed to have an even transporter expression in chemoresistant tissues. There was no statistically significant association between the expression of any of the drug transporters and ovarian cancer patient information (Table 3.6).

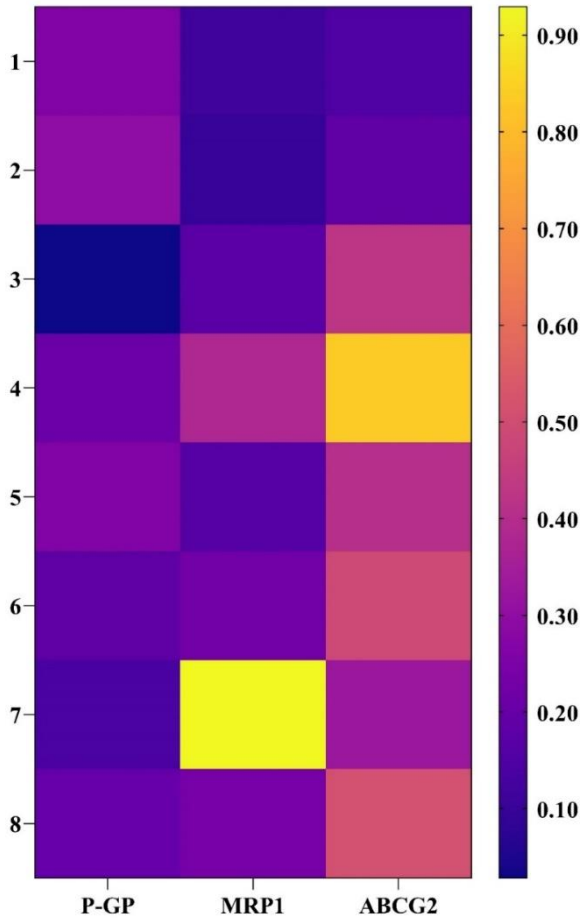

Figure 3.7: Heatmap illustrating the comparative levels of P-GP, MRP1 and ABCG2 in chemoresistant ovarian cancer tissues. Each row denotes a tissue sample and the color intensity bar reflects the relative expression levels.

Table 3.6: Association between ABC transporters expression and clinical features of chemoresistant ovarian cancer patients

Variables	P-GP		MRP1		ABCG2	
	mean ± sd	**P value**	**mean ± sd**	**P value**	**mean ± sd**	**P value**
Age (correlation coefficient)	-0.04	0.919	-0.33	0.42	0.45	0.267
Diagnosis						
Papillary serous carcinoma	0.20 ± 0.09	0.881	0.30 ± 0.29	1	0.40 ± 0.23	0.747
Squamous cell carcinoma	0.18 ± 0.00		0.23 ± 0.00		0.49 ± 0.00	
Differentiation						
Moderate	0.18 ± 0.00	0.881	0.23 ± 0.00	1	0.49 ± 0.00	0.747
Poor	0.20 ± 0.09		0.30 ± 0.29		0.40 ± 0.23	
Grade						
II	0.18 ± 0.00	0.881	0.23 ± 0.00	1	0.49 ± 0.00	0.747
III	0.20 ± 0.09		0.30 ± 0.29		0.40 ± 0.23	
T staging						
1	0.18 ± 0.00	0.531	0.23 ± 0.00	1	0.49 ± 0.00	0.354
3	0.23 ± 0.06		0.31 ± 0.35		0.31 ± 0.15	
N staging						
0	0.18 ± 0.00	0.855	0.23 ± 0.00	1	0.49 ± 0.00	0.311
1	0.22 ± 0.11		0.51 ± 0.59		0.25 ± 0.10	

** Pearson's correlation coefficient, Spearman correlation, independent samples T-test, Mann–Whitney U test were conducted.*

3.3. Expression of HIF1A in Chemoresistant Breast, Colorectal and Ovarian Cancer

The immunofluorescence image is showing DAPI staining of DNA and the expression of HIF1A in chemoresistant tissues with a scale bar of 25µm (Figure 3.8).

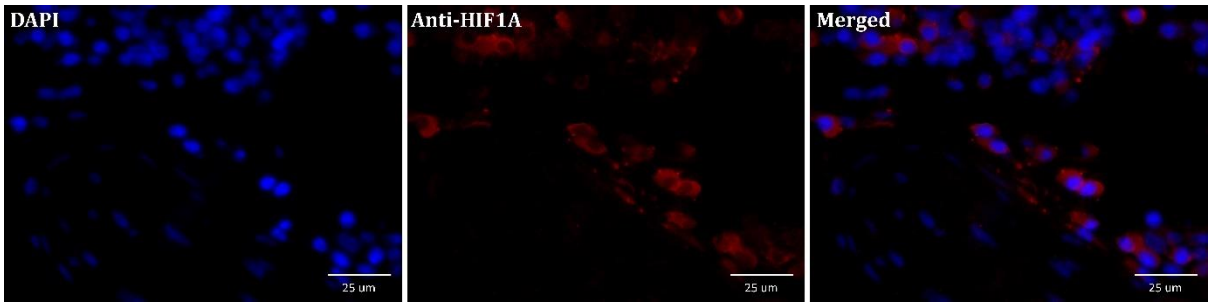

Figure 3.8: Immunofluorescence image of HIF1A expression. The image shows expression of HIF1A (red) in chemoresistant tissues and DAPI staining of DNA (blue). The scale bar is 25µm.

The fluctuations in HIF1A expression across chemoresistant and corresponding control tissues sourced from breast, colorectal and ovarian cancer patients are illustrated in Figure 3.9. Regarding breast cancer, the mean relative expression of HIF1A in chemoresistant tissues was 16.26%, contrasting with the lower percentage observed in controls (1.88%). This difference was found to be statistically significant (P value < 0.0001). For CRC, the average percentage was approximately 21.48% in chemoresistant tissues. But the percentage was nearly four folds less in controls (5.54%) (P value < 0.0001). Furthermore, the relative HIF1A expression in ovarian chemoresistant tissues was 21.93%, while in controls that was noted 3.91%, demonstrating a prominent difference with a statistically significant P value of 0.0020. No significant associations were identified between HIF1A expression in chemoresistant tissues and breast, colorectal and ovarian cancer patient data (Table 3.7).

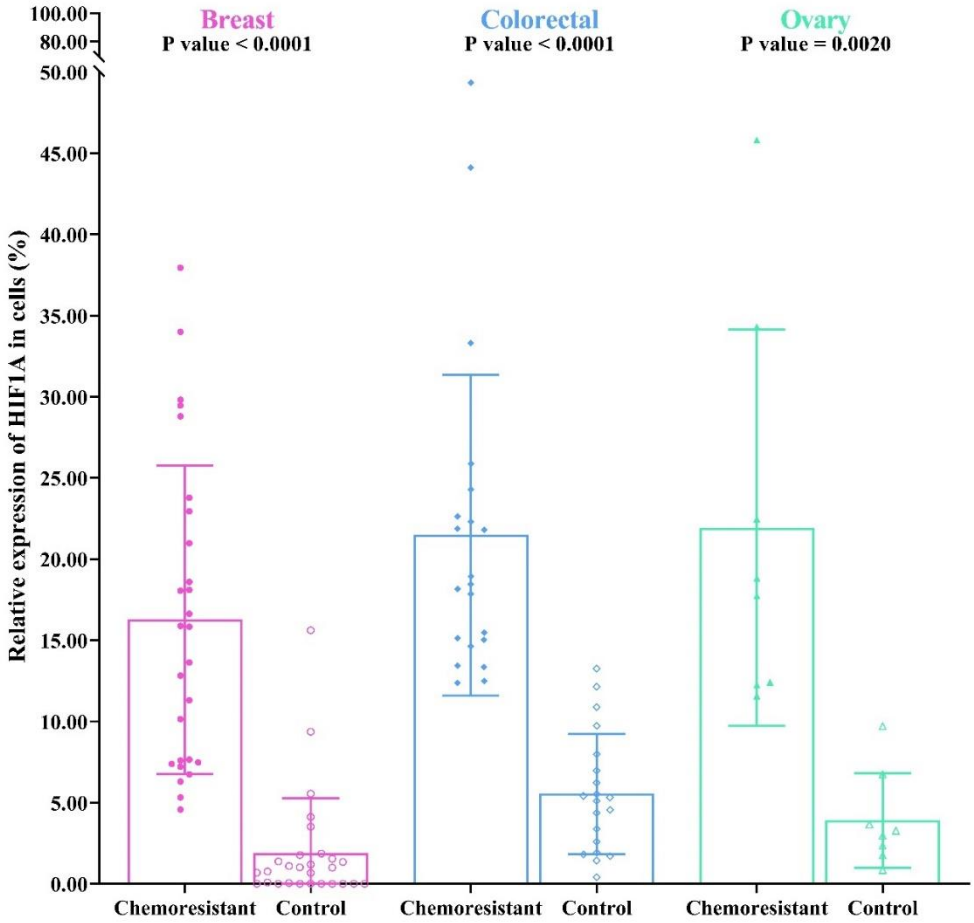

Figure 3.9: Comparison of HIF1A expression between chemoresistant and adjacent control tissues of breast, colorectal and ovarian cancers. X-axis represents breast (pink), colorectal (blue) and ovarian (green) cancers. Y-axis denotes the relative expression of HIF1A to total cells in percentage. Wilcoxon signed rank test for paired samples was conducted to validate the significance of differences for breast and colorectal cancers and paired samples T-test was run for ovarian cancer.

Table 3.7: Association between HIF1A expression and clinical features of chemoresistant breast, colorectal and ovarian cancer patients

Variables	Breast cancer		CRC		Ovarian cancer	
	mean ± sd	**P value**	**mean ± sd**	**P value**	**mean ± sd**	**P value**
Age (correlation coefficient)	-0.02	0.904	0.17	0.454	0.27	0.512
Sex						
Male	--	--	0.23 ± 0.11	0.336	--	--
Female	--		0.19 ± 0.08		--	
Diagnosis						
Infiltrating ductal carcinoma	0.16 ± 0.10	0.844	--	NA	--	0.744
Ductal carcinoma in situ	0.18 ± 0.00		--		--	
Infiltrating ductal and lobular carcinoma	0.17 ± 0.00		--		--	
Adenocarcinoma	--		0.21 ± 0.10		--	
Papillary serous carcinoma	--		--		0.23 ± 0.13	
Squamous cell carcinoma	--		--		0.18 ± 0.00	
Differentiation						
Well	--	0.395	0.22 ± 0.05	0.075	--	0.744
Moderate	0.16 ± 0.10		0.24 ± 0.15		0.18 ± 0.00	
Poor	0.19 ± 0.07		0.13 ± 0.01		0.23 ± 0.13	
Grade						
I	--	0.395	0.22 ± 0.05	0.075	--	0.744
II	0.16 ± 0.10		0.24 ± 0.15		0.18 ± 0.00	
III	0.19 ± 0.07		0.13 ± 0.01		0.23 ± 0.13	
T staging						
1	0.16 ± 0.10	0.881	0.49 ± 0.00	0.073	0.18 ± 0.00	0.843
2	0.16 ± 0.12		0.23 ± 0.06		--	
3	0.14 ± 0.03		0.19 ± 0.09		0.20 ± 0.09	
4	0.20 ± 0.04		0.12 ± 0.00		--	
Tis	0.18 ± 0.00		--		--	
N staging						
0	0.14 ± 0.09	0.338	0.22 ± 0.10	0.910	0.18 ± 0.00	0.836
1	0.15 ± 0.12		0.18 ± 0.04		0.23 ± 0.16	
2	0.24 ± 0.11		0.19 ± 0.06		--	
3	0.15 ± 0.08		--		--	

** Pearson's correlation coefficient, Spearman correlation, independent samples T-test, Mann–Whitney U test, Kruskal–Wallis test were conducted.*

3.4. Expression of HuR in Chemoresistant Breast, Colorectal and Ovarian Cancer

The immunofluorescence image is illustrating DAPI staining of DNA and the expression of HuR in chemoresistant tissues with a scale bar of 25µm (Figure 3.10).

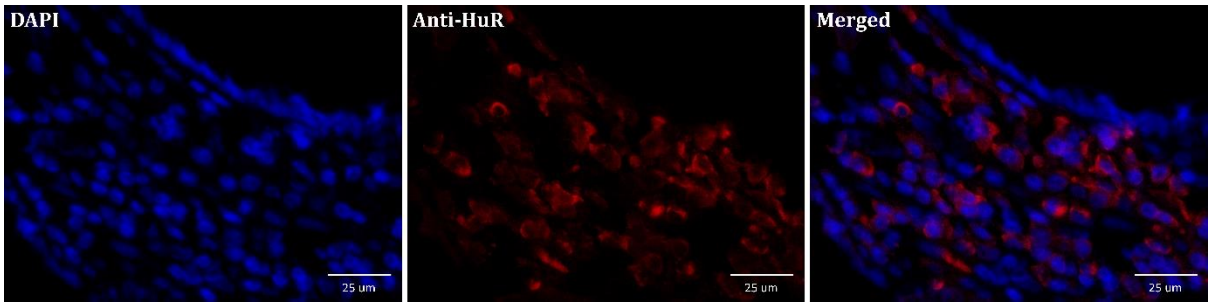

Figure 3.10: Immunofluorescence image of HuR expression. The image shows expression of HuR (red) and DAPI staining of DNA (blue) in chemoresistant tissues. The scale bar is 25µm.

The differences of HuR expression in chemoresistant and paired control tissues collected from breast, colorectal and ovarian cancer patients are portrayed in Figure 3.11. Mean relative HuR expression in breast cancer chemoresistant tissues (14.40%) was 19.2 times higher than control tissues (0.75%). This variation in ratio was statistically significant with a P value of < 0.0001. Likewise, HuR relative expression in CRC chemoresistant tissues was approximately 18.92%, which was significantly higher than the percentage detected in controls (3.58%) (P value < 0.0001). In addition, ovarian cancer chemoresistant tissues showed a mean percentage of 20.55% in case of HuR expression, though the controls had an average percentage of 2.87% (P value = 0.0078). There was no significant correlation between breast, colorectal and ovarian cancer patient data and HuR expression in chemoresistant tissues (Table 3.8).

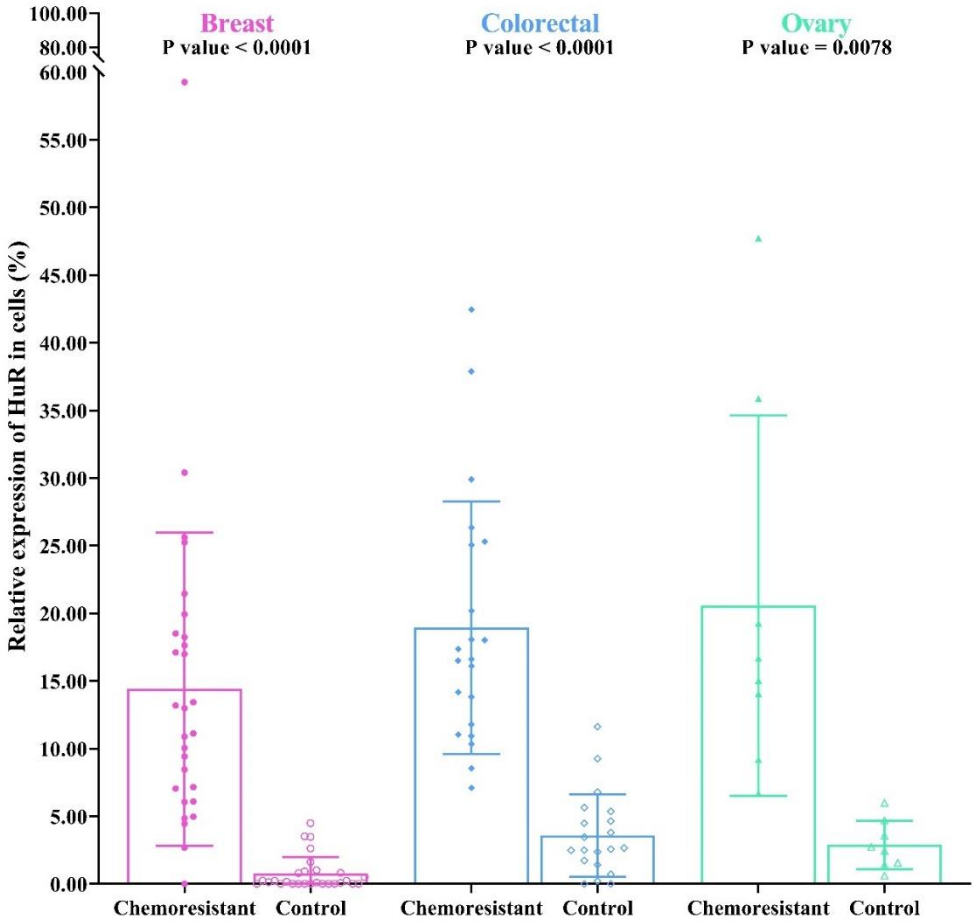

Figure 3.11: Comparison of HuR expression between chemoresistant and adjacent control tissues of breast, colorectal and ovarian cancers. X-axis represents breast (pink), colorectal (blue) and ovarian (green) cancers. Y-axis denotes the relative expression of HuR to total cells in percentage. Wilcoxon signed rank test for paired samples was conducted to validate the significance of differences for breast, colorectal and ovarian cancers.

Table 3.8: Association between HuR expression and clinical features of chemoresistant breast, colorectal and ovarian cancer patients

Variables	Breast cancer		CRC		Ovarian cancer	
	mean ± sd	**P value**	**mean ± sd**	**P value**	**mean ± sd**	**P value**
Age (correlation coefficient)	0.11	0.578	0.36	0.112	-0.24	0.570
Sex						
Male	--	--	0.22 ± 0.10	0.140	--	--
Female	--		0.15 ± 0.06		--	
Diagnosis						
Infiltrating ductal carcinoma	0.15 ± 0.12	0.600	--	NA	--	0.750
Ductal carcinoma in situ	0.17 ± 0.00		--		--	
Infiltrating ductal and lobular carcinoma	0.06 ± 0.00		--		--	
Adenocarcinoma	--		0.19 ± 0.09		--	
Papillary serous carcinoma	--		--		0.21 ± 0.15	
Squamous cell carcinoma	--		--		0.19 ± 0.00	
Differentiation						
Well	--	0.101	0.19 ± 0.06	0.646	--	0.750
Moderate	0.12 ± 0.08		0.20 ± 0.13		0.19 ± 0.00	
Poor	0.30 ± 0.25		0.19 ± 0.10		0.21 ± 0.15	
Grade						
I	--	0.395	0.19 ± 0.06	0.646	--	0.750
II	0.12 ± 0.08		0.20 ± 0.13		0.19 ± 0.00	
III	0.30 ± 0.25		0.19 ± 0.10		0.21 ± 0.15	
T staging						
1	0.15 ± 0.07	0.408	0.42 ± 0.00	0.241	0.19 ± 0.00	0.667
2	0.13 ± 0.17		0.18 ± 0.05		--	
3	0.11 ± 0.03		0.19 ± 0.09		0.18 ± 0.11	
4	0.18 ± 0.12		0.11 ± 0.00		--	
Tis	0.17 ± 0.00		--		--	
N staging						
0	0.12 ± 0.07	0.612	0.21 ± 0.09	0.098	0.19 ± 0.00	1.000
1	0.33 ± 0.37		0.12 ± 0.04		0.25 ± 0.15	
2	0.13 ± 0.10		0.17 ± 0.06		--	
3	0.18 ± 0.09		--		--	

** Spearman correlation, Mann–Whitney U test, Kruskal–Wallis test were conducted.*

3.5. Co-expression of ABC transporters and HIF1A in Chemoresistant Breast, Colorectal and Ovarian Cancer

The immunofluorescence image shows the co-expression of P-GP, MRP1 and ABCG2 with HIF1A within the same chemoresistant cells (Figure 3.12).

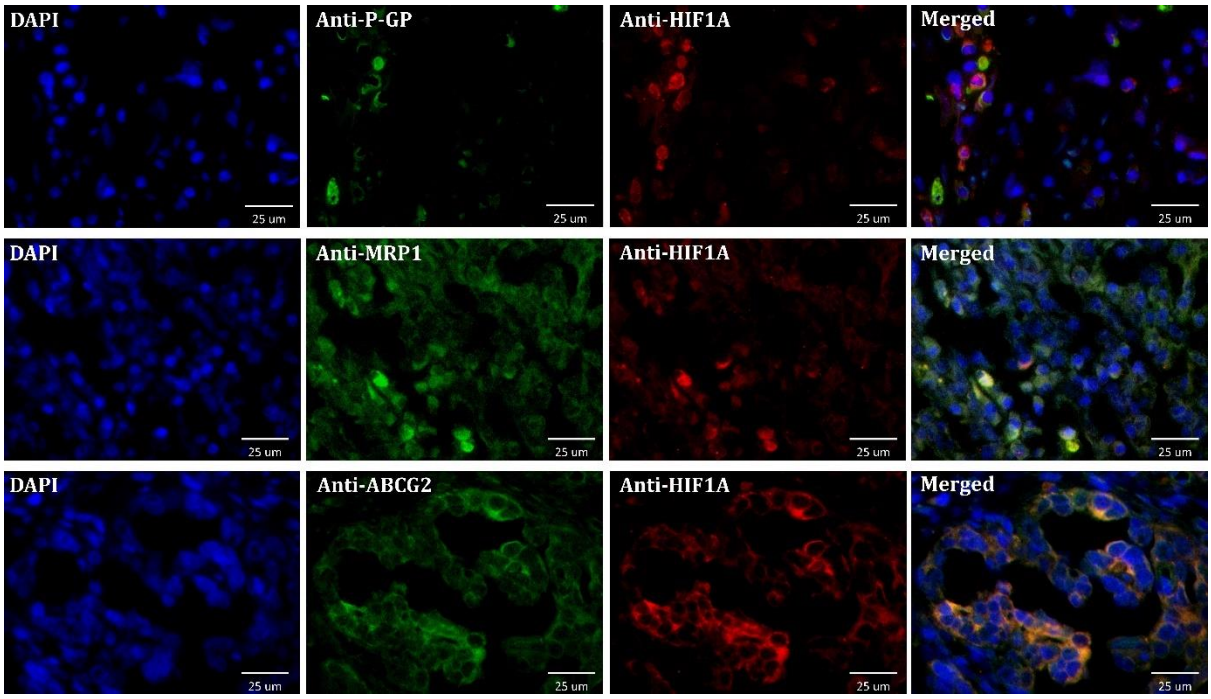

Figure 3.12: Immunofluorescence image of ABC transporter and HIF1A co-expression. The image shows expressions of P-GP, MRP1 and ABCG2 (green) and HIF1A (red) in chemoresistant tissues. The scale bar is 25µm.

3.5.1. ABC Transporters and HIF1A Co-expression in Chemoresistant Breast Cancer

Linear associations between the expression levels of ABC efflux transporters and HIF1A in breast tissues are illustrated in Figure 3.13. Remarkably, with an increase in the expression of HIF1A protein, there was a concurrent elevation in all transporter proteins expression. A one-unit increase in HIF1A corresponded to a 0.35 unit rise in P-GP (95% CI: 0.19-0.51), with < 0.0001 level of P value (Figure 3.13A). Similarly, a single unit raise in HIF1A resulted in a 0.78 unit increase in MRP1 expression (95% CI: 0.63-0.93) (P value < 0.0001) (Figure 3.13B). Furthermore, one-fold elevation of HIF1A led to a 1.08 unit rise in ABCG2 expression (95% CI: 0.70-1.45) with a statistically significant P value of < 0.0001 (Figure 3.13C).

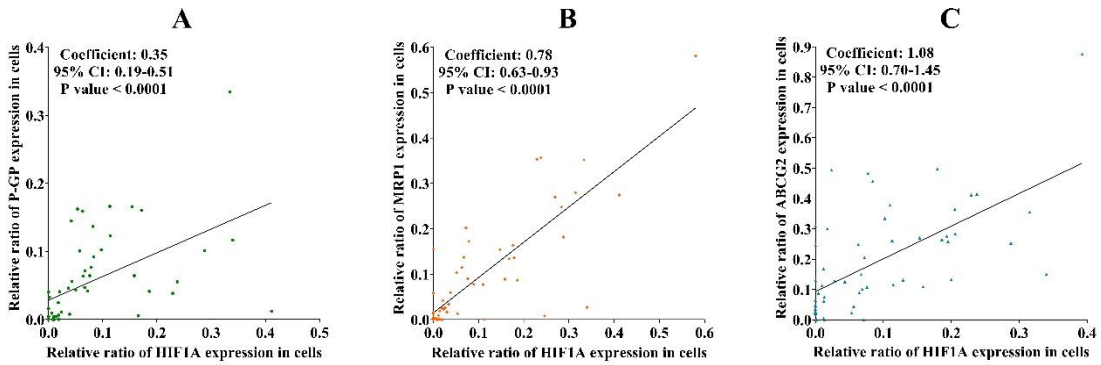

Figure 3.13: Correlation of individual ABC transporter and HIF1A expression in breast tissues. X-axis in (A), (B) and (C) denotes the relative ratio of HIF1A expression to total cells. Y-axis in (A), (B) and (C) denotes the relative ratio of P-GP, MRP1 and ABCG2 expression to total cells, respectively. The slopes indicate the linear relationship between transporters and HIF1A expression. Simple linear regression analysis was performed to identify the relationships.

The dynamics of co-expression between ABC transporters (P-GP, MRP1 and ABCG2) and HIF1A across chemoresistant and paired control tissues obtained from breast cancer patients are shown in Figure 3.14. For P-GP and HIF1A co-expression, the mean relative percentage in chemoresistant tissues was 60.90%, approximately 10 times higher than the controls (6.07%) (P value < 0.0001). In the context of MRP1 and HIF1A co-expression, the average percentage was 63.18% for chemoresistant tissues (slightly surpassing the P-GP and HIF1A co-expression). However, the percentage was around nine-fold less in controls (7.04%) (P value < 0.0001). Also, the relative co-expression regarding ABCG2 and HIF1A in breast chemoresistant tissues was 51.15%. In contrast, a noteworthy

variation in co-expression was seen in controls (3.35%) (P value < 0.0001). No significant associations were found when analyzing the relationship of ABC transporter-HIF1A co-expression with breast cancer patient data (Table 3.9).

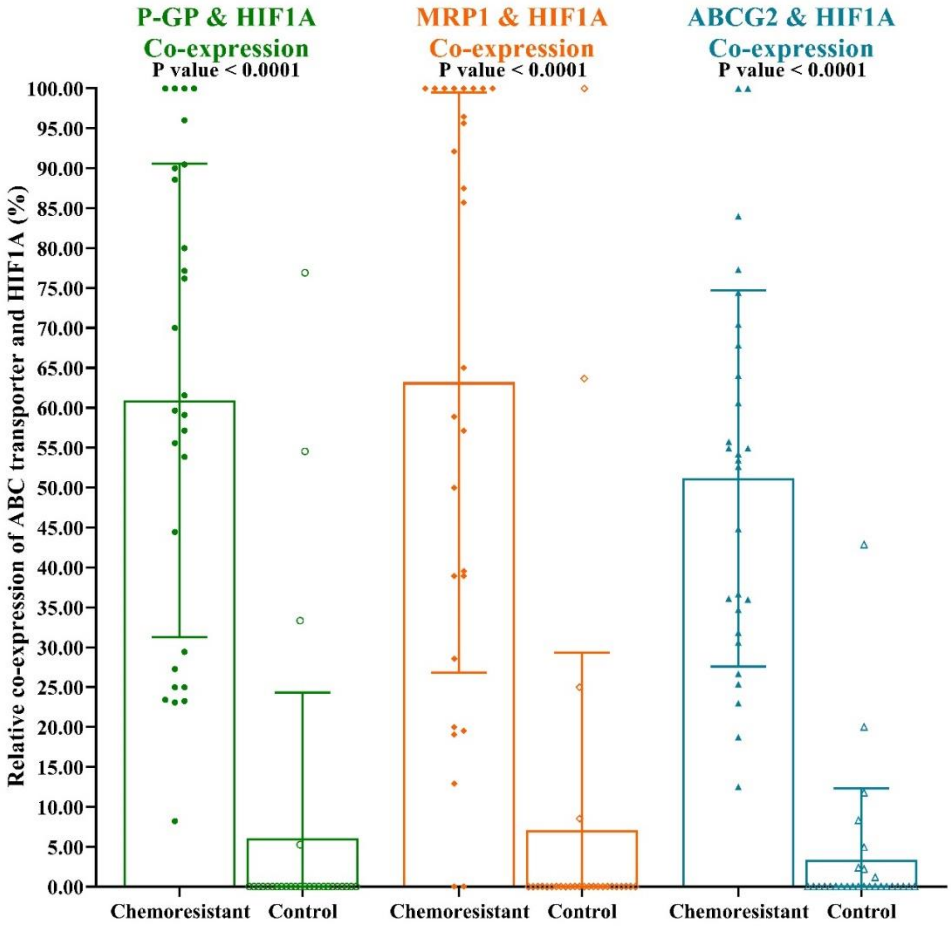

Figure 3.14: Comparison of ABC transporter and HIF1A co-expression in breast chemoresistant and adjacent control tissues. X-axis represents P-GP & HIF1A (green), MRP1 & HIF1A (orange) and ABCG2 & HIF1A (blue) co-expressions. Y-axis denotes the relative percentage of ABC transporter and HIF1A co-expression. Wilcoxon signed rank test for paired samples was conducted to validate the significance of differences for all types of co-expression.

Table 3.9: Association between ABC transporter and HIF1A co-expression and clinical features of chemoresistant breast cancer patients

Variables	Co_P-GP+HIF1A		Co_MRP1+HIF1A		Co_ABCG2+HIF1A	
	mean ± sd	**P value**	**mean ± sd**	**P value**	**mean ± sd**	**P value**
Age (correlation coefficient)	0.04	0.8538	-0.02	0.9096	-0.2	0.3248
Diagnosis						
Infiltrating ductal carcinoma	0.59 ± 0.30	0.4660	0.61 ± 036.	0.4260	0.50 ± 0.22	0.0719
Ductal carcinoma in situ	0.76 ± 0.00		1.00 ± 0.00		1.00 ± 0.00	
Infiltrating ductal and lobular carcinoma	0.96 ± 0.00		0.92 ± 0.00		0.31 ± 0.00	
Differentiation						
Moderate	0.60 ± 0.30	0.8210	0.65 ± 0.36	0.2420	0.51 ± 0.22	0.3090
Poor	0.62 ± 0.38		0.35 ± 0.33		0.38 ± 0.17	
Grade						
II	0.60 ± 0.30	0.8210	0.65 ± 0.36	0.2420	0.51 ± 0.22	0.3090
III	0.62 ± 0.38		0.35 ± 0.33		0.38 ± 0.17	
T staging						
1	0.57 ± 0.32	0.5530	0.74 ± 0.37	0.1870	0.59 ± 0.24	0.0773
2	0.64 ± 0.30		0.55 ± 0.34		0.41 ± 0.16	
3	0.39 ± 0.22		0.19 ± 0.27		0.50 ± 0.38	
4	0.79 ± 0.24		0.79 ± 0.19		0.43 ± 0.18	
Tis	0.76 ± 0.00		1.00 ± 0.00		1.00 ± 0.00	
N staging						
0	0.59 ± 0.31	0.7160	0.69 ± 0.38	0.4200	0.56 ± 0.27	0.5270
1	0.62 ± 0.54		0.26 ± 0.19		0.30 ± 0.07	
2	0.58 ± 0.22		0.61 ± 0.33		0.51 ± 0.20	
3	0.77 ± 0.20		0.74 ± 0.23		0.59 ± 0.07	

** Pearson's correlation coefficient, Spearman correlation, independent samples T-test, Mann–Whitney U test, ANOVA, Kruskal–Wallis test were conducted.*

3.5.2. ABC Transporters and HIF1A Co-expression in Chemoresistant CRC

The linear correlation of separate expressions between ABC drug transporters and HIF1A in colorectal tissues revealed that upregulation in HIF1A expression was concomitant with a simultaneous increase in the expression of all transporter proteins for colorectal tissues (Figure 3.15). One-unit escalation of HIF1A steered 1.08 unit increase in P-GP (95% CI: 0.96-1.20), exhibiting significance at a level of < 0.0001 (Figure 3.15A). Likewise, a singular unit ascent in HIF1A led to 1.17 unit rise in MRP1 expression (95% CI: 0.99-1.33) (P value < 0.0001) (Figure 3.15B). Besides, an elevation of one-fold in HIF1A resulted in a notable 1.75 unit increase in ABCG2, with a statistically significant P value of < 0.0001 (Figure 3.15C).

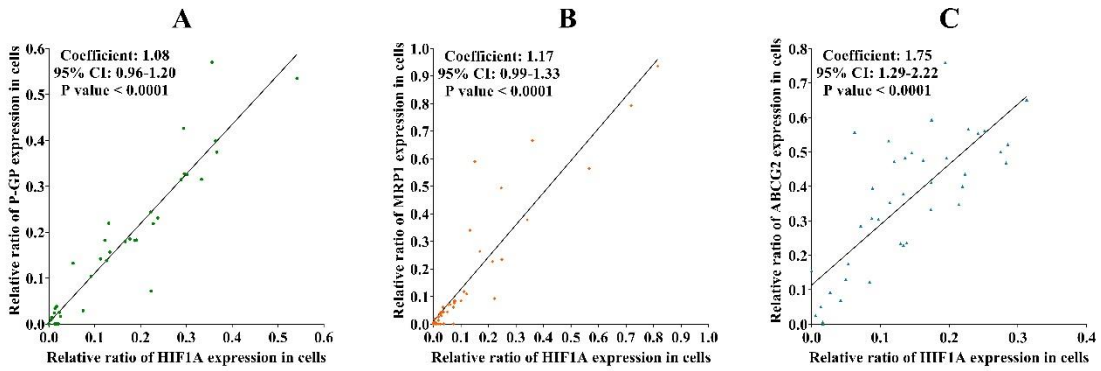

Figure 3.15: Correlation of individual ABC transporter and HIF1A expression in colorectal tissues. X-axis in (A), (B) and (C) denotes the relative ratio of HIF1A expression to total cells. Y-axis in (A), (B) and (C) denotes the relative ratio of P-GP, MRP1 and ABCG2 expression to total cells, respectively. The slopes indicate the linear relationship between transporters and HIF1A expression. Simple linear regression analysis was performed to identify the relationships.

ABC transporters (P-GP, MRP1 and ABCG2) and HIF1A co-expression variation in tissues obtained from chemoresistant and paired control samples of CRC patients are illustrated in Figure 3.16. The mean relative percentage observed in chemoresistant tissues was 83.24% for P-GP and HIF1A co-expression (highest among all the co-expressions), approximately 2.5-fold higher than in controls (33.12%) (P value < 0.0001). In the context of MRP1 and HIF1A co-expression, the relative percentage was 78.12% for CRC chemoresistant tissues. Conversely, the percentage was approximately half in controls (38.24%) (P value = 0.0001). In addition, the mean relative percentage of co-expression concerning ABCG2 and HIF1A in CRC chemoresistant tissues was 37.92%,

while it was 22.41% in adjacent controls (P value < 0.0001). Among chemoresistant CRC patients, the differentiation of cells and cancer grade was significantly correlated with P-GP and HIF1A co-expression (P value = 0.047) (Table 3.10). In Grade II and moderate differentiation of ovarian cancer, P-GP and HIF1A co-expression was the highest (0.91 ± 0.10).

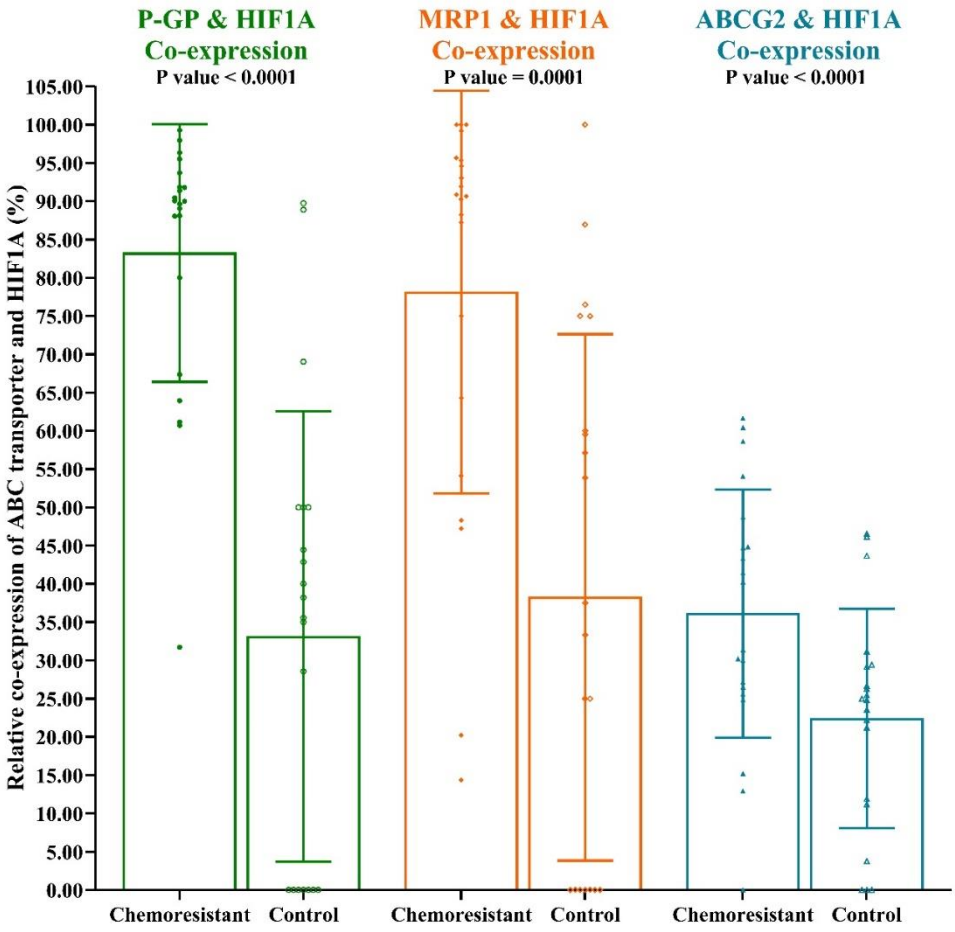

Figure 3.16: Comparison of ABC transporter and HIF1A co-expression in colorectal chemoresistant and adjacent control tissues. X-axis represents P-GP & HIF1A (green), MRP1 & HIF1A (orange) and ABCG2 & HIF1A (blue) co-expressions. Y-axis denotes the relative percentage of ABC transporter and HIF1A co-expression. Wilcoxon signed rank test for paired samples was conducted to validate the significance of differences for P-GP- and MRP1-HIF1A co-expression and paired samples T-test was run for ABCG2-HIF1A co-expression.

Table 3.10: Association between ABC transporter and HIF1A co-expression and clinical features of chemoresistant CRC patients

Variables	Co_P-GP+HIF1A		Co_MRP1+HIF1A		Co_ABCG2+HIF1A	
	mean ± sd	**P value**	**mean ± sd**	**P value**	**mean ± sd**	**P value**
Age (correlation coefficient)	0.09	0.7	-0.19	0.421	-0.21	0.365
Sex						
Male	0.89 ± 0.08	0.336	0.86 ± 0.15	0.595	0.40 ± 0.13	0.386
Female	0.74 ± 0.23		0.66 ± 0.36		0.34 ± 0.17	
Diagnosis						
Adenocarcinoma	0.83 ± 0.17	NA	0.78 ± 0.26	NA	0.38 ± 0.14	NA
Differentiation						
Well	0.85 ± 0.13	**0.047**	0.84 ± 0.19	0.521	0.38 ± 0.16	0.981
Moderate	0.91 ± 0.10		0.73 ± 0.29		0.39 ± 0.16	
Poor	0.48 ± 0.23		0.57 ± 0.53		0.40 ± 0.05	
Grade						
I	0.85 ± 0.13	**0.047**	0.84 ± 0.19	0.521	0.38 ± 0.16	0.981
II	0.91 ± 0.10		0.73 ± 0.29		0.39 ± 0.16	
III	0.48 ± 0.23		0.57 ± 0.53		0.40 ± 0.05	
T staging						
1	0.94 ± 0.00	0.436	0.91 ± 0.00	0.154	0.27 ± 0.00	0.666
2	0.79 ± 0.15		0.84 ± 0.23		0.37 ± 0.16	
3	0.85 ± 0.20		0.70 ± 0.29		0.41 ± 0.14	
4	0.91 ± 0.00		0.95 ± 0.00		0.00 ± 0.00	
N staging						
0	0.87 ± 0.10	0.978	0.84 ± 0.19	0.492	0.42 ± 0.14	0.315
1	0.81 ± 0.19		0.61 ± 0.38		0.29 ± 0.18	
2	0.75 ± 0.28		0.74 ± 0.33		0.42 ± 0.12	

** Pearson's correlation coefficient, Spearman correlation, independent samples T-test, Mann–Whitney U test, ANOVA, Kruskal–Wallis test were conducted.*

3.5.3. ABC Transporters and HIF1A Co-expression in Chemoresistant Ovarian Cancer

The linear regression models from Figure 3.17 elucidates the associations between ABC drug transporters and HIF1A individual expressions in the ovary. Interestingly, like in breast and colorectal cancers, elevation in the relative expression of all transporter proteins was observed as HIF1A expression inclined. A one-unit raise in HIF1A related to a 1.24-unit rise in P-GP (95% CI: 0.83-1.66) (P < 0.0001) (Figure 3.17A). Alike the previous one, solitary unit elevation of HIF1A led to a 1.09-unit increase in the expression of MRP1 (95% CI: 1.04-1.14) with a highly significant P value of < 0.0001 (Figure 3.17B). In addition, a one-fold elevation in HIF1A promoted ABCG2 expression by 0.96-unit (95% CI: 0.55-1.38) (P value = 0.0002) (Figure 3.17C).

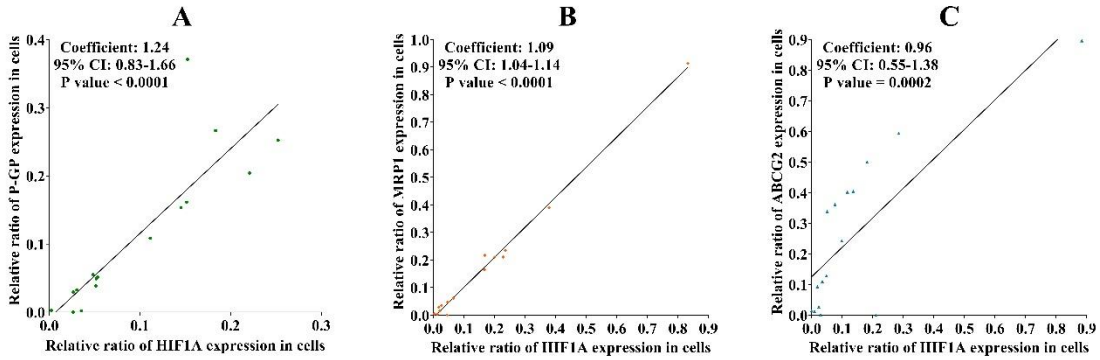

Figure 3.17: Correlation of individual ABC transporter and HIF1A expression in ovarian tissues. X-axis in (A), (B) and (C) denotes the relative ratio of HIF1A expression to total cells. Y-axis in (A), (B) and (C) denotes relative ratio of P-GP, MRP1 and ABCG2 expression to total cells, respectively. The slopes indicate the linear relationship between transporters and HIF1A expression. Simple linear regression analysis was performed to identify the relationships.

The differences in ABC transporters and HIF1A co-expression across the tissues collected from chemoresistant and paired control samples from ovarian cancer patients are portrayed in Figure 3.18. Co-expression ratio was the highest for MRP1 and HIF1A in chemoresistant tissue of ovarian cancer. In the context of P-GP and HIF1A relative co-expression, the mean percentages in chemoresistant and control tissues were 84.66% and 55.85%, respectively (P value = 0.0156). The relative average percentage in chemoresistant tissues was 92.40% for MRP1 and HIF1A co-expression. On the contrary, the percentage was approximately half (58.47%) in controls (P value = 0.0313). It was

noticed that there was not any significant association between ovarian cancer patient information and ABC drug transporter and HIF1A co-expression (Table 3.11).

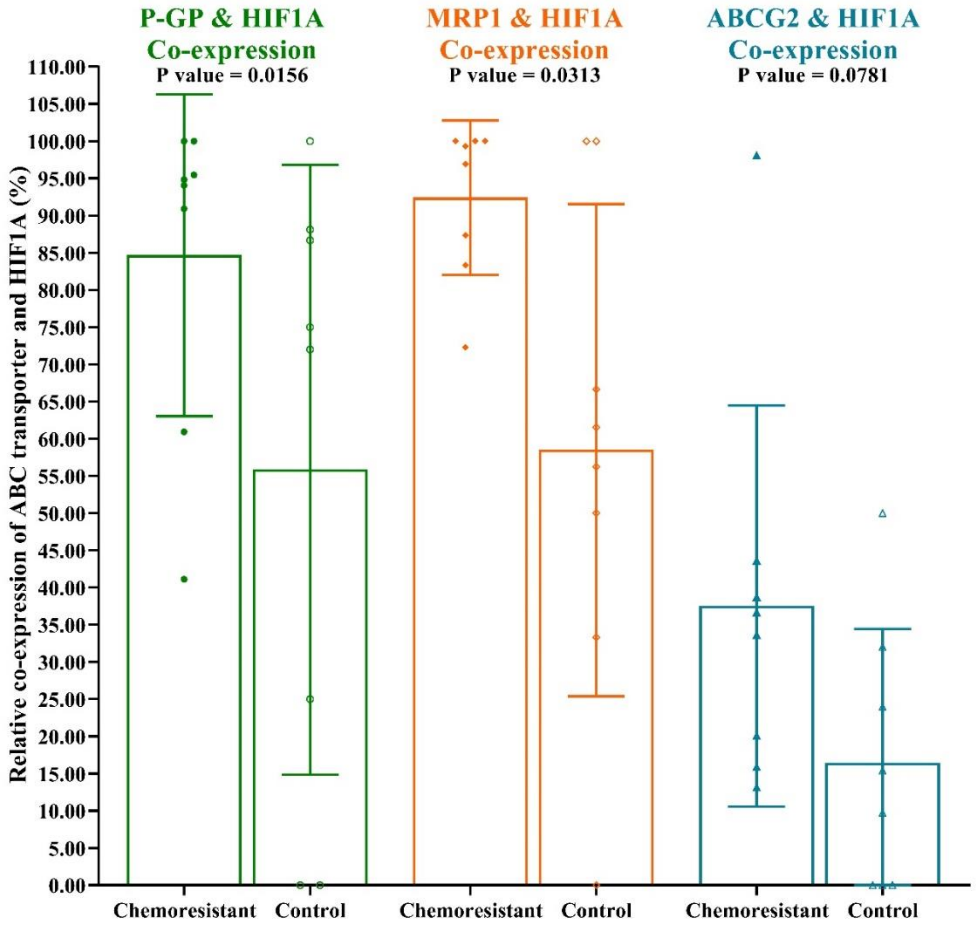

Figure 3.18: Comparison of ABC transporter and HIF1A co-expression in ovarian chemoresistant and adjacent control tissues. X-axis represents P-GP & HIF1A (green), MRP1 & HIF1A (orange) and ABCG2 & HIF1A (blue) co-expressions. Y-axis denotes the relative percentage of ABC transporter and HIF1A co-expression. Wilcoxon signed rank test for paired samples was conducted to validate the significance of differences for all types of co-expression.

Table 3.11: Association between ABC transporter and HIF1A co-expression and clinical features of chemoresistant ovarian cancer patients

Variables	Co_P-GP_HIF1A		Co_MRP1_HIF1A		Co_ABCG2_HIF1A	
	mean ± sd	**P value**	**mean ± sd**	**P value**	**mean ± sd**	**P value**
Age (correlation coefficient)	-0.07	0.87	0.586	0.127	0.45	0.26
Diagnosis						
Papillary serous carcinoma	0.83 ± 0.23	1	0.94 ± 0.10	0.5	0.38 ± 0.29	1
Squamous cell carcinoma	0.94 ± 0.00		0.83 ± 0.00		0.34 ± 0.00	
Differentiation						
Moderate	0.94 ± 0.00	1	0.83 ± 0.00	0.5	0.34 ± 0.00	1
Poor	0.83 ± 0.23		0.94 ± 0.10		0.38 ± 0.29	
Grade						
II	0.94 ± 0.00	1	0.83 ± 0.00	0.5	0.34 ± 0.00	1
III	0.83 ± 0.23		0.94 ± 0.10		0.38 ± 0.29	
T staging						
1	0.94 ± 0.00	1	0.83 ± 0.00	0.667	0.34 ± 0.00	1
3	0.78 ± 0.26		0.92 ± 0.12		0.30 ± 0.13	
N staging						
0	0.94 ± 0.00	1	0.83 ± 0.00	1	0.34 ± 0.00	1
1	0.78 ± 0.24		0.94 ± 0.09		0.26 ± 0.18	

** Spearman correlation, Mann–Whitney U test were conducted.*

3.5.4. 3D modelling of HIF1A Protein and its target binding site

The predicted structure of the HIF1A protein is presented in Figure 3.19A. An estimation of the quality of the predicted protein model is provided in Figures 3.19B, 3.19C and 3.19D. From the Ramachandran plot, it was observed that a total of 98.10% {most favored region (91.60%) + additional allowed region (6.20%) + generally allowed region (0.30%)} of the AA residues were in allowed region (Figure 3.19B). Based on the evaluations, the structure of HIF1A was determined to be acceptable.

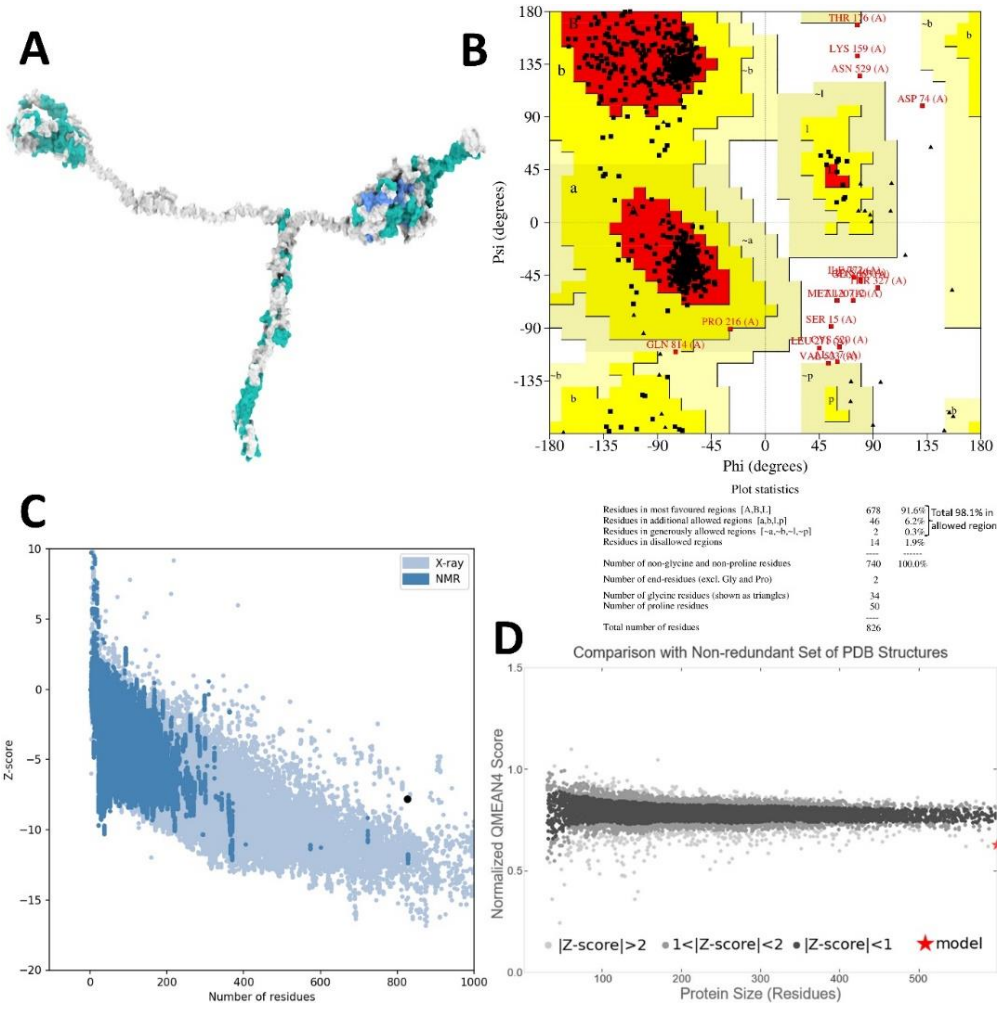

Figure 3.19: HIF1A protein structure prediction and validation. (A) Predicted structure of HIF1A protein. (B) Ramachandran plot for HIF1A protein. Percentages of residues in allowed region and disallowed region were 98.1% and 1.9%, respectively. (C) Z-score plot for HIF1A protein. The black dot denotes the position predicted model in the Z-score plot. (D) Q-mean score plot for HIF1A protein. The red star indicates the position of predicted model in the Q-mean score plot.

The 'CGTG' regions were identified within 2000 bp range of the promoter regions for *P-GP* (from -1000 to -1003, from -1592 to -1595, from -1625 to -1628 and from -1630 to -

1633) and *MRP1* (from -1516 to -1520 and from -1742 to - 1745) genes, but a similar region was located within 6500 bp range for *ABCG2* (from -6111 to -6114) gene. Utilizing the 3D DNA models from Figure 3.20, molecular docking experiments were conducted with the HIF1A protein from Figure 3.19A.

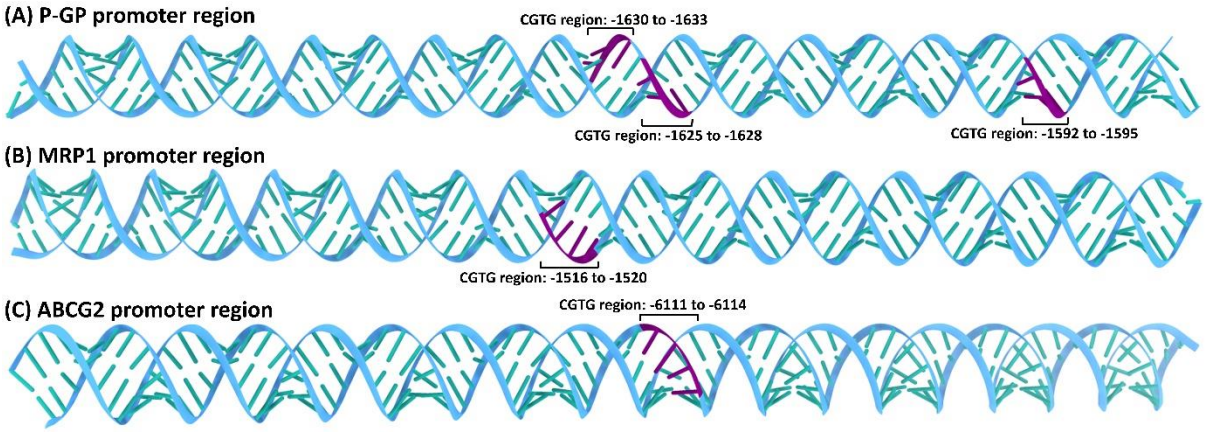

Figure 3.20: 3D DNA models of the promoter regions for ABC transporter genes. (A) Promoter region of the *P-GP* gene. (B) Promoter region of the *MRP1* gene. (C) Promoter region of the *ABCG2* gene. 'CGTG' regions are highlighted in purple. The prediction of the 3D structure includes 50 nucleotides both before and after the CGTG region.

3.5.5. Molecular docking between HIF1A and Promoter Regions of ABC Transporter Genes

Representative figures of docking simulations are presented in Figure 3.21. Table 3.12 represents Z-scores of molecular docking analyses between the HIF1A protein and the DNA of ABC drug transporters (P-GP, MRP1 and ABCG2) promoter regions, specifically with the 'CGTG' region. Molecular docking was conducted using five AA regions of HIF1A protein for which structures were determined via X-ray crystallography. These selected regions include AA sequences of 238-348, 395-411, 549-582, 717-757 and 775-826. We observed that all the Z-scores found from docking were negative. Z-scores provide a way to determine how a particular docking score compares to a distribution of scores from random or non-specific docking poses and a negative Z-score from HADDOCK 2.4 means that the docking score is better than average when compared to the distribution of decoy or random docking scores. Additionally, other comprehensive information such as the Haddock score, cluster size, RMSD from the overall lowest-energy structure, Van der Waals energy, electrostatic energy, desolvation energy, restraints violation energy and buried surface area for all dockings are provided in Supplementary table 10.

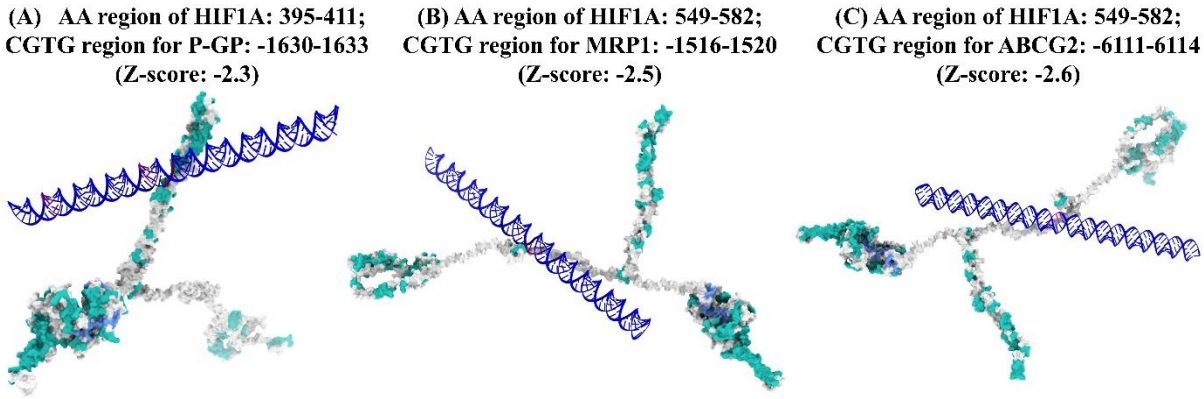

Figure 3.21: Molecular docking of HIF1A with 'CGTG' sequence of ABC transporter genes promoter regions. (A) Representative docking of HIF1A (AA region: 395-411) and *P-GP* gene promoter region (Z-score: -2.3). (B) Representative docking of HIF1A (AA region: 549-582) and *MRP1* gene promoter region (Z-score: -2.5). (C) Representative docking of HIF1A (AA region: 549-582) and *ABCG2* gene promoter region (Z-score: -2.6). More details are in Table 3.16.

Table 3.12: Molecular docking of HIF1A protein and 'CGTG' sequence from the promoter region of ABC transporters DNA and their Z-scores (More details are provided in Supplementary table 10)

AA region of HIF1A	Z-Score
P-GP promoter region	
238--348	-1.7
395-411	-2.3
549-582	-2.1
717-757	-1.7
775-826	-1.3
MRP1 promoter region	
238--348	-1.1
395-411	-1.8
549-582	-2.5
717-757	-2.3
775-826	-2.3
ABCG2 promoter region	
238--348	-2
395-411	-1.6
549-582	-2.6
717-757	-1.9
775-826	-1.1

3.6. Co-expression of ABC transporters and HuR in Chemoresistant Breast, Colorectal and Ovarian Cancers

The immunofluorescence image shows the co-expression of P-GP, MRP1 and ABCG2 with HuR within the same chemoresistant cells (Figure 3.22).

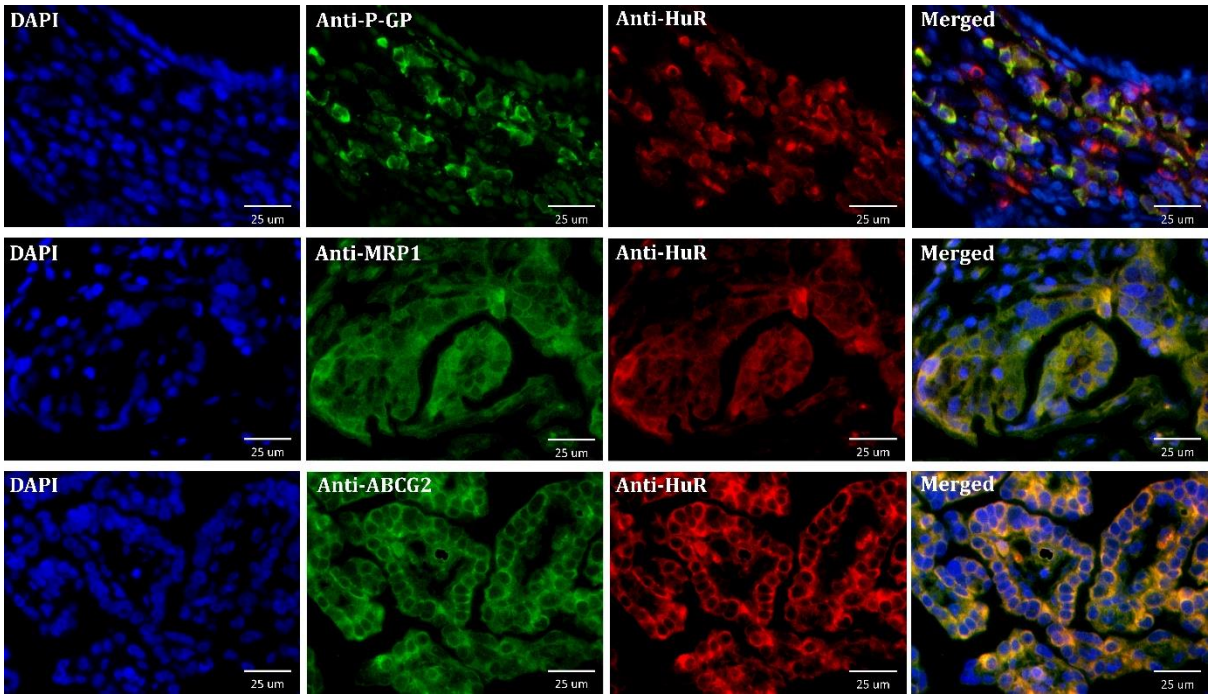

Figure 3.22: Immunofluorescence image of ABC transporter and HuR co-expression. The image shows expressions of P-GP, MRP1 and ABCG2 (green) and HuR (red) in chemoresistant tissues. The scale bar is 25µm.

3.6.1. ABC Transporters and HuR Co-expression in Chemoresistant Breast Cancer

Linear regression analysis between the expression levels of ABC efflux transporters (P-GP, MRP1 and ABCG2) and HuR in breast tissues revealed that the expression of transporter proteins is directly proportional to HuR protein expression (Figure 3.23). A one-unit increase in HuR corresponded to a 0.39 unit rise in P-GP (95% CI: 0.21-0.56) (P value < 0.0001) (Figure 3.23A). Similarly, a single unit raise in HuR expression propelled 0.68 unit increase in MRP1 expression (95% CI: 0.49-0.88) and this relation was significant at < 0.0001 level (Figure 3.23B). Likewise, one-fold elevation of HuR resulted in 0.72 unit rise in ABCG2 expression (95% CI: 0.32-1.13) (P value = 0.0008) (Figure 3.23C).

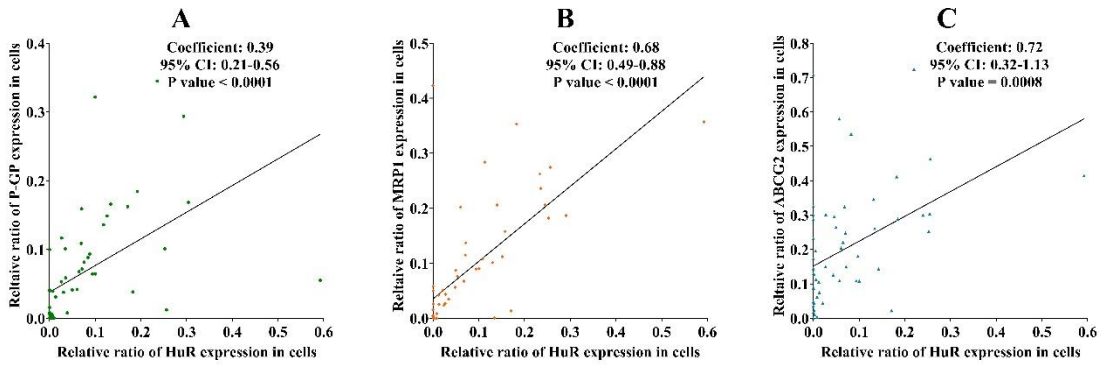

Figure 3.23: Correlation of individual ABC transporter and HuR expression in breast tissues. X-axis in (A), (B) and (C) denotes the relative ratio of HuR expression to total cells. Y-axis in (A), (B) and (C) denotes relative ratio of P-GP, MRP1 and ABCG2 expression to total cells, respectively. The slopes indicate the linear relationship between transporters and HuR expression. Simple linear regression analysis was performed to identify the relationships.

The deviations of ABC transporters (P-GP, MRP1 and ABCG2) and HuR co-expression in the breast chemoresistant and adjacent control tissues and their significance levels are exhibited in Figure 3.24. For P-GP and HuR co-expression, the mean relative percentage in chemoresistant tissues was 54.99%, almost 10 times higher than controls (5.27%) (P value < 0.0001). The average relative percentage was 74.16% in chemoresistant tissues for MRP1 and HuR co-expression (highest amongst all other co-expressions). However, that was 6.43% in controls (P value < 0.0001). In breast chemoresistant tissues, the mean relative co-expression for ABCG2 and HuR was 35.48%, whereas it was 0.68% in control tissues (P value < 0.0001). There was no significant association between ABC

transporters (P-GP, MRP1 and ABCG2) and HuR co-expression and breast cancer patient information (Table 3.13).

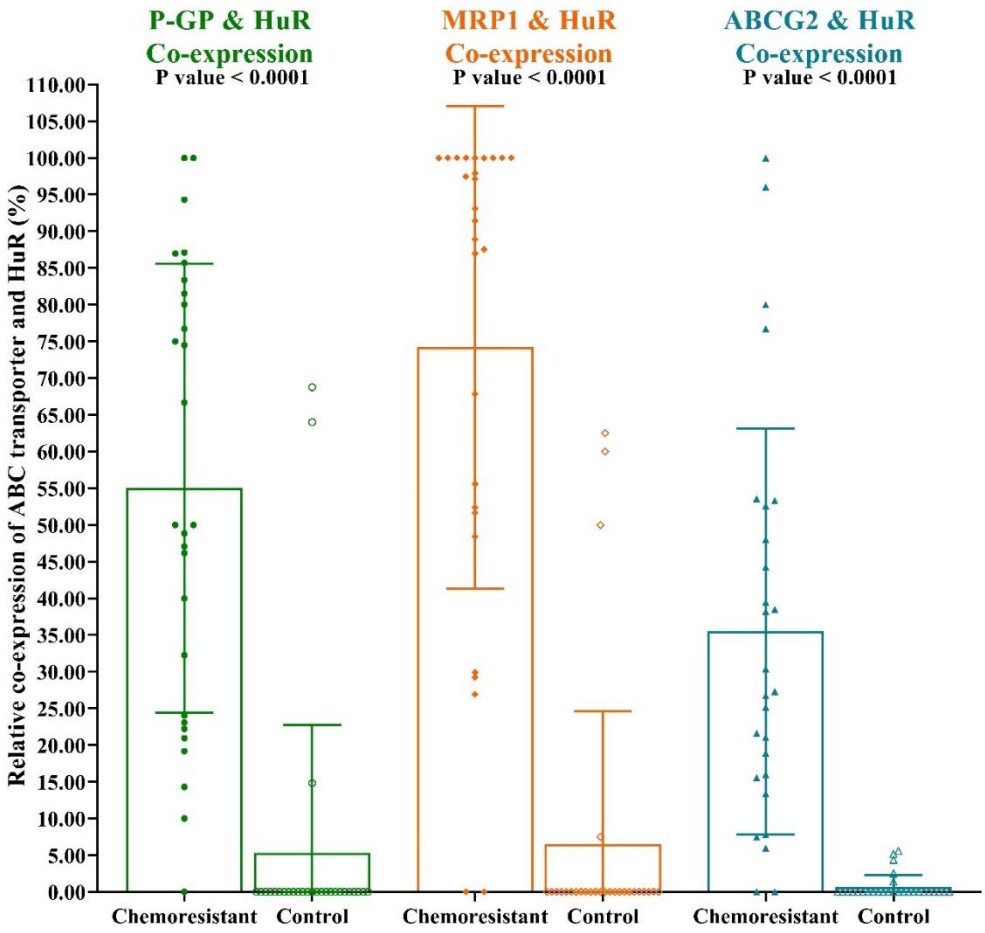

Figure 3.24: Comparison of ABC transporter and HuR co-expression in breast chemoresistant and adjacent control tissues. X-axis represents P-GP & HuR (green), MRP1 & HuR (orange) and ABCG2 & HuR (blue) co-expressions. Y-axis denotes the relative percentage of ABC transporter and HuR co-expression. Wilcoxon signed rank test for paired samples was conducted to validate the significance of differences for all types of co-expression.

Table 3.13: Association between ABC transporter and HuR co-expression and clinical features of chemoresistant breast cancer patients

Variables	Co_P-GP+HuR		Co_MRP1+HuR		Co_ABCG2+HuR	
	mean ± sd	**P value**	**mean ± sd**	**P value**	**mean ± sd**	**P value**
Age (correlation coefficient)	-0.05	0.7934	-0.02	0.9349	0.27	0.1727
Diagnosis						
Infiltrating ductal carcinoma	0.52 ± 0.30	0.2510	0.73 ± 0.34	0.4710	0.34 ± 0.26	0.1910
Ductal carcinoma in situ	0.81 ± 0.00		1.00 ± 0.00		0.96 ± 0.00	
Infiltrating ductal and lobular carcinoma	0.94 ± 0.00		0.87 ± 0.00		0.13 ± 0.00	
Differentiation						
Moderate	0.55 ± 0.30	0.7430	0.76 ± 0.31	0.4900	0.32 ± 0.26	0.4900
Poor	0.47 ± 0.46		0.51 ± 0.50		0.39 ± 0.18	
Grade						
II	0.55 ± 0.30	0.7430	0.76 ± 0.31	0.4900	0.32 ± 0.26	0.4900
III	0.47 ± 0.46		0.51 ± 0.50		0.39 ± 0.18	
T staging						
1	0.61 ± 0.30	0.3960	0.79 ± 0.34	0.6050	0.43 ± 0.32	0.4530
2	0.47 ± 0.31		0.72 ± 0.29		0.26 ± 0.18	
3	0.33 ± 0.19		0.50 ± 0.71		0.23 ± 0.06	
4	0.68 ± 0.39		0.69 ± 0.25		0.29 ± 0.22	
Tis	0.81 ± 0.00		1.00 ± 0.00		0.96 ± 0.00	
N staging						
0	0.56 ± 0.29	0.3950	0.75 ± 0.35	0.6960	0.38 ± 0.32	0.7030
1	0.60 ± 0.56		0.74 ± 0.36		0.30 ± 0.33	
2	0.39 ± 0.27		0.82 ± 0.25		0.33 ± 0.27	
3	0.69 ± 0.31		0.77 ± 0.22		0.45 ± 0.08	

** Spearman correlation, Mann–Whitney U test, Kruskal–Wallis test were conducted.*

3.6.2. ABC Transporters and HuR Co-expression in Chemoresistant CRC

A linear regression association between the independent expressions of ABC transporters and HuR in colorectal tissues is presented in Figure 3.25. Similar to Figure 3.23, it was observed that the transporter protein expression level is directly proportional to the expression HuR protein for colorectal tissues. A singular unit elevation in HuR drove the rise of P-GP by 1.01 unit (95% CI: 0.94-1.08) (P value < 0.0001) (Figure 3.25A). Besides, one-fold increase in HuR expression induced MRP1 to overexpress by 1.14 unit (95% CI: 1.01-1.26) (P < 0.0001) (Figure 3.25B). Also, one-fold raise in HuR steered 1.38 unit rise in ABCG2 expression (95% CI: 0.60-2.16) (P value = 0.0010) (Figure 3.25C).

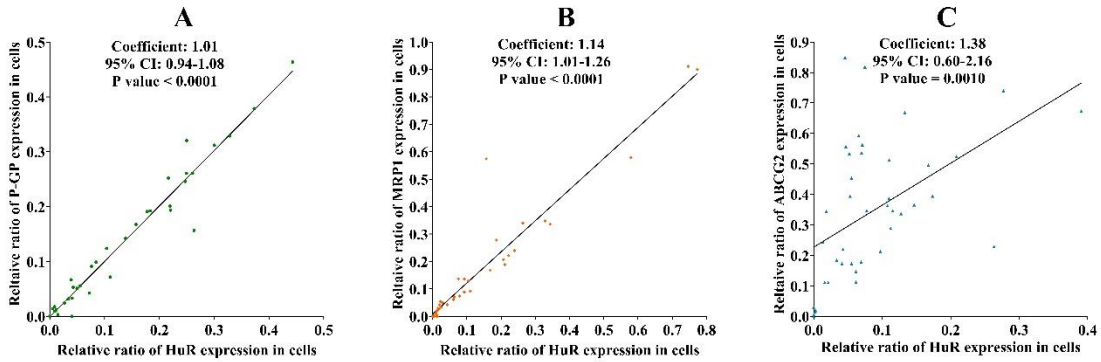

Figure 3.25: Correlation of individual ABC transporter and HuR expression in colorectal tissues. X-axis in (A), (B) and (C) denotes the relative ratio of HuR expression to total cells. Y-axis in (A), (B) and (C) denotes relative ratio of P-GP, MRP1 and ABCG2 expression to total cells, respectively. The slopes indicate the linear relationship between transporters and HuR expression. Simple linear regression analysis was performed to identify the relationships.

The variations of ABC transporters and HuR co-expression across the colorectal chemoresistant and adjacent control tissues are exhibited in Figure 3.26. Highest relative mean percentage was found for P-GP and HuR co-expression in the context of colorectal chemoresistant tissues (88.43%). However, in control tissues the percentage was 38.87% (P value < 0.0001). Slightly lower than the co-expression of P-GP and HuR, the average percentage was 84.46% in chemoresistant tissues for MRP1 and HuR co-expression. But the controls showed a mean relative percentage of 46.95% (P value = 0.0023). The average percentage of ABCG2 and HuR co-expression in CRC was 29.64% and 11.43% in chemoresistant and matched control tissues, respectively (P value < 0.0001). There was

no significant association between ABC transporters (P-GP, MRP1 and ABCG2) and HuR co-expression and ovarian cancer patient data (Table 3.14).

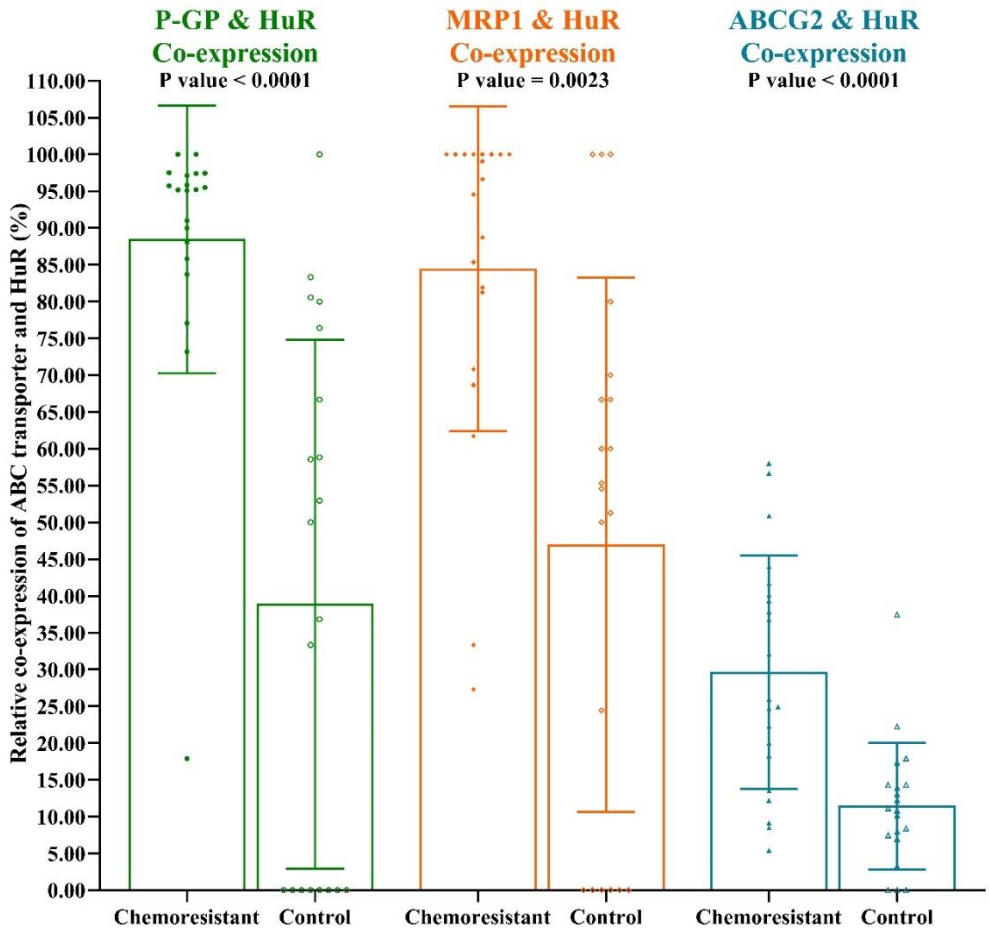

Figure 3.26: Comparison of ABC transporter and HuR co-expression in colorectal chemoresistant and adjacent control tissues. X-axis represents P-GP & HuR (green), MRP1 & HuR (orange) and ABCG2 & HuR (blue) co-expressions. Y-axis denotes the relative percentage of ABC transporter and HuR co-expression. Wilcoxon signed rank test for paired samples was conducted to validate the significance of differences for all types of co-expression.

Table 3.14: Association between ABC transporter and HuR co-expression and clinical features of chemoresistant CRC patients

Variables	Co_P-GP+HuR		Co_MRP1+HuR		Co_ABCG2+HuR	
	mean ± sd	**P value**	**mean ± sd**	**P value**	**mean ± sd**	**P value**
Age (correlation coefficient)	-0.04	0.868	-0.24	0.31	0.21	0.362
Sex						
Male	0.93 ± 0.07	0.588	0.85 ± 0.22	0.817	0.34 ± 0.14	0.165
Female	0.81 ± 0.29		0.84 ± 0.25		0.23 ± 0.17	
Diagnosis						
Adenocarcinoma	0.88 ± 0.18	NA	0.84 ± 0.22	NA	0.30 ± 0.16	NA
Differentiation						
Well	0.85 ± 0.24	0.421	0.79 ± 0.28	0.745	0.30 ± 0.18	0.721
Moderate	0.93 ± 0.08		0.90 ± 0.15		0.30 ± 0.11	
Poor	0.84 ± 0.16		0.85 ± 0.21		0.39 ± 0.24	
Grade						
I	0.85 ± 0.24	0.421	0.79 ± 0.28	0.745	0.30 ± 0.18	0.721
II	0.93 ± 0.08		0.90 ± 0.15		0.30 ± 0.11	
III	0.84 ± 0.16		0.85 ± 0.21		0.39 ± 0.24	
T staging						
1	0.96 ± 0.00	0.795	0.85 ± 0.00	0.276	0.38 ± 0.00	0.344
2	0.81 ± 0.29		0.88 ± 0.25		0.22 ± 0.14	
3	0.91 ± 0.08		0.79 ± 0.23		0.36 ± 0.16	
4	0.97 ± 0.00		1.00 ± 0.00		0.26 ± 0.00	
N staging						
0	0.95 ± 0.05	0.155	0.87 ± 0.14	0.911	0.37 ± 0.13	0.054
1	0.64 ± 0.41		0.78 ± 0.38		0.16 ± 0.07	
2	0.88 ± 0.10		0.79 ± 0.32		0.27 ± 0.19	

** Pearson's correlation coefficient, Spearman correlation, independent samples T-test, Mann–Whitney U test, ANOVA, Kruskal–Wallis test were conducted.*

3.6.3. ABC Transporters and HuR Co-expression in Chemoresistant Ovarian Cancer

The linear regression testing illustrates the connection between separate expressions of ABC drug transporters and HuR protein in ovarian tissues (Figure 3.27). Consistent with the patterns observed in Figures 3.23 and 3.25, it is evident that expression of HuR protein directly affects the levels of transporter protein expressions. A rise of one unit in HuR led to a corresponding upsurge of 1.06 units in P-GP (95% CI: 0.93-1.20) with a significant P value of < 0.0001 (Figure 3.27A). On the other hand, a one-fold rise in HuR expression boosted a MRP1 expression by 1.06-unit (95% CI: 0.95-1.16) (P value < 0.0001) (Figure 3.27B). Moreover, one-fold elevation of HuR induced 0.95-unit increase in ABCG2 expression (95% CI: 0.60-1.29) (P value of < 0.0001) (Figure 3.27C).

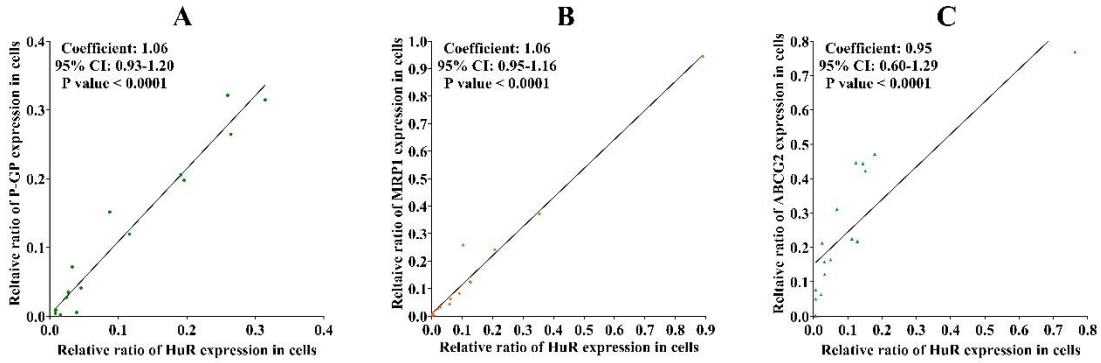

Figure 3.27: Correlation of individual ABC transporter and HuR expression in ovarian tissues. X-axis in (A), (B) and (C) denotes the relative ratio of HuR expression to total cells. Y-axis in (A), (B) and (C) denotes relative ratio of P-GP, MRP1 and ABCG2 expression to total cells, respectively. The slopes indicate the linear relationship between transporters and HuR expression. Simple linear regression analysis was performed to identify the relationships.

The differences of ABC transporters and HuR co-expression across the ovarian chemoresistant and paired control tissues are displayed in Figure 3.28. Only the difference of MRP1 and HuR co-expression between ovarian chemoresistant and control tissues was found significant (P value = 0.0156), where the average relative co-expression percentage was 86.58% and 43.09% in chemoresistant and control tissues, respectively. There was no significant association between ABC transporters (P-GP, MRP1 and ABCG2) and HuR co-expression and ovarian cancer patient data (Table 3.15).

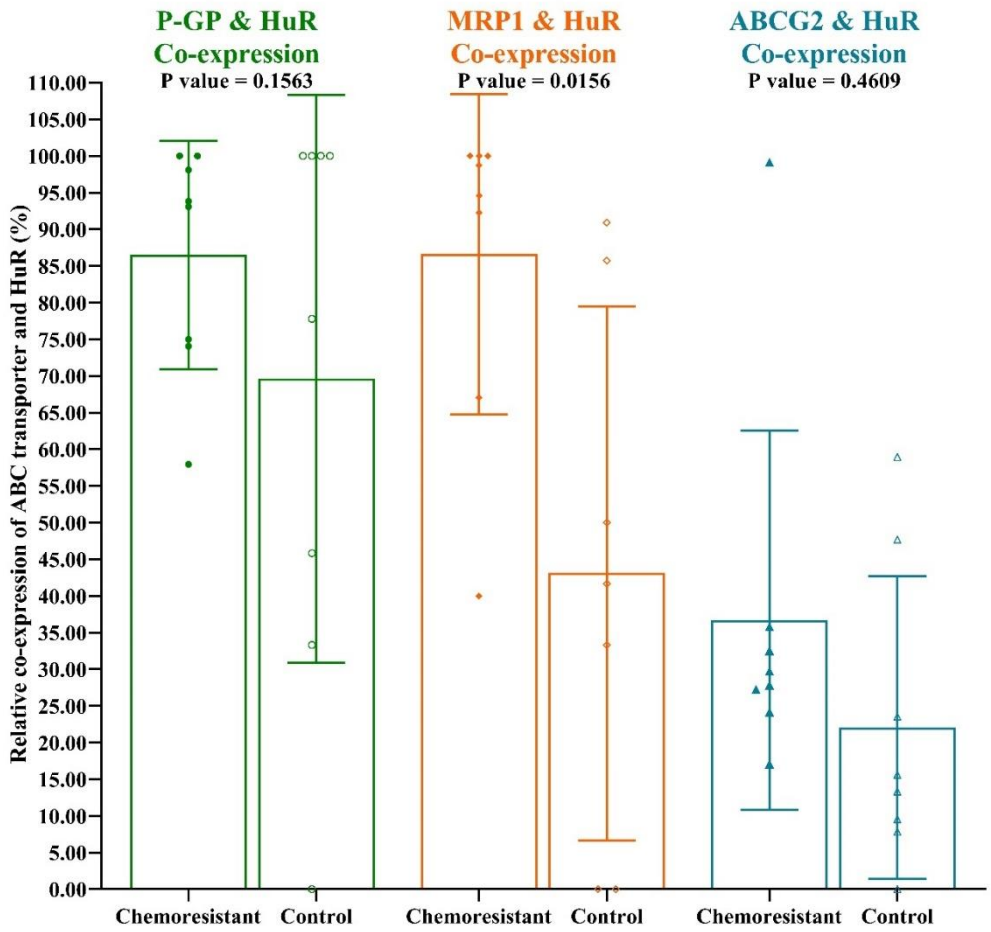

Figure 3.28: Comparison of ABC transporter and HuR co-expression in ovarian chemoresistant and adjacent control tissues. X-axis represents P-GP & HuR (green), MRP1 & HuR (orange) and ABCG2 & HuR (blue) co-expressions. Y-axis denotes the relative percentage of ABC transporter and HuR co-expression. Wilcoxon signed rank test for paired samples was conducted to validate the significance of differences for all types of co-expression.

Table 3.15: Association between ABC transporter and HuR co-expression and clinical features of chemoresistant ovarian cancer patients

Variables	Co_P-GP+HuR		Co_MRP1+HuR		Co_ABCG2+HuR	
	mean ± sd	**P value**	**mean ± sd**	**P value**	**mean ± sd**	**P value**
Age (correlation coefficient)	-0.07	0.866	0.49	0.22	0.55	0.16
Diagnosis						
Papillary serous carcinoma	0.86 ± 0.17	1	0.89 ± 0.22	0.5	0.38 ± 0.27	0.5
Squamous cell carcinoma	0.93 ± 0.00		0.67 ± 0.00		0.24 ± 0.00	
Differentiation						
Moderate	0.93 ± 0.00	1	0.67 ± 0.00	0.5	0.24 ± 0.00	0.5
Poor	0.86 ± 0.17		0.89 ± 0.22		0.38 ± 0.27	
Grade						
II	0.93 ± 0.00	1	0.67 ± 0.00	0.5	0.24 ± 0.00	0.5
III	0.86 ± 0.17		0.89 ± 0.22		0.38 ± 0.27	
T staging						
1	0.93 ± 0.00	1	0.67 ± 0.00	0.667	0.24 ± 0.00	0.667
3	0.85 ± 0.18		0.86 ± 0.26		0.28 ± 0.07	
N staging						
0	0.93 ± 0.00	1	0.67 ± 0.00	1	0.24 ± 0.00	1
1	0.84 ± 0.14		0.96 ± 0.05		0.22 ± 0.07	

** Spearman correlation, Mann–Whitney U test were conducted.*

3.6.4. 3D Modelling of HuR protein and its target binding site

The anticipated 3D structure of the HuR protein is presented in Figure 3.29A. The quality assessments of the protein model prediction are provided in Figures 3.29B, 3.29C and 3.29D. From the Ramachandran plot, it was observed that a total of 100.00% {most favored region (89.40%) + additional allowed region (9.90%) + generally allowed region (0.70%)} of the AA residues were in allowed region (Figure 3.29B). According to the validation methods, the HuR structure was considered satisfactory. AU-rich regions from 3'UTR of the mRNAs (Figure 3.30) were selected for molecular docking analyses with the predicted structure of HuR from Figure 3.29A.

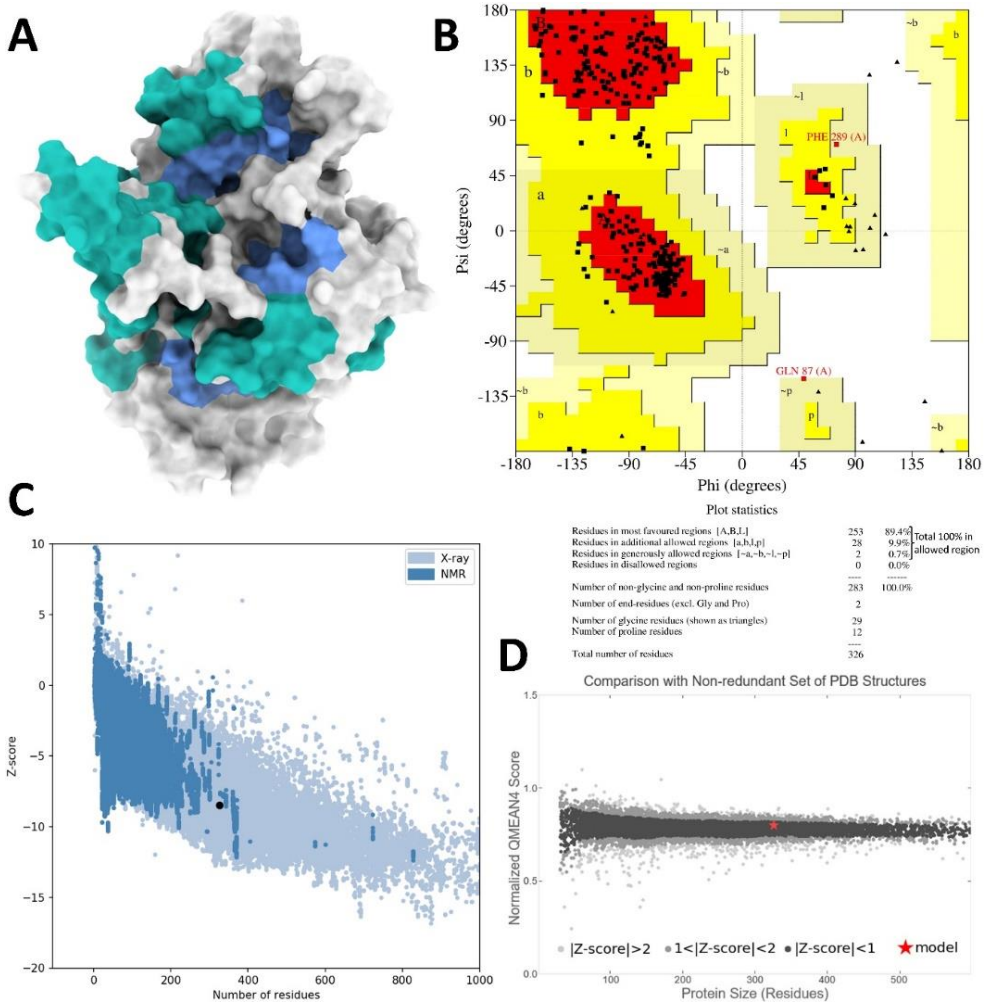

Figure 3.29: HuR protein structure prediction and validation. (A) Predicted structure of HuR protein. (B) Ramachandran plot for HuR protein. Percentages of residues in the allowed region and disallowed region were 100.0% and 0.0%, respectively. (C) Z-score plot for HuR protein. The black dot denotes the position of predicted model in the Z-score plot. (D) Q-mean score plot for HuR protein. The red star indicates the position of predicted model in the Q-mean score plot.

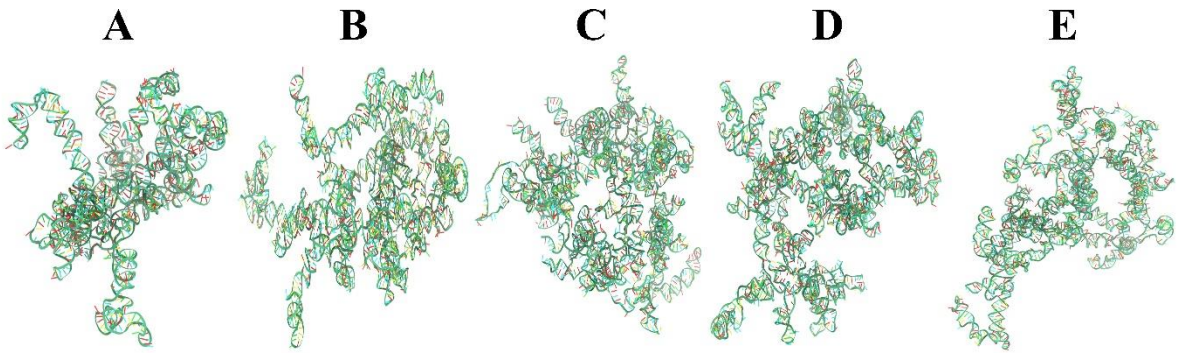

Figure 3.30: Predicted 3D structures of 3'UTR regions of ABC transporter mRNA. (A) 3'UTR of *P-GP* mRNA. (B) 3'UTR of *MRP1* mRNA. (C) 3'UTR of *ABCG2* TV1 mRNA. (D) 3'UTR of *ABCG2* TV2 mRNA. (E) 3'UTR of *ABCG2* TV3 mRNA.

3.6.5. Molecular docking between HuR and AU-rich regions from 3'UTR of ABC Transporter mRNA

Representative figures of docking simulations are presented in Figure 3.31A, 3.31B, 3.31C, 3.31D and 3.31E. Z-scores of molecular docking analyses between RRM1 of HuR protein and AU-rich regions from the 3'UTR of *P-GP*, *MRP1*, *ABCG2* TV1, *ABCG2* TV2 and *ABCG2* TV3 mRNA are exhibited in Tables 3.16, 3.17, 3.18, 3.19 and 3.20. RRM1 includes AA sequences of 18-99. It was noticed that all the Z-scores were negative. Interpretation method of Z-scores is previously described in section 3.5.5. All other information such as the Haddock score, cluster size, RMSD from the overall lowest-energy structure, Van der Waals energy, electrostatic energy, desolvation energy, restraints violation energy and buried surface area for all dockings are provided in Supplementary table 14, 15, 16, 17 and 18.

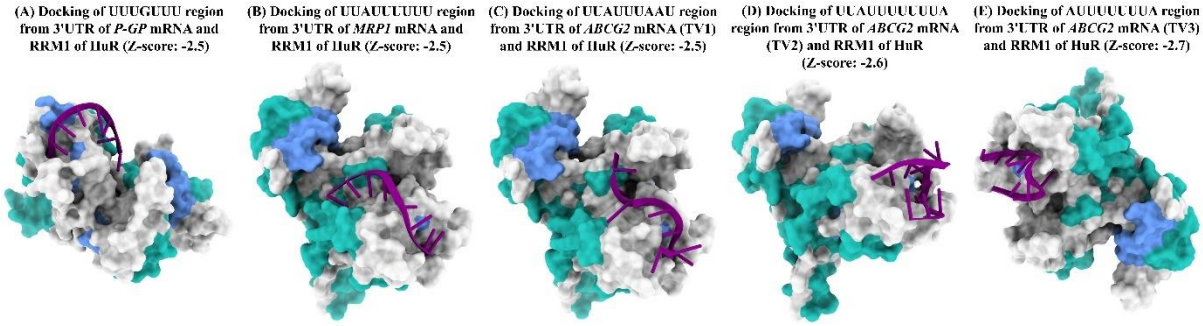

Figure 3.31: Molecular docking of RRM1 of HuR with AU-rich regions from 3'UTR of ABC transporters mRNA. (A) Representative docking of HuR RRM1 (AA region: 18-99) and UUUGUUU region from 3'UTR of *P-GP* mRNA (Z-score: -2.5) (More details are in Table 3.20). (B) Representative docking of HuR RRM1 (AA region: 18-99) and UUAUUUUUU region from 3'UTR of *MRP1* mRNA (Z-score: -2.5) (More details are in Table 3.21). (C) Representative docking of HuR RRM1 (AA region: 18-99) and UUAUUUAAU region from 3'UTR of *ABCG2* TV1 mRNA (Z-score: -2.5) (More details are in Table 3.22). (D) Representative docking of HuR RRM1 (AA region: 18-99) and UUAUUUUUUUA region from 3'UTR of *ABCG2* TV2 mRNA (Z-score: -2.6) (More details are in Table 3.23). (E) Representative docking of HuR RRM1 (AA region: 18-99) and AUUUUUUUA region from 3'UTR of *ABCG2* TV3 mRNA (Z-score: -2.7) (More details are in Table 3.24).

Table 3.16: Molecular docking of RRM1 of HuR protein and AU-rich region from the 3'UTR of *P-GP* mRNA and their Z-scores (More details are provided in Supplementary table 14)

AU-rich regions of 3'UTR	Z-Score
UUUGUUU	-2.5
AAAUUUUAUAA	-2.2
AUUUU	-2.2
AAAUUUUAU	-2.1
AUUUUAU	-1.9
AUUUA	-1.7
UUUUA	-1.7
GUUUG	-1.6
AAUUUUAUA	-1.5
AUAAAUUUUAUAA	-1.5
AUUUUAA	-1.5
UAAAUUUUAUA	-1.5
AUUAAA	-1.4
AAUUUUA	-1.3
UUUUU	-1.3
UUUUUAA	-1.2
AAUAAA	-0.9

Table 3.17: Molecular docking of RRM1 of HuR protein and AU-rich region from the 3'UTR of *MRP1* mRNA (More details are provided in Supplementary table 15)

AU-rich regions of 3'UTR	Z-Score
UUAUUUUUU	-2.5
UUUUUUUUUAA	-2.3
UUUUUUUUUUUAA	-2.3
UAUAUUUAUUU	-2.2
UUUUUUA	-2.2
AUUUU	-2.1
UAUUUUU	-2.1
UUUUUUUUUUUUA	-2.1
UUUUUUU	-2
UUUUUUUAA	-1.9
UUUUUUUUA	-1.9
AUUUUUU	-1.8
AUUUUUUUUUU	-1.8
UAUUUAU	-1.8
UUUUA	-1.8
UUUUU	-1.7
UUUUUAA	-1.7
UUUUUUUUUUA	-1.7
UUUUUUUUUUU	-1.7
AUAUAUUUAUUUU	-1.5
AUUUA	-1.4
AUUUUUUUU	-1.4
AUAUUUAUU	-1.2
AUUUUUUUUUUUU	-1.2
GUUUG	-1.2
UUUUUUUUU	-1.2

Table 3.18: Molecular docking of RRM1 of HuR protein and AU-rich region from the 3'UTR of *ABCG2* TV1 mRNA (More details are provided in Supplementary table 16)

AU-rich regions of 3'UTR	Z-Score
UUAUUUAAU	-2.5
UAAUUUAUU	-2.4
UUUUUUU	-2.3
AUAUUUUUA	-2.1
UAUUUAA	-2.1
AUUAUUUAAUA	-2
UUAAUUUUAUU	-2
UUUAAUUUUAUUU	-2
UUUUAUUUUUUUA	-2
UUAUUUUUUUA	-1.8
UUUAUUUUUUU	-1.8
UUUGUUU	-1.8
UUUUUAA	-1.8
UUUUUUA	-1.8
AUUUUAU	-1.7
GUUUG	-1.7
UUUUUUAAA	-1.7
AAUAAA	-1.6
AUUUUUU	-1.6
UUUUA	-1.6
AAUUUAU	-1.5
AUUAAA	-1.5
UAUUUUUAU	-1.5
UUUUU	-1.5
UUUUUAU	-1.5
AAUUUUA	-1.4
AUUUA	-1.4
AUUUUUUUA	-1.4
UAUUUUUUU	-1.4
AAUUUUAUU	-1.3
AUUUU	-1.3
UAAUUUUAUUU	-1.3
UUAAUUUUAUUUU	-1.3
AAUUUAA	-1.2
UAAUUUUAU	-1.2
UAUAUUUUUAU	-1.2
UAUUUUU	-1.2

UUAUUUUUU	-1.2
AUUUUUA	-1.1

Table 3.19: Molecular docking of RRM1 of HuR protein and AU-rich region from the 3'UTR of *ABCG2* TV2 mRNA (More details are provided in Supplementary table 17)

AU-rich regions of 3'UTR	**Z-Score**
UUAUUUUUUUA	-2.6
AAUUUUA	-2.3
UAUUUUU	-2.3
UUUGUUU	-2.3
UAUUUAA	-2.2
AUUUUAU	-2.1
UUUUU	-2.1
UUUUUUA	-2.1
UUUUUUAAA	-2.1
UUUUUUU	-2
AUUUUUA	-1.9
GUUUG	-1.9
UAUUUUUAU	-1.9
AUUUUUUUA	-1.8
UAAUUUUAUUU	-1.8
UAUAUUUUUAU	-1.8
UAUUUUUUU	-1.8
UUUUUAA	-1.8
AUUUU	-1.7
AUUUUUU	-1.7
UUAAUUUUAUU	-1.7
UUUAAUUUUAUUU	-1.7
AAUUUAU	-1.6
AUAUUUUUA	-1.6
AUUAUUUAAUA	-1.6
UUUUAUUUUUUUA	-1.6
UUUUUAU	-1.6
AAUUUAA	-1.5
UAAUUUUAU	-1.5
UUAUUUUUU	-1.5
AAUAAA	-1.4
UUAAUUUUAUUUU	-1.4
UUAUUUAAU	-1.4
AUUAAA	-1.3

AUUUA	-1.3
UAAUUUAUU	-1.3
UUUAUUUUUUU	-1.2
AAUUUUAUU	-1.1
UUUUA	-1

Table 3.20: Molecular docking of RRM1 of HuR protein and AU-rich region from the 3'UTR of *ABCG2* TV3 mRNA (More details are provided in Supplementary table 18)

AU-rich regions of 3'UTR	**Z-Score**
AUUUUUUUA	-2.7
UUUUAUUUUUUUA	-2.6
AAUUUUA	-2.4
UAUUUUUUU	-2.4
UUAAUUUUAUUUU	-2.4
UUAAUUUUAUU	-2.3
UUUAUUUUUUU	-2.3
UUUUUAA	-2.2
AUUUUUU	-2.1
GUUUG	-2.1
UAAUUUUAU	-2.1
AUUAUUUAAUA	-2
UAAUUUUAUUU	-2
UUUGUUU	-2
UUUUUUA	-2
UUAUUUUUUUA	-1.9
UUUUU	-1.9
AAUUUAU	-1.8
AUUUUAU	-1.8
AUUUUUA	-1.8
UAAUUUAUU	-1.8
UUUUUUU	-1.8
AAUAAA	-1.7
AAUUUAA	-1.7
AUUAAA	-1.7
UUAUUUUUU	-1.7
UUUAAUUUUAUUU	-1.7
UUUUUAU	-1.7
AAUUUUAUU	-1.5
AUAUUUUUA	-1.5
AUUUU	-1.5
UAUAUUUUUAU	-1.5
UAUUUAA	-1.5
UAUUUUUAU	-1.5
UUAUUUAAU	-1.5
UAUUUUU	-1.4
UUUUA	-1.3
AUUUA	-1.2
UUUUUUAAA	-1

Chapter 4

Discussion

4.1. ABC transporters in Chemoresistant Breast, Colorectal and Ovarian Cancer

Chemoresistance, by reducing the survival rate, poses one of the significant challenges in the treatment of advanced cancer patients undergoing chemotherapy [261]. There are a multitude of molecular mechanisms connected to this phenomenon [10,262]. Among those mechanisms, diminished intracellular accumulation of drugs has been a prominent contributor to developing anti-cancer drug resistance [262]. The cell membrane transporters facilitate the diminution of drug accumulation inside cells; thus, creating chemoresistance to commonly employed chemotherapeutic agents [263]. ABC transporters are the most eminent transmembrane protein group in actively ejecting various structurally and mechanistically distinct chemotherapeutic agents outside cells [47]. Thereby protecting the cells from being destroyed. While this protein superfamily comprises 49 members, only three – P-GP, MRP1 and ABCG2– have been extensively causing multidrug resistance [4,10]. These three proteins are also the most studied ones and they exhibit broad and overlapping substrate specificity, promoting the elimination of various hydrophobic compounds, that includes key anti-cancer therapeutics like taxanes, topoisomerase inhibitors and antimetabolites [10]. Previously, one study from Japan also revealed the differences of ABCG2 dysfunction among three different ethnic groups including Japanese, Caucasians and African Americans [264]. Additionally, ABC transporter population specific variations have been stated to contribute to their functions and the chemotherapeutic regimens [265]. Despite worldwide research on ABC transporter overexpression in chemoresistant cancers, to the best of our knowledge, there is a notable gap in Bangladesh while addressing this critical issue. In an effort to fill this void, this study aimed at delineating the expression patterns of P-GP, MRP1 and ABCG2 in chemoresistant breast, colorectal and ovarian cancers among the Bangladeshi population.

For breast, colorectal and ovarian cancers, findings of this study indicate that there was a substantial overexpression of P-GP, MRP1 and ABCG2 proteins in chemoresistant tissues than the corresponding control tissues. Higher P-GP expression has already been linked to increased rates of cancer recurrence, diminished survival rates and chemoresistance [266–268], which is consistent to the results of this experiment. P-GP was revealed to be overexpressing by 11-, 4.4- and 7.7-fold in breast, colorectal and ovarian chemoresistant

tissues, respectively, in comparison to matched controls (Figure 3.2, 3.4, 3.6). This ATP-driven transporter relies on energy and operates by binding hydrophobic drug substrates (which can be either neutral or positively charged) within the transmembrane regions [8,269]. These substrates are possibly introduced to the transporter directly from the lipid bilayer [8]. Many previous studies also established the connection of P-GP overexpression in developing chemoresistance in breast, colorectal and ovarian carcinomas. In triple-negative breast cancer (TNBC), a rise in P-GP expression after conventional chemotherapeutic treatment has been observed by Chevillard *et al* [95]. Also, by utilizing immunohistochemistry in breast cancer tissues, Kim *et al.* and Zhang *et al.* revealed an upswing in P-GP expression, particularly those with no pathological response after neoadjuvant chemotherapy [270,271]. In another study, the same transporter was found to be upregulated following preoperative chemotherapy for breast cancer [272]. Investigations have also shed light on the association between the AKT/PI3K signaling pathway and P-GP upregulation in CRC chemoresistance [273]. Reversal of oxaliplatin resistance in CRC was also verified upon suppressing P-GP [274]. In case of ovarian cancer, Penson *et al.* underscored the relationship between P-GP expression and paclitaxel dependent chemotherapy [99]. The role of P-GP in drug resistant ovarian cancer is substantiated with multiple evidences, which indicate that its overexpression leads to adverse prognosis for the patients and it also may appear as a predictive factor [275–279]. P-gp expression is regulated by a variety of biochemical pathways, including metabolic and signal transduction pathways such as COX-2 and NF-kB [280].

MRP1 is also a crucial drug resistance-associated ABC transporter. It was noted that MRP1 overexpressed by 9.4, 11.5 and 15.6 times more in breast, colorectal and ovarian chemoresistant tissues, respectively, than the corresponding control tissues (Figure 3.2, 3.4, 3.6). Aligning to the data from our study, similar Austrian experimental research showed that MRP1 caused resistance against cyclophosphamide, methotrexate and fluorouracil treatment in breast cancer patients [281]. Upregulation of this transporter in breast cancer tissues was also reported in a study by Chang *et al* [282]. On the contrary, some prior studies identified no association between MRP1 mRNA levels and CRC chemoresistance [283,284]. But experiments by Cao *et al.*, Ji *et al.* and Xing *et al.* support the outcome of our study and stated MRP1 overexpression as a poor prognostic marker for CRC [115,285,286]. Moreover, *MRP1* gene was found to be undergoing alternative

splicing at a higher rate in ovarian tumor tissues [287]. Other studies indicated that targeting *MRP1* with siRNA can increase paclitaxel-sensitization in chemoresistant ovarian cancer cells [89,288]. Clinical significance of MRP1 expression as a prognostic marker in patients with ovarian carcinoma is also reported in investigations [89,288]. Besides, MRP1 expression is regulated by oxidative stress [289].

ABCG2— in chemoresistant breast, colorectal and ovarian tissues— demonstrated overexpression levels of 2.2-, 1.5- and 4.-fold higher compared to their matched controls in this study (Figure 3.2, 3.4, 3.6). It operates as a half-transporter, thereby this protein engages in homodimerization or even oligomerization (pairing with another ABCG2) to achieve functionality [15,290]. Multiple previous research showed the relationship of ABCG2 efflux transporter in promoting chemotherapeutic drug resistance for patients with breast carcinoma [291,292]. One study suggested CD147 as a potential therapeutic target for reversing multidrug resistance facilitated by ABCG2 in breast cancer [293]. Another study indicated the involvement of ABCG2 in resistance to flavopiridol [134]. Concerning CRC cells, 5-fluorouracil (5-FU) treatment was found to induce the upregulation of miR-21, thus repressing PDCD4 and subsequently activating the JNK pathway, finally resulting in the overexpression of ABCG2 [294]. Further investigation in CRC cell lines uncovered that the crosstalk between miR-519c, HuR and 3'UTR of ABCG2 contributed to ABCG2 overexpression [244]. Besides, the upregulation of ABCG2 partially mediating NOS1-induced chemoresistance has been stated in a study by Li *et al* [295]. They implied the connection between ABCG2-associated cisplatin chemoresistance and NOS1 expression in ovarian carcinoma. Clinical trials have also demonstrated universal ABCG2 expression in primary or recurrent ovarian cancer patients [296]. Additionally, another study has attempted to overcome the topotecan-resistant ovarian carcinoma by utilizing ABCG2 antagonists to the cells [297]. ABCG2 expression is regulated by various transcription factors and signaling pathways such as Nrf2, ERK1/2 and Akt [298–300].

In this investigation of ABC drug transporter expression level in Bangladeshi population, it was observed that P-GP, MRP1 and ABCG2 notably co-expressed (but, not equally) in all the cases of three cancer types. Many previous research stated the common pathways shared by these ABC transporters. Among them, PXR, COX-2/NF-kB, and Wnt/β-catenin pathways are some of the key common regulatory mechanisms [301–303]. Therefore, we

suggest that combinatorial therapeutic approach to target all the key ABC transporters could lead to a better patient outcome. Results, as illustrated in Figures 3.3, 3.5 and 3.7, portray a constant scenario, where the overexpression of one efflux transporter corresponds to lesser expression of the others. The order of expression from highest to lowest was consistently ABCG2 > MRP1 > P-GP; a trend that aligns with the observations made by Bark *et al* [304]. ABCG2 consistently transcended P-GP and MRP1 in most chemoresistant tissue samples of breast, colorectal and ovarian cancer. The Nrf2 pathway plays a critical role in upregulating ABCG2 expression in cancer cells [298]. Nrf2 binds to antioxidant response elements in the promoter region of ABCG2, leading to its increased transcription and subsequent higher protein levels [298]. This pathway is often constitutively activated in chemoresistant cancers, contributing to the robust expression of ABCG2 compared to other transporters. In many cancers, particularly breast and ovarian cancers, ABCG2 is overexpressed more frequently than P-GP and MRP1 due to specific transcriptional regulators, oncogenic pathways and chemotherapeutic drug specificity which are commonly used for breast and ovarian cancers [295]. This opposite connection between P-GP and ABCG2 expression was further supported by a study, where defective P-GP was related to an increase in *ABCG2* mRNA at the mouse blood–brain barrier [305]. The phenomenon of MRP1 and P-GP having inverse relationship has also been documented in various reports [306–309]. Fascinatingly, it was also noted that ABCG2 demonstrated higher expression levels in adjacent tissues than the other two investigated ABC proteins, suggesting that the disparities in expression between chemoresistant and control tissues were more pronounced for P-GP and MRP1. These collective findings underscore the intricate dynamics of ABC transporter expression in different types of chemoresistant tissues and the multifaceted role of P-GP, MRP1 and ABCG2 in mediating chemoresistance across different cancer types. That also emphasizes the necessity of further exploring these connections to improve our understanding of resistance mechanisms and develop potential therapeutic strategies by targeting these transporters for cancer patients.

4.2. HIF1A in Chemoresistant Breast, Colorectal and Ovarian Cancer

Dysregulation of HIF1A expression is crucial in cancer biology that affects biological processes like tumor angiogenesis, invasion, energy metabolism and cell survival [185,186]. HIF1A, under hypoxic conditions, advances rapid accumulation and subsequent transactivation of various genes [188]. Additionally, heightened expression of this protein has been reported in diverse malignant tumors, spanning breast cancer, pancreatic carcinoma, renal cancer, ovarian, uterine and cervical carcinoma, colorectal and gastric cancer, prostate cancer and bladder cancer [185,190,192–196]. Although hypoxic cells demonstrate increased resistance to chemotherapy [310], there is a notable gap in research addressing hypoxia-mediated chemoresistance among Bangladeshi population. So, this study represents an initial exploration of HIF1A expression level in chemoresistant tissues collected from patients with breast, colorectal and ovarian carcinoma within the specific demographic of Bangladesh.

One mechanism behind chemoresistance is the inhibition of apoptosis [311]. To interrupt the apoptotic pathway, tumor hypoxia potentially overexpresses the antiapoptotic gene *Bcl2* and decrease drug sensitivity by upregulation of drug transporter proteins, therefore contributing to resistance against radio- and chemotherapy [312,313]. The *P-GP* gene was found to be hypoxia-responsive by Comerford *et al* [202]. In another study, researchers showed that inhibition of HIF-1A withdrew multidrug resistance in colon cancer cells by downregulating P-GP expression [201].

While examining breast, colorectal and ovarian cancers, the mean relative HIF1A expression in chemoresistant tissues were found to be significantly 8.9-, 3.8- and 5.6-times higher than in controls, respectively (Figure 3.9). One study concluded that hypoxia followed by extracellular matrix (ECM) stiffness suppresses miR-326, a tumor suppressor miRNA, in chemoresistant TNBC [314]. Notably, raised level of HIF1A was identified as predictive factor for endocrine therapy-resistance in breast cancer [315,316]. In the context of colon cancer, HIPK2, by preventing HIF1A to express, has been shown to re-establish the apoptosis-inducing capability of chemotherapy, thus sensitizing chemoresistant tumor cells [203]. In ovarian cancer, HIF1A-induced chemoresistance has been linked to oxidative stress responses of cells followed by cellular senescence [317].

Additionally, HIF1A triggering drug resistance in gastric and bladder malignancies has also been reported in previous studies [318,319].

The observed overexpression of HIF1A protein in chemoresistant tissues highlights its potential as a key player in chemoresistance mechanisms. Addressing these aspects could potentially pave the way for HIF1A-targeted therapeutic strategies aimed at overcoming chemoresistance and improving the efficacy of anti-cancer treatments in this population.

4.3. HuR in Chemoresistant Breast, Colorectal and Ovarian Cancer

By mRNA trafficking, stabilization and protein-translation enhancement, either cytoplasmic or nuclear overexpression of HuR plays a distinctive role in the expression of many cancer-associated molecules, thus contributing to carcinogenesis [217,223–225,320]. This also includes processes such as influencing immune evasion, cell proliferation, angiogenesis and cell survival [321]. Prior research underscored the substantial correlation between HuR expression level and adverse clinicopathological features, like advanced malignant stages, lymph node metastasis and poor survival rates that involves breast, lung, ovarian, colon, oral, gastric, renal and skin cancer [217,226,322,227–229,231–233,235,238]. Moreover, elevated HuR levels have been linked to multidrug resistant pancreatic, colorectal, breast, ovary and urinary cancer cells [223,225,241,242,323,324]. Multiple strategies had also been undertaken to suppress HuR in malignancy by inhibiting cytoplasmic translocation, using siRNAs in order to decrease expression, or impeding its binding to target mRNAs [325]. Diminished cytoplasmic expression of this protein was revealed to reverse therapeutic resistance to anti-cancer drugs in breast and ovarian cancers [326,327].

HuR overexpression, as a potential part of chemoresistance mechanism, has been assessed in various experiments. One of the mechanisms is HuR playing a protective role for tumor cells (under nutrient-deprived conditions) by regulating the isocitrate dehydrogenase 1 (IDH1) [328]. One study concluded that HuR knockdown, followed by the prevention of PIM1 posttranscriptional regulation, retreated hypoxia-induced resistance and enhanced sensitivity to oxaliplatin [328]. Additionally, chemotherapeutic agents such as oxaliplatin, cisplatin, gemcitabine, mitomycin C and carboplatin, as well as PARP inhibitor, can induce the HuR cytoplasmic accumulation [323,329]. In diverse experimental studies, application of HuR inhibitors with various chemotherapeutic agents proved to be essential in cancer treatment [330–334].

Wei *et al.* highlighted the critical role of HuR in fostering docetaxel resistance in TNBC, particularly through the post-transcriptional upregulation of *BCL2* and β-Catenin [335]. Inhibitiion of HuR cytoplasmic localization through JNK inactivation was also found to be a potential novel therapeutic strategy for breast cancer treatment [326]. In the context of CRC, an investigation identified that HuR impacts chemotherapeutic sensitivity by

inhibiting the IRES-dependent translation of caspase-2, obstructing miR-519c by modulating the miR-519c-HuR-ABCG2 pathway, upregulating galectin-3 signaling and multidrug resistance transporters, or binding to the 3'UTR of *CDC6,* followed by its upregulation [244,324,336,337]. In this study, the expression level of HuR in drug resistant breast, colorectal and ovarian cancers was examined. We detected a substantial increase of HuR expression in chemoresistant tissues (19.2-, 5.3- and 7.2-fold higher) compared to the controls (Figure 3.11). In addition, ursolic acid has been identified as an agent which promotes the translocation of HuR protein from cytoplasm to nucleus, therefore lowers MDR1 mRNA stability and accordingly reduces MDR1 expression in ovarian cancer cells [327].

HuR protein elevation in drug resistant tissues emphasizes its function as a significant factor to chemoresistance mechanisms in various types of malignancies. Delving into this intricacy holds the potential to lay the groundwork for additional clinical studies targeting HuR to conquer over multidrug resistance in this particular population.

4.4. ABC transporters and HIF1A co-expression in Chemoresistant Breast, Colorectal and Ovarian Cancer

Many scientific studies have recognized the individual links of ABC efflux transporters and HIF1A in multidrug resistance across several cancers [203,263,314,315,317]. But the precise nature of HIF1A in ABC transporter-mediated chemoresistance mechanism remains largely elusive. Addressing this issue, the current study aims to unravel the co-expression patterns between the transporters and HIF1A in the context of chemoresistant breast, colorectal and ovarian cancers.

Through immunofluorescence staining in chemoresistant breast, colorectal and ovarian tissues, the co-expression patterns of these transporters and HIF1A were observed. Intriguingly, concurrent co-expression of HIF1A and all three transporters was noted in the chemoresistant tissues for the patients in all cancers. Findings from this study also indicate that HIF1A expression linearly increases the expressions of P-GP, MRP1 and ABCG2 proteins (Figure 3.13, 3.15, 3.17). In this study, P-GP and HIF1A co-expressed approximately 10 times higher in chemoresistant breast tissues than the controls (Figure 3.14). Similar overexpression trends were seen in case of CRC and ovarian cancer by 2.5- and 1.5-times (Figure 3.16, 3.18). These findings aligned with some previous research stated below: Under hypoxic conditions, both HIF1A and *P-GP* mRNAs exhibit a substantial rise compared to normoxia across the same cell populations [338]. On the other hand, HIF1A protein was also found to be binding to the *P-GP* gene promoter under normoxic conditions [201]. Another study reported the hypoxia responsiveness of the *ABCB1* gene [202]. Moreover, overexpression of HIPK2 has been observed to diminish HIF1 transcriptional activity which resulted in P-GP abolition and adverse drug reaction induced apoptosis [203].

Similar to P-GP and HIF1A co-expression, MRP1 and HIF1A also showed higher co-expression level in chemoresistant tissues, which was about 9 folds higher for the breast tissues, 2-fold higher for the colorectal tissues and 1.6-fold higher for the ovarian tissues (Figure 3.14, 3.16, 3.18). Like P-GP, MRP1 was also documented as a drug resistance protein associated with hypoxia [339,340]. Also, inhibition of HIF1A by means of siRNA and dominant-negative HIF1A, has been demonstrated to drive MRP1 expression down

[341]. Furthermore, study by Chen et al. proved that HIF1A suppression can decrease MRP1-regulated drug resistance in lung and liver carcinomas [201].

In case of co-expression concerning ABCG2 and HIF1A in chemoresistant breast cancer and CRC, the overexpression followed the same trend as P-GP & HIF1A and MRP1 & HIF1A co-expressions. Throughout the drug-resistant tissues, the co-expression levels were 15.3- (breast cancer) and 1.7-fold (CRC) higher than the adjacent control tissues (Figure 3.14, 3.16). This relation of HIF1A regulating the transcription of *ABCG2* mRNA was first addressed by Krishnamurthy *et al.* in 2004 [126]. They reported that HIF1A binds with the hypoxia response element (HRE) in the ABCG2 promoter region under hypoxic conditions. Another research revealed that activation of HIF1A stimulates the ERK1/2/HIF1A that translocate the ABCG2 efflux pump from the cytoplasm to the cell membrane [342].

After analyzing the co-expression patterns, our aim was to investigate the interplay between HIF1A and ABC transporters. By binding to the 'CGTG' region of the promoter sequence of a gene, HIF1A exerts its influence in transcription induction [343,344]. Through bioinformatic analysis, the 'CGTG' sequences were found within -2000bp before 5' end for *P-GP* and *MRP1*, whereas -6500bp for *ABCG2*, respectively. Molecular docking analyses of these regions with HIF1A helped us discern their binding capabilities. Interestingly, all the Z-scores derived from the docking experiments were highly negative (Table 3.12), supporting the proposition that HIF1A potentially promotes the transcription of all the three selected ABC transporters via binding with this region.

By examining the linear associations of individual expressions (Figure 3.13, 3.15, 3.17), the co-expression patterns (Figure 3.14, 3.16, 3.18) and the molecular docking analyses (Table 3.12) between the transporters and HIF1A, we propose that HIF1A directly regulates the transcription of key efflux pumps (P-GP, MRP1 and ABCG2) possibly by binding to the 'CGTG' sequence upstream the promoter regions of their respective genes. Interestingly, P-GP and MRP1 demonstrated almost comparable co-expression levels with HIF1A, surpassing that of ABCG2. This discrepancy may be attributed to the proximity of the 'CGTG' sequence in the promoter regions, situated within 2000 bp for *P-GP* and 1000 bp for *MRP1*, while ranging to 6500 bp for *ABCG2*. Findings of this study also suggest that HIF1A could enhance the transcription of all three transporters concurrently for the same patients, potentially leading to a poorer prognosis. Therefore,

inhibition of HIF1A from binding to the ‘CGTG’ region of ABC efflux pump promoters could drastically reverse chemoresistance mechanisms.

4.5. ABC transporters and HuR co-expression in Chemoresistant Breast, Colorectal and Ovarian Cancer

Several studies have described the correlation between the cytoplasmic localization of HuR and the prevalence of post-chemotherapeutic multidrug resistance in various cancer cells, thereby causing poor prognosis [225,241,242]. The role of HuR in cancers is encoding a multitude of proto-oncogenes, consisting of cytokines, cell cycle regulators, invasion factors, chemokines, growth factors and proinflammatory factors [217,345]. While researchers are still investigating the concurrent upregulation of HuR and ABC efflux pumps in chemoresistance [40,225,243,244], the details of intrinsic mechanism of this remain somewhat elusive. Thus, more comprehensive research is needed to unravel the precise association between these two protein types. This study intends to elucidate the potential role of HuR on the overexpression of drug transporters (P-GP, MRP1 and ABCG2), offering a better insight into the mechanisms of chemoresistance.

To delve deeper into this mechanism, immunofluorescence staining was conducted on chemoresistant breast, colorectal and ovarian tissues which revealed distinct co-expression patterns of these drug transporters and HuR. Interestingly, we noticed that HuR and all three transporters concomitantly co-expressed in the same chemoresistant tissues across different cancers. Our findings also point to a linear correlation between these two types of proteins, indicating that elevated HuR expression corresponds to increased levels of P-GP, MRP1 and ABCG2 proteins (Figure 3.23, 3.25, 3.27).

Breast cancer tissues revealed a mean relative percentage 10.4 times greater in chemoresistant samples compared to paired controls for P-GP and HuR co-expression (Figure 3.24). Whereas CRC chemoresistant tissues exhibited 2.3 times upsurge in P-GP and HuR co-expression (Figure 3.26). Notably, the association between cytoplasmic expression of HuR expression and P-GP overexpression implies that HuR may exert regulatory control over multidrug resistance genes, suggesting a new mechanism influencing therapeutic sensitivity of cancer cells [225]. In a recent study, Gong *et al.* assumed HuR expression as a newfound factor affecting the efficacy of chemotherapy in NSCLC [243]. They asserted that direct and particular binding of FENDRR toward the 3'UTR of *P-GP* inhibits the binding of HuR to *P-GP* 3'UTR, resulting in a decline in the translation of this transporter.

A study concluded that HuR potentially have control over the galectin-3 signaling pathway, that orchestrates the sequential transcriptional expressions of diverse array of genes including *galectin-3*, *β-catenin*, *cyclin D1*, *Bcl-2*, *c-Myc*, *P-GP* and *MRP* [337]. According to the findings of this study, MRP1 and HuR co-expression was 11.5 times higher in breast cancer chemoresistant tissues compared to control tissues (Figure 3.24). Similarly, CRC and ovarian cancer chemoresistant tissues also demonstrated increase (1.8- and 2-times, respectively) in MRP1 and HuR co-expression compared to controls (Figure 3.26, 3.28).

In breast cancer and CRC cells, ABCG2 and HuR co-expressed nearly 52.2 times and 2.6 times higher, respectively in chemoresistant tissues compared to controls (Figure 3.24, 3.26). Supporting these findings, a study by To *et al.* demonstrated that the heightened ABCG2 expression in CRC tumors coincided with the decreased levels of miR-519c and increased levels of HuR [244]. miR-519c can target both HuR and ABCG2. So, the overexpression of ABCG2 was assumed to be triggered by the interplay of HuR, miR-519c and the 3'UTR of ABCG2 [244]. They also stated HuR as a potential drug target for ABCG2-modulated chemoresistance in CRC.

After investigating the co-expression profiles, our goal was to explore the relationship between HuR and ABC transporters. By typically binding to the ARE sequence positioned in the 3'UTR of the target mRNAs, HuR protein enhance the posttranscriptional stability. As RRM1 recognizes hairpin-loops of AREs in target mRNAs [210], we simulated molecular docking of HuR RRM1 with the ARE sequqnces in the 3'UTRs of the selected three transporter mRNAs. We observed that all the Z-scores were consistently negative (Table 3.16, 3.17, 3.18, 3.19, 3.20). This bioinformatic investigation suggests that HuR may facilitate the stability of ABC transporter mRNAs, consequently contributing to efflux pump-induced chemoresistance.

Through scrutinizing linear connections among individual expressions (Figure 3.23, 3.25, 3.27), co-expression patterns (Figure 3.24, 3.26, 3.28) and molecular docking analyses (Table 3.16, 3.17, 3.18, 3.19, 3.20) between transporters (P-GP, MRP1 and ABCG2) and HuR, we postulate that HuR directly regulates the posttranscriptional mRNA stabilization of crucial efflux pumps by linking to the AREs located in the 3'UTR regions of their respective mRNAs during cancer state, helping the efflux pumps overexpress, thus resulting in chemoresistance. As per our results, P-GP and MRP1 also showed nearly

equivalent co-expression levels with HuR, exceeding those of ABCG2. Findings from this study further suggest that HuR has the capacity to simultaneously enhance the mRNA-stabilization of all three transporters in the same patients, potentially leading to a less favorable prognosis. Accordingly, preventing HuR from binding to the AREs of ABC efflux pump 3'UTRs could substantially reverse resistance to chemotherapy.

Limitations:

Despite several strengths, there are also some limitations of this study. We collected a total of 57 (chemoresistant) and 57 (paired control) tissues regarding breast, colorectal and ovarian cancers. A larger sample size might provide better insight into the results. Due to resource limitations, laboratory experiments such as western blotting, immunoprecipitation and cell line analysis to determine the protein expressions could not be conducted. These experimental methods would have enhanced the strengths of the study.

Chapter 5

Conclusion

In the pursuit of focusing on the crucial gap in research on cancer chemoresistance in Bangladeshi population, this multifaceted study aimed to elucidate the intricate mechanisms behind therapeutic resistance in breast, colorectal and ovarian cancer. This investigation centered on the expression patterns and co-expression associations of key proteins (P-GP, MRP1, ABCG2, HIF1A and HuR) in chemoresistant tissues obtained from Bangladeshi cancer patients. The results revealed the persistent co-expression of P-GP, MRP1 and ABCG2 in all examined cases across the three cancer types, revealing a potential synergistic function in chemoresistance. Therefore, we propose a combinatorial therapeutic approach against these key ABC transporters to enhance treatment outcomes. Besides, ABCG2 consistently surpassed P-GP and MRP1 in expression levels, implying a complex interplay between these transporters in facilitating chemoresistance. The observed overexpression of HIF1A and HuR in chemoresistant tissues implicates their pivotal roles behind resistance mechanisms across various malignancies. We also propose that HIF1A directly regulates the transcription of key efflux pumps by binding to the ‘CGTG’ sequence in their promoter regions, while HuR facilitates posttranscriptional mRNA stabilization through interaction with AREs in the 3'UTR regions. Inhibition of HIF1A and HuR binding to these regulatory regions may appear as a promising avenue for reversing chemoresistance. This study contributes to the comprehension of complex dynamics of ABC transporter expression in chemoresistant tissues and emphasizes the need for targeted therapeutic strategies for improved treatment outcomes in Bangladeshi cancer patients. Lastly, the findings of this study provide a foundation for upcoming research endeavors focusing on the molecular intricacies of chemoresistance.

References

1. Rich JN, Bao S. Chemotherapy and Cancer Stem Cells. Vol. 1, Cell Stem Cell. 2007. p. 353–5.
2. Szakács G, Paterson JK, Ludwig JA, Booth-Genthe C, Gottesman MM. Targeting multidrug resistance in cancer. Vol. 5, Nature Reviews Drug Discovery. 2006. p. 219–34.
3. Nath SD, Shoily SS, Fatema K, Khan A, Mostafa MG, Sajib AA. Pan-cancer chemoresistance-associated genes, affected pathways and potential therapeutic targets. Hum Gene. 2023;35.
4. Gottesman MM, Fojo T, Bates SE. Multidrug resistance in cancer: Role of ATP-dependent transporters. Vol. 2, Nature Reviews Cancer. 2002. p. 48–58.
5. Corrie PG. Cytotoxic chemotherapy: clinical aspects. Vol. 36, Medicine. 2008. p. 24–8.
6. Krishna R, Mayer LD. Multidrug resistance (MDR) in cancerMechanisms, reversal using modulators of MDR and the role of MDR modulators in influencing the pharmacokinetics of anticancer drugs. Vol. 11, European Journal of Pharmaceutical Sciences. 2000. p. 265–83.
7. Zheng HC. The molecular mechanisms of chemoresistance in cancers. Vol. 8, Oncotarget. 2017. p. 59950–64.
8. Ambudkar S V., Dey S, Hrycyna CA, Ramachandra M, Pastan I, Gottesman MM. Biochemical, cellular, and pharmacological aspects of the multidrug transporter. Vol. 39, Annual Review of Pharmacology and Toxicology. 1999. p. 361–98.
9. Luqmani YA. Mechanisms of drug resistance in cancer chemotherapy. In: Medical Principles and Practice. 2005. p. 35–48.
10. Holohan C, Van Schaeybroeck S, Longley DB, Johnston PG. Cancer drug resistance: An evolving paradigm. Vol. 13, Nature Reviews Cancer. 2013. p. 714–26.
11. Swanton C. Intratumor heterogeneity: Evolution through space and time. Vol. 72, Cancer Research. 2012. p. 4875–82.
12. Lowe SW, Cepero E, Evan G. Intrinsic tumour suppression. Vol. 432, Nature. 2004. p. 307–15.
13. Chen WX, Liu XM, Lv MM, Chen L, Zhao JH, Zhong SL, Ji MH, Hu Q, Luo Z, Wu JZ, Tang JH. Exosomes from drug-resistant breast cancer cells transmit chemoresistance by a horizontal transfer of micrornas. PLoS One. 2014 Apr;9(4):e95240.
14. Fojo T, Bates S. Strategies for reversing drug resistance. Vol. 22, Oncogene. 2003. p. 7512–23.
15. Kachalaki S, Ebrahimi M, Mohamed Khosroshahi L, Mohammadinejad S, Baradaran B. Cancer chemoresistance; Biochemical and molecular aspects: A brief overview. Vol. 89, European Journal of Pharmaceutical Sciences. 2016. p. 20–30.
16. Lowe SW, Ruley HE, Jacks T, Housman DE. p53-dependent apoptosis modulates the cytotoxicity of anticancer agents. Cell. 1993;74(6):957–67.
17. Thomas H, Coley HM. Overcoming multidrug resistance in cancer: An update on the clinical strategy of inhibiting P-glycoprotein. Vol. 10, Cancer Control. 2003. p. 159–65.
18. Moscow JA, Cowan KH. Multidrug Resistance. JNCI J Natl Cancer Inst [Internet]. 1988;80(1):14–20. Available from: https://doi.org/10.1093/jnci/80.1.14
19. Longley DB, Johnston PG. Molecular mechanisms of drug resistance. J Pathol [Internet]. 2005;205(2):275–92. Available from: https://pathsocjournals.onlinelibrary.wiley.com/doi/abs/10.1002/path.1706
20. Andersen MH, Sørensen RB, Schrama D, Svane IM, Becker JC, Thor Straten P. Cancer treatment: The combination of vaccination with other therapies. Cancer Immunol Immunother. 2008;57(11):1735–43.
21. Martin HL, Smith L, Tomlinson DC. Multidrug-resistant breast cancer: Current perspectives. Vol. 6, Breast Cancer: Targets and Therapy. 2014. p. 1–13.

22. War AR. Curcumin Co-Treatment Sensitizes Multi-Drug Resistant Ht29 Colon Cancer Cell Line. J Cancer Res Immuno-Oncology. 2018;04(02).

23. Wang X, Zhang H, Chen X. Drug resistance and combating drug resistance in cancer. Vol. 2, Cancer Drug Resistance. 2019. p. 141–60.

24. Kim H, Kim K, No JH, Jeon YT, Jeon HW, Kim YB. Prognostic value of biomarkers related to drug resistance in patients with advanced epithelial ovarian cancer. Anticancer Res. 2012;32(2):589–94.

25. Uramoto H, Tanaka F. Recurrence after surgery in patients with NSCLC. Vol. 3, Translational Lung Cancer Research. 2014. p. 242–9.

26. Ferrone CR, Brennan MF, Gonen M, Coit DG, Fong Y, Chung S, Tang L, Klimstra D, Allen PJ. Pancreatic adenocarcinoma: The actual 5-year survivors. J Gastrointest Surg. 2008;12(4):701–6.

27. Ferrone CR, Pieretti-Vanmarcke R, Bloom JP, Zheng H, Szymonifka J, Wargo JA, Thayer SP, Lauwers GY, Deshpande V, Mino-Kenudson M, Fernández-Del Castillo C, Lillemoe KD, Warshaw AL. Pancreatic ductal adenocarcinoma: Long-term survival does not equal cure. Surg (United States). 2012;152(3):S43–9.

28. Fischer R, Breidert M, Keck T, Makowiec F, Lohrmann C, Harder J. Early recurrence of pancreatic cancer after resection and during adjuvant chemotherapy. Saudi J Gastroenterol. 2012;18(2):118–21.

29. Pattison S, Mitchell C, Lade S, Leong T, Busuttil RA, Boussioutas A. Early relapses after adjuvant chemotherapy suggests primary chemoresistance in diffuse gastric cancer. PLoS One. 2017;12(9):e0183891.

30. Uddin AFMK, Mahmud A, Islam J, Khan Z. Cancer care scenario in Bangladesh. South Asian J Cancer. 2013;2(2):102–4.

31. Noronha V, Tsomo U, Jamshed A, Hai MA, Wattegama S, Baral RP, Piya M, Prabhash K. A fresh look at oncology facts on south central Asia and SAARC countries. Vol. 1, South Asian Journal of Cancer. 2012. p. 01–4.

32. Zong L, Pi Z, Liu S, Liu Z, Song F. Metabolomics analysis of multidrug-resistant breast cancer cells: In vitro using methyl- tert -butyl ether method. RSC Adv. 2018;8(28):15831–41.

33. World Health Organization. Global Cancer Observatory [Internet]. [cited 2024 Mar 16]. Available from: https://gco.iarc.fr/en

34. Sung H, Ferlay J, Siegel RL, Laversanne M, Soerjomataram I, Jemal A, Bray F. Global Cancer Statistics 2020: GLOBOCAN Estimates of Incidence and Mortality Worldwide for 36 Cancers in 185 Countries. CA Cancer J Clin. 2021;71(3):209–49.

35. Shetty P. India faces growing breast cancer epidemic. Vol. 379, The Lancet. 2012. p. 992–3.

36. Hussain SMA. Comprehensive update on cancer scenario of Bangladesh. South Asian J Cancer. 2013;2(04):279–84.

37. Legrand N, Dixon DA, Sobolewski C. AU-rich element-binding proteins in colorectal cancer. Vol. 11, World Journal of Gastrointestinal Oncology. 2019. p. 71–90.

38. Takács D, Csonka Á, Horváth Á, Windt T, Gajdács M, Riedl Z, Hajós G, Amaral L, Molnár J, Spengler G. Reversal of ABCB1-related multidrug resistance of colonic adenocarcinoma cells by phenothiazines. Anticancer Res. 2015;35(6):3245–51.

39. Yuan Z, Shi X, Qiu Y, Jia T, Yuan X, Zou Y, Liu C, Yu H, Yuan Y, He X, Xu K, Yin P. Reversal of P-gp-mediated multidrug resistance in colon cancer by cinobufagin. Oncol Rep. 2017;37(3):1815–25.

40. Huang YH, Peng W, Furuuchi N, Gerhart J, Rhodes K, Mukherjee N, Jimbo M, Gonye GE, Brody JR, Getts RC, Sawicki JA. Delivery of Therapeutics Targeting the mRNA Binding Protein HuR Using 3DNA Nanocarriers Suppresses Ovarian Tumor Growth. Cancer Res. 2016;76(6):1549–59.

41. Ferlay J, Shin HR, Bray F, Forman D, Mathers C, Parkin DM. Estimates of worldwide burden of cancer in 2008: GLOBOCAN 2008. Int J Cancer. 2010;127(12):2893–917.

42. Sankaranarayanan R, Ferlay J. Worldwide burden of gynaecological cancer: The size of the problem. Vol. 20, Best Practice and Research: Clinical Obstetrics and Gynaecology. 2006. p. 207–25.

43. Zheng X, Andruska N, Lambrecht MJ, He S, Parissenti A, Hergenrother PJ, Nelson ER, Shapiro DJ. Targeting multidrug-resistant ovarian cancer through estrogen receptor a dependent ATP depletion caused by hyperactivation of the unfolded protein response. Oncotarget. 2018;9(19):14741–53.

44. Leslie EM, Deeley RG, Cole SPC. Multidrug resistance proteins: Role of P-glycoprotein, MRP1, MRP2, and BCRP (ABCG2) in tissue defense. Vol. 204, Toxicology and Applied Pharmacology. 2005. p. 216–37.

45. Ambudkar S V., Kimchi-Sarfaty C, Sauna ZE, Gottesman MM. P-glycoprotein: From genomics to mechanism. Vol. 22, Oncogene. 2003. p. 7468–85.

46. Cole SPC. Targeting multidrug resistance protein 1 (MRP1, ABCC1): Past, present, and future. Vol. 54, Annual Review of Pharmacology and Toxicology. 2014. p. 95–117.

47. Fletcher JI, Haber M, Henderson MJ, Norris MD. ABC transporters in cancer: More than just drug efflux pumps. Vol. 10, Nature Reviews Cancer. 2010. p. 147–56.

48. Dassa E, Bouige P. The ABC of ABCs: A phylogenetic and functional classification of ABC systems in living organisms. Vol. 152, Research in Microbiology. 2001. p. 211–29.

49. Choi CH. ABC transporters as multidrug resistance mechanisms and the development of chemosensitizers for their reversal. Vol. 5, Cancer Cell International. 2005. p. 1–13.

50. Löscher W, Potschka H. Role of multidrug transporters in pharmacoresistance to antiepileptic drugs. Vol. 301, Journal of Pharmacology and Experimental Therapeutics. 2002. p. 7–14.

51. Lu JF, Pokharel D, Bebawy M. MRP1 and its role in anticancer drug resistance. Vol. 47, Drug Metabolism Reviews. 2015. p. 406–19.

52. Walker JE, Saraste M, Runswick MJ, Gay NJ. Distantly related sequences in the alpha- and beta-subunits of ATP synthase, myosin, kinases and other ATP-requiring enzymes and a common nucleotide binding fold. EMBO J. 1982;1(8):945–51.

53. Smith PC, Karpowich N, Millen L, Moody JE, Rosen J, Thomas PJ, Hunt JF. ATP binding to the motor domain from an ABC transporter drives formation of a nucleotide sandwich dimer. Mol Cell. 2002;10(1):139–49.

54. Wikipedia TFE. ABC transporter [Internet]. [cited 2024 Sep 27]. Available from: https://en.wikipedia.org/wiki/ABC_transporter

55. Rees DC, Johnson E, Lewinson O. ABC transporters: The power to change. Vol. 10, Nature Reviews Molecular Cell Biology. 2009. p. 218–27.

56. Klein I, Sarkadi B, Váradi A. An inventory of the human ABC proteins. Vol. 1461, Biochimica et Biophysica Acta - Biomembranes. 1999. p. 237–62.

57. Mack JT, Brown CB, Tew KD. ABCA2 as a therapeutic target in cancer and nervous system disorders. Vol. 12, Expert Opinion on Therapeutic Targets. 2008. p. 491–504.

58. Aung T, Chapuy B, Vogel D, Wenzel D, Oppermann M, Lahmann M, Weinhage T, Menck K, Hupfeld T, Koch R, Trümper L, Wulf GG. Exosomal evasion of humoral immunotherapy in aggressive B-cell lymphoma modulated by ATP-binding cassette transporter A3. Proc Natl Acad Sci U S A. 2011;108(37):15336–41.

59. De Waard NE, Kolovou PE, McGuire SP, Cao J, Frank NY, Frank MH, Jager MJ, Ksander BR. Expression of Multidrug Resistance Transporter ABCB5 in a Murine Model of Human Conjunctival Melanoma. Vol. 1, Ocular Oncology and Pathology. 2015. p. 182–9.

60. Munoz M, Henderson M, Haber M, Norris M. Role of the MRP1/ABCC1 multidrug transporter protein in cancer. Vol. 59, IUBMB Life. 2007. p. 752–7.

61. Yamasaki M, Makino T, Masuzawa T, Kurokawa Y, Miyata H, Takiguchi S, Nakajima K, Fujiwara Y, Matsuura N, Mori M, Doki Y. Role of multidrug resistance protein 2 (MRP2) in chemoresistance and clinical outcome in oesophageal squamous cell carcinoma. Br J Cancer. 2011;104(4):707–13.

62. Scheffer GL, Kool M, de Haas M, de Vree JML, Pijnenborg ACLM, Bosman DK, Oude Elferink RPJ, Der Valk P Van, Borst P, Scheper RJ. Tissue distribution and induction of human multidrug resistant protein 3. Lab Investig. 2002;82(2):193–201.

63. Yang JY, Ha SA, Yang YS, Kim JW. P-Glycoprotein ABCB5 and YB-1 expression plays a role in increased heterogeneity of breast cancer cells: Correlations with cell fusion and doxorubicin resistance. BMC Cancer. 2010;10(388):1–10.

64. Oguri T, Ozasa H, Uemura T, Bessho Y, Miyazaki M, Maeno K, Maeda H, Sato S, Ueda R. MRP7/ABCC10 expression is a predictive biomarker for the resistance to paclitaxel in non-small cell lung cancer. Mol Cancer Ther. 2008;7(5):1150–5.

65. Natarajan K, Xie Y, Baer MR, Ross DD. Role of breast cancer resistance protein (BCRP/ABCG2) in cancer drug resistance. Vol. 83, Biochemical Pharmacology. 2012. p. 1084–103.

66. Katayama K, Noguchi K, Sugimoto Y. Regulations of P-Glycoprotein/ABCB1/ MDR1 in Human Cancer Cells. New J Sci. 2014;2014.

67. Januchowski R, Sterzyńska K, Zaorska K, Sosińska P, Klejewski A, Brązert M, Nowicki M, Zabel M. Analysis of MDR genes expression and cross-resistance in eight drug resistant ovarian cancer cell lines. J Ovarian Res. 2016;9(1):1–11.

68. Ye Q, Liu K, Shen Q, Li Q, Hao J, Han F, Jiang RW. Reversal of multidrug resistance in cancer by multi-functional flavonoids. Vol. 9, Frontiers in Oncology. 2019.

69. Wesołowska O, Wiśniewski J, Środa-Pomianek K, Bielawska-Pohl A, Paprocka M, Duś D, Duarte N, Ferreira MJU, Michalak K. Multidrug resistance reversal and apoptosis induction in human colon cancer cells by some flavonoids present in citrus plants. J Nat Prod. 2012;75(11):1896–902.

70. Kuo MT. Roles of multidrug resistance genes in breast cancer chemoresistance. Vol. 608, Advances in Experimental Medicine and Biology. 2007. p. 23–30.

71. Staud F, Pavek P. Breast cancer resistance protein (BCRP/ABCG2). Int J Biochem Cell Biol. 2005;37(4):720–5.

72. Gottesman MM, Pastan I. The multidrug transporter, a double-edged sword. Vol. 263, The Journal of biological chemistry. 1988. p. 12163–6.

73. Biedler JL, Riehm H. Cellular resistance to actinomycin D in Chinese hamster cells in vitro: cross-resistance, radioautographic, and cytogenetic studies. Cancer Res. 1970;30(4):1174–84.

74. Juliano RL, Ling V. A surface glycoprotein modulating drug permeability in Chinese hamster ovary cell mutants. BBA - Biomembr. 1976;455(1):152–62.

75. Ling V. Drug resistance and membrane alteration in mutants of mammalian cells. Can J Genet Cytol. 1975;17(4):503–15.

76. Jones PM, George AM. The ABC transporter structure and mechanism: Perspectives on recent research. Vol. 61, Cellular and Molecular Life Sciences. 2004. p. 682–99.

77. Rosenberg MF, Callaghan R, Ford RC, Higgins CF. Structure of the multidrug resistance p-glycoprotein to 2.5 nm resolution determined by electron microscopy and image analysis. J Biol Chem. 1997;272(16):10685–94.

78. Croop JM. P-glycoprotein structure and evolutionary homologies. Cytotechnology. 1993;12(1–3):1–32.

79. Chen C jie, Chin JE, Ueda K, Clark DP, Pastan I, Gottesman MM, Roninson IB. Internal

duplication and homology with bacterial transport proteins in the mdr1 (P-glycoprotein) gene from multidrug-resistant human cells. Cell. 1986;47(3):381–9.

80. Hodges LM, Markova SM, Chinn LW, Gow JM, Kroetz DL, Klein TE, Altman RB. Very important pharmacogene summary: ABCB1 (MDR1, P-glycoprotein). Pharmacogenet Genomics. 2011;21(3):152–61.

81. Li J, Jaimes KF, Aller SG. Refined structures of mouse P-glycoprotein. Protein Sci. 2014;23(1).

82. Senior AE, Bhagat S. P-glycoprotein shows strong catalytic cooperativity between the two nucleotide sites. Biochemistry. 1998;37(3):831–6.

83. Ramachandra M, Ambudkar S V., Chen D, Hrycyna CA, Dey S, Gottesman MM, Pastan I. Human P-glycoprotein exhibits reduced affinity for substrates during a catalytic transition state. Biochemistry. 1998;37(14):5010–9.

84. Sauna ZE, Ambudkar S V. Evidence for a requirement for ATP hydrolysis at two distinct steps during a single turnover of the catalytic cycle of human P-glycoprotein. Proc Natl Acad Sci U S A. 2000;97(6):2515–20.

85. Ueda K, Cardarelli C, Gottesman MM, Pastan T. Expression of a full-length cDNA for the human "MDR1" gene confers resistance to colchicine, doxorubicin, and vinblastine. Proc Natl Acad Sci U S A. 1987;84(9):3004–8.

86. Triller N, Korošec P, Kern I, Košnik M, Debeljak A. Multidrug resistance in small cell lung cancer: Expression of P-glycoprotein, multidrug resistance protein 1 and lung resistance protein in chemo-naive patients and in relapsed disease. Lung Cancer. 2006;54(2):235–40.

87. Szakács G, Annereau JP, Lababidi S, Shankavaram U, Arciello A, Bussey KJ, Reinhold W, Guo Y, Kruh GD, Reimers M, Weinstein JN, Gottesman MM. Predicting drug sensitivity and resistance: Profiling ABC transporter genes in cancer cells. Cancer Cell. 2004;6(2):129–37.

88. Baran Y, Gür B, Kaya P, Ural AU, Avcu F, Gündüz U. Upregulation of multi drug resistance genes in doxorubicin resistant human acute myelogeneous leukemia cells and reversal of the resistance. Hematology. 2007;12(6):511–7.

89. Duan Z, Brakora KA, Seiden M V. Inhibition of ABCB1 (MDR1) and ABCB4 (MDR3) expression by small interfering RNA and reversal resistance in human ovarian cancer cells. Mol Cancer Ther. 2004;3(7):833–8.

90. Lu C, Shervington A. Chemoresistance in gliomas. Mol Cell Biochem. 2008;312(1–2):71–80.

91. Takara K, Sakaeda T, Okumura K. An Update on Overcoming MDR1-Mediated Multidrug Resistance in Cancer Chemotherapy. Curr Pharm Des. 2005;12(3):273–86.

92. Cole SPC, Bhardwaj G, Gerlach JH, Mackie JE, Grant CE, Almquist KC, Stewart AJ, Kurz EU, Duncan AMV, Deeley RG. Overexpression of a transporter gene in a multidrug-resistant human lung cancer cell line. Science (80-). 1992;258(5088):1650–4.

93. Deeley RG, Cole SPC. Substrate recognition and transport by multidrug resistance protein 1 (ABCC1). Vol. 580, FEBS Letters. 2006. p. 1103–11.

94. Koh EH, Chung HC, Lee KB, Lim HY, Kim JH, Roh JK, Min JS, Lee KS, Kim BS. The value of immunohistochemical detection of P-glycoprotein in breast cancer before and after induction chemotherapy. Yonsei Med J. 1992;33(2):137–42.

95. Chevillard S, Pouillart P, Beldjord C, Asselain B, Beuzeboc P, Magdelénat H, Vielh P. Sequential assessment of multidrug resistance phenotype and measurement of S-phase fraction as predictive markers of breast cancer response to neoadjuvant chemotherapy. Cancer. 1996;77(2):292–300.

96. Mechetner E, Kyshtoobayeva A, Zonis S, Kim H, Stroup R, Garcia R, Parker RJ, Fruehauf JP. Levels of multidrug resistance (MDR1) P-glycoprotein expression by human breast cancer correlate with in vitro resistance to taxol and doxorubicin. Clin Cancer Res. 1998;4(2):389–98.

97. Kanzaki A, Toi M, Nakayama K, Bando H, Mutoh M, Uchida T, Fukumoto M, Takebayashi Y. Expression of multidrug resistance-related transporters in human breast carcinoma. Japanese J

Cancer Res. 2001;92(4):452–8.

98. Van Der Zee AGJ, Hollema H, Suurmeijer AJH, Krans M, Sluiter WJ, Willemse PHB, Aalders JG, De Vries EGE. Value of P-glycoprotein, glutathione S-transferase pi, c-erbB-2, and p53 as prognostic factors in ovarian carcinomas. J Clin Oncol. 1995;13(1):70–8.

99. Penson RT, Oliva E, Skates SJ, Glyptis T, Fuller AF, Goodman A, Seiden M V. Expression of multidrug resistance-1 protein inversely correlates with paclitaxel response and survival in ovarian cancer patients: A study in serial samples. Gynecol Oncol. 2004;93(1):98–106.

100. Baekelandt MM, Holm R, Nesland JM, Tropé CG, Kristensen GB. P-glycoprotein expression is a marker for chemotherapy resistance and prognosis in advanced ovarian cancer. Anticancer Res. 2000;20(2B):1061–7.

101. Linn SC, Giaccone G. MDR1/P-glycoprotein expression in colorectal cancer. Eur J Cancer. 1995;31(7–8):1291–4.

102. Slovak ML, Pelkey Ho J, Bhardwaj G, Kurz EU, Deeley RG, Cole SPC. Localization of a Novel Multidrug Resistance-associated Gene in the HT1080/DR4 and H69AR Human Tumor Cell Lines. Cancer Res. 1993;53(14):3221–5.

103. Hollenstein K, Dawson RJ, Locher KP. Structure and mechanism of ABC transporter proteins. Vol. 17, Current Opinion in Structural Biology. 2007. p. 412–8.

104. Johnson ZL, Chen J. Structural Basis of Substrate Recognition by the Multidrug Resistance Protein MRP1. Cell. 2017;168(6).

105. Chaptal V, Magnard S, Gueguen-Chaignon V, Falson P, Pietro A Di, Baubichon-Cortay H. Nucleotide-free Crystal Structure of Nucleotide-binding Domain 1 from Human ABCC1 Supports a 'General-Base Catalysis' Mechanism for ATP Hydrolysis. Biochem Pharmacol Open Access. 2014;3(6):1–4.

106. Manciu L, Chang XB, Buyse F, Hou YX, Gustot A, Riordani JR, Ruysschaert JM. Intermediate structural states involved in MRP1-mediated drug transport. Role of glutathione. J Biol Chem. 2003;278(5):3347–56.

107. Amram S, Ganoth A, Tichon O, Peer D, Nachliel E, Gutman M, Tsfadia Y. Structural Characterization of the Drug Translocation Path of MRP1/ABCC1. Isr J Chem. 2014;54(8–9):1382–93.

108. Zhou SF, Wang LL, Di Y, Xue C, Duan W, Li C, Li Y. Substrates and Inhibitors of Human Multidrug Resistance Associated Proteins and the Implications in Drug Development. Curr Med Chem. 2008;15(20):1981–2039.

109. Slot AJ, Molinski S V., Cole SPC. Mammalian multidrug-resistance proteins (MRPs). Essays Biochem. 2011;50(1):179–207.

110. Ni Z, Bikadi Z, F. Rosenberg M, Mao Q. Structure and Function of the Human Breast Cancer Resistance Protein (BCRP/ABCG2). Curr Drug Metab. 2010;11(7):603–17.

111. Loe DW, Deeley RG, Cole SPC. Characterization of vincristine transport by the M(r) 190,000 multidrug resistance protein (MRP): Evidence for cotransport with reduced glutathione. Cancer Res. 1998;58(22):5130–6.

112. Jedlitschky G, Leier I, Buchholz U, Barnouin K, Kurz G, Keppler D. Transport of glutathione, glucuronate, and sulfate conjugates by the MRP gene-encoded conjugate export pump. Cancer Res. 1996;56(5):988–94.

113. Müller M, Meijer C, Zaman GJR, Borst P, Scheper RJ, Mulder NH, De Vries EGE, Jansen PLM. Overexpression of the gene encoding the multidrug resistance-associated protein results in increased ATP-dependent glutathione S-conjugate transport. Proc Natl Acad Sci U S A. 1994;91(26):13033–7.

114. Deeley RG, Westlake C, Cole SPC. Transmembrane transport of endo- and xenobiotics by mammalian ATP-binding cassette multidrug resistance proteins. Vol. 86, Physiological Reviews.

2006. p. 849–99.

115. Cao D, Qin S, Mu Y, Zhong M. The role of MRP1 in the multidrug resistance of colorectal cancer. Oncol Lett. 2017;13(4):2471–6.

116. Tong X, Zhao J, Zhang Y, Mu P, Wang X. Expression levels of MRP1, GST-π, and GSK3B in ovarian cancer and the relationship with drug resistance and prognosis of patients. Oncol Lett. 2019;18(1):22–8.

117. Austin Doyle L, Yang W, Abruzzo L V., Krogmann T, Gao Y, Rishi AK, Ross DD. A multidrug resistance transporter from human MCF-7 breast cancer cells. Proc Natl Acad Sci U S A. 1998;95(26):15665–70.

118. Bates SE, Robey R, Miyake K, Rao K, Ross DD, Litman T. The role of half-transporters in multidrug resistance. J Bioenerg Biomembr. 2001;33(6):503–11.

119. Mao Q, Unadkat JD. Role of the Breast Cancer Resistance Protein (BCRP/ABCG2) in Drug Transport—an Update. AAPS J. 2015;17(1):65–82.

120. Robey RW, To KKK, Polgar O, Dohse M, Fetsch P, Dean M, Bates SE. ABCG2: A perspective. Vol. 61, Advanced Drug Delivery Reviews. 2009. p. 3–13.

121. Diestra JE, Scheffer GL, Català I, Maliepaard M, Schellens JHM, Scheper RJ, Germà-Lluch JR, Izquierdo MA. Frequent expression of the multi-drug resistance-associated protein BCRP/MXR/ABCP/ABCG2 in human tumours detected by the BXP-21 monoclonal antibody in paraffin-embedded material. J Pathol. 2002;198(2):213–9.

122. Gutmann H, Hruz P, Zimmermann C, Beglinger C, Drewe J. Distribution of breast cancer resistance protein (BCRP/ABCG2) mRNA expression along the human GI tract. Biochem Pharmacol. 2005;70(5):695–9.

123. Bailey-Dell KJ, Hassel B, Doyle LA, Ross DD. Promoter characterization and genomic organization of the human breast cancer resistance protein (ATP-binding cassette transporter G2) gene. Biochim Biophys Acta - Gene Struct Expr. 2001;1520(3):234–41.

124. Taylor NMI, Manolaridis I, Jackson SM, Kowal J, Stahlberg H, Locher KP. Structure of the human multidrug transporter ABCG2. Nature. 2017;546(7659).

125. Ee PLR, Kamalakaran S, Tonetti D, He X, Ross DD, Beck WT. Identification of a Novel Estrogen Response Element in the Breast Cancer Resistance Protein (ABCG2) Gene. Cancer Res. 2004;64(4):1247–51.

126. Krishnamurthy P, Ross DD, Nakanishi T, Bailey-Dell K, Zhou S, Mercer KE, Sarkadi B, Sorrentino BP, Schuetz JD. The stem cell marker Bcrp/ABCG2 enhances hypoxic cell survival through interactions with heme. J Biol Chem. 2004;279(23):24218–25.

127. Szatmari I, Vámosi G, Brazda P, Balint BL, Benko S, Széles L, Jeney V, Özvegy-Laczka C, Szántó A, Barta E, Balla J, Sarkadi B, Nagy L. Peroxisome proliferator-activated receptor γ-regulated ABCG2 expression confers cytoprotection to human dendritic cells. J Biol Chem. 2006;281(33):23812–23.

128. Nakanishi T, Bailey-Dell KJ, Hassel BA, Shiozawa K, Sullivan DM, Turner J, Ross DD. Novel 5′ untranslated region variants of BCRP mRNA are differentially expressed in drug-selected cancer cells and in normal human tissues: Implications for drug resistance, tissue-specific expression, and alternative promoter usage. Cancer Res. 2006;66(10):5007–11.

129. Khunweeraphong N, Stockner T, Kuchler K. The structure of the human ABC transporter ABCG2 reveals a novel mechanism for drug extrusion. Sci Rep. 2017;7(1):13767.

130. Polgar O, Robey RW, Bates SE. ABCG2: Structure, function and role in drug response. Vol. 4, Expert Opinion on Drug Metabolism and Toxicology. 2008. p. 1–15.

131. Kawabata S, Oka M, Shiozawa K, Tsukamoto K, Nakatomi K, Soda H, Fukuda M, Ikegami Y, Sugahara K, Yamada Y, Kamihira S, Doyle LA, Ross DD, Kohno S. Breast cancer resistance protein directly confers SN-38 resistance of lung cancer cells. Biochem Biophys Res Commun.

2001;280(5):1216–23.

132. Özvegy-Laczka C, Cserepes J, Elkind NB, Sarkadi B. Tyrosine kinase inhibitor resistance in cancer: Role of ABC multidrug transporters. Drug Resist Updat. 2005;8(1–2):15–26.

133. Maliepaard M, Van Gastelen MA, Tohgo A, Hausheer FH, Van Waardenburg RCAM, De Jong LA, Pluim D, Beijnen JH, Schellens JHM. Circumvention of breast cancer resistance protein (BCRP)-mediated resistance to camptothecins in vitro using non-substrate drugs or the BCRP inhibitor GF120918. Clin Cancer Res. 2001;7(4):935–41.

134. Robey RW, Medina-Peèrez WY, Nishiyama K, Lahusen T, Miyake K, Litman T, Senderowicz AM, Ross DD, Bates SE. Overexpression of the ATP-binding cassette half-transporter, ABCG2 (MXR/BCRP/ABCP1), in flavopiridol-resistant human breast cancer cells. Clin Cancer Res. 2001;7(1):145–52.

135. Honjo Y, Hrycyna CA, Yan QW, Medina-Pérez WY, Robey RW, Van de Laar A, Litman T, Dean M, Bates SE. Acquired mutations in the MXR/BCRP/ABCP gene alter substrate specificity in MXR/BCRP/ABCP-overexpressing cells. Cancer Res. 2001;61(18):6635–9.

136. Zhao R, Goldman ID. Resistance to antifolates. Vol. 22, Oncogene. 2003. p. 7431–57.

137. Yang JP, Liu Y, Zhong W, Yu D, Wen LJ, Jin CS. Chemoresistance of CD133+ cancer stem cells in laryngeal carcinoma. Chin Med J (Engl). 2011;124(7):1055–60.

138. Yajima T, Ochiai H, Uchiyama T, Takano N, Shibahara T, Azuma T. Resistance to cytotoxic chemotherapy-induced apoptosis in side population cells of human oral squamous cell carcinoma cell line Ho-1-N-1. Int J Oncol. 2009;35(2):273–80.

139. Chu TS, Chen JS, Lopez JP, Pardo FS, Aguilera J, Ongkeko WM. Imatinib-mediated inactivation of Akt regulates ABCG2 function in head and neck squamous cell carcinoma. Arch Otolaryngol - Head Neck Surg. 2008;134(9):979–84.

140. Nakanishi T, Chumsri S, Khakpour N, Brodie AH, Leyland-Jones B, Hamburger AW, Ross DD, Burger AM. Side-population cells in luminal-type breast cancer have tumour-initiating cell properties, and are regulated by HER2 expression and signalling. Br J Cancer. 2010;102(5):815–26.

141. Fang DD, Kim YJ, Lee CN, Aggarwal S, McKinnon K, Mesmer D, Norton J, Birse CE, He T, Ruben SM, Moore PA. Expansion of CD133+ colon cancer cultures retaining stem cell properties to enable cancer stem cell target discovery. Br J Cancer. 2010;102(8):1265–75.

142. Chikazawa N, Tanaka H, Tasaka T, Nakamura M, Tanaka M, Onishi H, Katano M. Inhibition of Wnt signaling pathway decreases chemotherapy-resistant side-population colon cancer cells. Anticancer Res. 2010;30(6):2041–8.

143. Hong Y Bin, Kang HJ, Kwon SY, Kim HJ, Kwon KY, Cho CH, Lee JM, Kallakury BVS, Bae I. Nuclear factor (Erythroid-Derived 2)-like 2 regulates drug resistance in pancreatic cancer cells. Pancreas. 2010;39(4):463–72.

144. Wang YH, Li F, Luo B, Wang XH, Sun HC, Liu S, Cui YQ, Xu XX. A side population of cells from a human pancreatic carcinoma cell line harbors cancer stem cell characteristics. Neoplasma. 2009;56(5):371–8.

145. Hu L, McArthur C, Jaffe RB. Ovarian cancer stem-like side-population cells are tumourigenic and chemoresistant. Br J Cancer. 2010;102(8):1276–83.

146. Adhikari AS, Agarwal N, Wood BM, Porretta C, Ruiz B, Pochampally RR, Iwakuma T. CD117 and Stro-1 identify osteosarcoma tumor-initiating cells associated with metastasis and drug resistance. Cancer Res. 2010;70(11):4602–12.

147. Di Fiore R, Santulli A, Drago Ferrante R, Giuliano M, De Blasio A, Messina C, Pirozzi G, Tirino V, Tesoriere G, Vento R. Identification and expansion of human osteosarcoma-cancer-stem cells by long-term 3-aminobenzamide treatment. J Cell Physiol. 2009;219(2):301–13.

148. Liu T, Xu F, Du X, Lai D, Liu T, Zhao Y, Huang Q, Jiang L, Huang W, Cheng W, Liu Z. Establishment and characterization of multi-drug resistant, prostate carcinoma-initiating stem-like

cells from human prostate cancer cell lines 22RV1. Mol Cell Biochem. 2010;340(1–2):265–73.

149. Ning ZF, Huang YJ, Lin TX, Zhou YX, Jiang C, Xu KW, Huang H, Yin XB, Huang J. Subpopulations of stem-like cells in side population cells from the human bladder transitional cell cancer cell line T24. J Int Med Res. 2009;37(3):621–30.

150. Mahller YY, Williams JP, Baird WH, Mitton B, Grossheim J, Saeki Y, Cancelas JA, Ratner N, Cripe TP. Neuroblastoma cell lines contain pluripotent tumor initiating cells that are susceptible to a targeted oncolytic virus. PLoS One. 2009;4(1):e4235.

151. Karin M. Too many transcription factors: Positive and negative interactions. Vol. 2, New Biologist. 1990. p. 126–31.

152. Latchman DS. Transcription factors: An overview. Int J Biochem Cell Biol. 1997;29(12):1305–12.

153. Fulton DL, Sundararajan S, Badis G, Hughes TR, Wasserman WW, Roach JC, Sladek R. TFCat: The curated catalog of mouse and human transcription factors. Genome Biol. 2009;10(3):1–14.

154. Vaquerizas JM, Kummerfeld SK, Teichmann SA, Luscombe NM. A census of human transcription factors: Function, expression and evolution. Vol. 10, Nature Reviews Genetics. 2009. p. 252–63.

155. Lambert SA, Jolma A, Campitelli LF, Das PK, Yin Y, Albu M, Chen X, Taipale J, Hughes TR, Weirauch MT. The Human Transcription Factors. Cell [Internet]. 2018;172(4):650–65. Available from: https://www.sciencedirect.com/science/article/pii/S0092867418301065

156. Babu MM, Luscombe NM, Aravind L, Gerstein M, Teichmann SA. Structure and evolution of transcriptional regulatory networks. Vol. 14, Current Opinion in Structural Biology. 2004. p. 283–91.

157. Gertz J, Reddy TE, Varley KE, Garabedian MJ, Myers RM. Genistein and bisphenol A exposure cause estrogen receptor 1 to bind thousands of sites in a cell type-specific manner. Genome Res. 2012;22(11):2153–62.

158. Wärnmark A, Treuter E, Wright APH, Gustafsson JÅ. Activation Functions 1 and 2 of Nuclear Receptors: Molecular Strategies for Transcriptional Activation. Vol. 17, Molecular Endocrinology. 2003. p. 1901–9.

159. Geertz M, Shore D, Maerkl SJ. Massively parallel measurements of molecular interaction kinetics on a microfluidic platform. Proc Natl Acad Sci U S A. 2012;109(41):16540–5.

160. Damante G, Fabbro D, Pellizzari L, Civitareale D, Guazzi S, Polycarpou-schwartz M, Cauci S, Quadrifoglio F, Formisano S, Di Lauro R. Sequence-specific DNA recognition by the thyroid transcription factor-1 homeodomain. Nucleic Acids Res. 1994;22(15):3075-3083.

161. Gill G. Regulation of the initiation of eukaryotic transcription. Essays Biochem. 2001;37:33–43.

162. Narlikar GJ, Fan HY, Kingston RE. Cooperation between complexes that regulate chromatin structure and transcription. Vol. 108, Cell. 2002. p. 475–87.

163. Lan X, Glass CK, Rosenfeld MG. Coactivator and corepressor complexes in nuclear receptor function. Curr Opin Genet Dev. 1999;9(2):140–7.

164. Lee TI, Young RA. Transcriptional regulation and its misregulation in disease. Vol. 152, Cell. 2013. p. 1237–51.

165. Fong AP, Tapscott SJ. Skeletal muscle programming and re-programming. Vol. 23, Current Opinion in Genetics and Development. 2013. p. 568–73.

166. Takahashi K, Yamanaka S. A decade of transcription factor-mediated reprogramming to pluripotency. Vol. 17, Nature Reviews Molecular Cell Biology. 2016. p. 183–93.

167. Lobe CG. Transcription Factors and Mammalian Development. Curr Top Dev Biol. 1992;27:351–83.

168. Pawson T. Signal transduction—a conserved pathway from the membrane to the nucleus. Vol. 14, Developmental Genetics. 1993. p. 333–8.

169. Wheaton K, Atadja P, Riabowol K. Regulation of transcription factor activity during cellular aging. Vol. 74, Biochemistry and Cell Biology. 1996. p. 523–34.

170. Meyyappan M, Atadja PW, Riabowol KT. Regulation of gene expression and transcription factor binding activity during cellular aging. NeuroSignals. 1996;5(3):130–8.

171. Vaupel P, Mayer A. Hypoxia in cancer: Significance and impact on clinical outcome. Vol. 26, Cancer and Metastasis Reviews. 2007. p. 225–39.

172. Cimmino F, Avitabile M, Lasorsa VA, Montella A, Pezone L, Cantalupo S, Visconte F, Corrias MV, Iolascon A, Capasso M. HIF-1 transcription activity: HIF1A driven response in normoxia and in hypoxia. BMC Med Genet. 2019;20(1):1–15.

173. Semenza GL. Regulation of mammalian O2 homeostasis by hypoxia-inducible factor 1. Vol. 15, Annual Review of Cell and Developmental Biology. 1999. p. 551–78.

174. Semenza GL. HIF-1: Mediator of physiological and pathophysiological responses to hypoxia. Vol. 88, Journal of Applied Physiology. 2000. p. 1474–80.

175. Jaakkola P, Mole DR, Tian YM, Wilson MI, Gielbert J, Gaskell SJ, Von Kriegsheim A, Hebestreit HF, Mukherji M, Schofield CJ, Maxwell PH, Pugh CW, Ratcliffe PJ. Targeting of HIF-α to the von Hippel-Lindau ubiquitylation complex by O2-regulated prolyl hydroxylation. Science (80-). 2001;292(5516):468–72.

176. Iyer N V., Kotch LE, Agani F, Leung SW, Laughner E, Wenger RH, Gassmann M, Gearhart JD, Lawler AM, Yu AY, Semenza GL. Cellular and developmental control of O2 homeostasis by hypoxia- inducible factor 1α. Genes Dev. 1998;12(2):149–62.

177. Semenza GL, Rue EA, Iyer N V., Pang MG, Kearns WG. Assignment of the hypoxia-inducible factor 1α gene to a region of conserved synteny on mouse chromosome 12 and human chromosome 14q. Genomics. 1996;34(3):437–9.

178. Hogenesch JB, Chan WK, Jackiw VH, Brown RC, Gu YZ, Pray-Grant M, Perdew GH, Bradfield CA. Characterization of a subset of the basic-helix-loop-helix-PAS superfamily that interacts with components of the dioxin signaling pathway. J Biol Chem. 1997;272(13):8581–93.

179. Wang FS, Wang CJ, Chen YJ, Chang PR, Huang YT, Sun YC, Huang HC, Yang YJ, Yang KD. Ras Induction of Superoxide Activates ERK-dependent Angiogenic Transcription Factor HIF-1α and VEGF-A Expression in Shock Wave-stimulated Osteoblasts. J Biol Chem. 2004;279(11):10331–7.

180. Bateman A, Martin MJ, Orchard S, Magrane M, Ahmad S, Alpi E, Bowler-Barnett EH, Britto R, Bye-A-Jee H, Cukura A, Denny P, Dogan T, Ebenezer TG, Fan J, Garmiri P, da Costa Gonzales LJ, Hatton-Ellis E, Hussein A, Ignatchenko A, Insana G, Ishtiaq R, Joshi V, Jyothi D, Kandasaamy S, Lock A, Luciani A, Lugaric M, Luo J, Lussi Y, MacDougall A, Madeira F, Mahmoudy M, Mishra A, Moulang K, Nightingale A, Pundir S, Qi G, Raj S, Raposo P, Rice DL, Saidi R, Santos R, Speretta E, Stephenson J, Totoo P, Turner E, Tyagi N, Vasudev P, Warner K, Watkins X, Zaru R, Zellner H, Bridge AJ, Aimo L, Argoud-Puy G, Auchincloss AH, Axelsen KB, Bansal P, Baratin D, Batista Neto TM, Blatter MC, Bolleman JT, Boutet E, Breuza L, Gil BC, Casals-Casas C, Echioukh KC, Coudert E, Cuche B, de Castro E, Estreicher A, Famiglietti ML, Feuermann M, Gasteiger E, Gaudet P, Gehant S, Gerritsen V, Gos A, Gruaz N, Hulo C, Hyka-Nouspikel N, Jungo F, Kerhornou A, Le Mercier P, Lieberherr D, Masson P, Morgat A, Muthukrishnan V, Paesano S, Pedruzzi I, Pilbout S, Pourcel L, Poux S, Pozzato M, Pruess M, Redaschi N, Rivoire C, Sigrist CJA, Sonesson K, Sundaram S, Wu CH, Arighi CN, Arminski L, Chen C, Chen Y, Huang H, Laiho K, McGarvey P, Natale DA, Ross K, Vinayaka CR, Wang Q, Wang Y, Zhang J. UniProt: the Universal Protein Knowledgebase in 2023. Nucleic Acids Res. 2023;51(D1):D523–31.

181. Wang GL, Jiang BH, Rue EA, Semenza GL. Hypoxia-inducible factor 1 is a basic-helix-loop-helix-PAS heterodimer regulated by cellular O2 tension. Proc Natl Acad Sci U S A. 1995;92(12):5510–4.

182. Jiang BH, Zheng JZ, Leung SW, Roe R, Semenza GL. Transactivation and inhibitory domains of Hypoxia-inducible factor 1α: Modulation of transcriptional activity by oxygen tension. J Biol Chem. 1997;272(31):19253–60.

183. Alves CC, Donadi EA, Giuliatti S. Structural characterization of the interaction of hypoxia inducible factor-1 with its hypoxia responsive element at the −964g > a variation site of the hla-g promoter region. Int J Mol Sci. 2021;22(23).

184. Thomlinson RH, Gray LH. The histological structure of some human lung cancers and the possible implications for radiotherapy. Br J Cancer. 1955;9(4):539–49.

185. Semenza GL. Targeting HIF-1 for cancer therapy. Vol. 3, Nature Reviews Cancer. 2003. p. 721–32.

186. Shan B, Gerez J, Haedo M, Fuertes M, Theodoropoulou M, Buchfelder M, Losa M, Stalla GK, Arzt E, Renner U. RSUME is implicated in HIF-1-induced VEGF-A production in pituitary tumour cells. Endocr Relat Cancer. 2012;19(1):13–27.

187. Bos R, Van der Groep P, Greijer AE, Shvarts A, Meijer S, Pinedo HM, Semenza GL, Van Diest PJ, Van der Wall E. Levels of hypoxia-inducible factor-1α independently predict prognosis in patients with lymph node negative breast carcinoma. Cancer. 2003;97(6):1573–81.

188. Jia X, Hong Q, Lei L, Li D, Li J, Mo M, Wang Y, Shao Z, Shen Z, Cheng J, Liu G. Basal and therapy-driven hypoxia-inducible factor-1α confers resistance to endocrine therapy in estrogen receptor-positive breast cancer. Oncotarget. 2015;6(11):8648–62.

189. Aebersold DM, Burri P, Beer KT, Laissue J, Djonov V, Greiner RH, Semenza GL. Expression of hypoxia-inducible factor-1alpha: a novel predictive and prognostic parameter in the radiotherapy of oropharyngeal cancer. Cancer Res. 2001 Apr;61(7):2911–6.

190. Höckel M, Vaupel P. Tumor hypoxia: Definitions and current clinical, biologic, and molecular aspects. Vol. 93, Journal of the National Cancer Institute. 2001. p. 266–76.

191. Dvorák K. [Intravenous systemic thrombolysis using streptokinase in the treatment of developing cardiogenic shock in myocardial infarct]. Vnitr Lek. 1990 May;36(5):426–34.

192. Birner P, Schindl M, Obermair A, Breitenecker G, Oberhuber G. Expression of hypoxia-inducible factor 1alpha in epithelial ovarian tumors: its impact on prognosis and on response to chemotherapy. Clin cancer Res an Off J Am Assoc Cancer Res. 2001 Jun;7(6):1661–8.

193. Ezzeddini R, Taghikhani M, Somi MH, Samadi N, Rasaee MJ. Clinical importance of FASN in relation to HIF-1α and SREBP-1c in gastric adenocarcinoma. Life Sci. 2019;224:169–76.

194. Ezzeddini R, Taghikhani M, Salek Farrokhi A, Somi MH, Samadi N, Esfahani A, Rasaee MJ. Downregulation of fatty acid oxidation by involvement of HIF-1α and PPARγ in human gastric adenocarcinoma and related clinical significance. J Physiol Biochem. 2021;77(2):249–60.

195. Talks KL, Turley H, Gatter KC, Maxwell PH, Pugh CW, Ratcliffe PJ, Harris AL. The expression and distribution of the hypoxia-inducible factors HIF-1α and HIF-2α in normal human tissues, cancers, and tumor-associated macrophages. Am J Pathol. 2000;157(2):411–21.

196. H. Z, A.M. DM, E. L, M. L, D.A. H, D. Z, P. B, W.B. I, G.L. S, J.W. S. Overexpression of hypoxia-inducible factor 1α in common human cancers and their metastases. Cancer Res. 1999;59(22):5830–5.

197. Semenza GL. Hypoxia-inducible factors: Mediators of cancer progression and targets for cancer therapy. Vol. 33, Trends in Pharmacological Sciences. 2012. p. 207–14.

198. Hayashi Y, Yokota A, Harada H, Huang G. Hypoxia/pseudohypoxia-mediated activation of hypoxia-inducible factor-1α in cancer. Vol. 110, Cancer Science. 2019. p. 1510–7.

199. Warburg O. On respiratory impairment in cancer cells. Science (80-). 1956;124(3215):269–70.

200. Nakano A, Tsuji D, Miki H, Cui Q, El Sayed SM, Ikegame A, Oda A, Amou H, Nakamura S, Harada T, Fujii S, Kagawa K, Takeuchi K, Sakai A, Ozaki S, Okano K, Nakamura T, Itoh K, Matsumoto T, Abe M. Glycolysis inhibition inactivates ABC transporters to restore drug sensitivity in malignant cells. PLoS One. 2011;6(11):e27222.

201. Chen J, Ding Z, Peng Y, Pan F, Li J, Zou L, Zhang Y, Liang H. HIF-1α inhibition reverses multidrug resistance in colon cancer cells via downregulation of MDR1/P-Glycoprotein. PLoS One. 2014;9(6):e98882.

202. Comerford KM, Wallace TJ, Karhausen J, Louis NA, Montalto MC, Colgan SP. Hypoxia-inducible factor-1-dependent regulation of the multidrug resistance (MDR1) gene. Cancer Res. 2002;62(12):3387–94.

203. Nardinocchi L, Puca R, Sacchi A, D'Orazi G. Inhibition of HIF-1alpha activity by homeodomain-interacting protein kinase-2 correlates with sensitization of chemoresistant cells to undergo apoptosis. Mol Cancer. 2009;8(1):1–9.

204. Gerstberger S, Hafner M, Tuschl T. A census of human RNA-binding proteins. Nat Rev Genet. 2014;15(12):829–45.

205. Wang ZL, Li B, Luo YX, Lin Q, Liu SR, Zhang XQ, Zhou H, Yang JH, Qu LH. Comprehensive Genomic Characterization of RNA-Binding Proteins across Human Cancers. Cell Rep. 2018;22(1):286–98.

206. Lunde BM, Moore C, Varani G. RNA-binding proteins: Modular design for efficient function. Vol. 8, Nature Reviews Molecular Cell Biology. 2007. p. 479–90.

207. Liu S, Li B, Liang Q, Liu A, Qu L, Yang J. Classification and function of RNA–protein interactions. Vol. 11, Wiley Interdisciplinary Reviews: RNA. 2020. p. e1601.

208. Glisovic T, Bachorik JL, Yong J, Dreyfuss G. RNA-binding proteins and post-transcriptional gene regulation. Vol. 582, FEBS Letters. 2008. p. 1977–86.

209. Campos AR, And DG, White K. Mutant alleles at the locus elav in drosophila melanogaster lead to nervous system defects. A developmental-genetic analysis. J Neurogenet. 1985;2(3):197–218.

210. Wang H, Zeng F, Liu Q, Liu H, Liu Z, Niu L, Teng M, Li X. The structure of the ARE-binding domains of Hu antigen R (HuR) undergoes conformational changes during RNA binding. Acta Crystallogr Sect D Biol Crystallogr. 2013;69(3):373–80.

211. Ma WJ, Cheng S, Campbell C, Wright A, Furneaux H. Cloning and characterization of HuR, a ubiquitously expressed Elav-like protein. J Biol Chem. 1996;271(14):8144–51.

212. Ma WJ, Furneaux H. Localization of the human HuR gene to chromosome 19p13.2. Hum Genet. 1996;99(1):32–3.

213. Tran H, Maurer F, Nagamine Y. Stabilization of Urokinase and Urokinase Receptor mRNAs by HuR Is Linked to Its Cytoplasmic Accumulation Induced by Activated Mitogen-Activated Protein Kinase-Activated Protein Kinase 2. Mol Cell Biol. 2003;23(20):7177–88.

214. Doller A, Akool ES, Huwiler A, Müller R, Radeke HH, Pfeilschifter J, Eberhardt W. Posttranslational Modification of the AU-Rich Element Binding Protein HuR by Protein Kinase Cδ Elicits Angiotensin II-Induced Stabilization and Nuclear Export of Cyclooxygenase 2 mRNA. Mol Cell Biol. 2008;28(8):2608–25.

215. Chen X, Li A, Sun BF, Yang Y, Han YN, Yuan X, Chen RX, Wei WS, Liu Y, Gao CC, Chen YS, Zhang M, Ma XD, Liu ZW, Luo JH, Lyu C, Wang HL, Ma J, Zhao YL, Zhou FJ, Huang Y, Xie D, Yang YG. 5-methylcytosine promotes pathogenesis of bladder cancer through stabilizing mRNAs. Nat Cell Biol. 2019;21(8):978–90.

216. Meisner NC, Hintersteiner M, Mueller K, Bauer R, Seifert JM, Naegeli HU, Ottl J, Oberer L, Guenat C, Moss S, Harrer N, Woisetschlaeger M, Buehler C, Uhl V, Auer M. Identification and mechanistic characterization of low-molecular-weight inhibitors for HuR. Nat Chem Biol. 2007;3(8):508–15.

217. Wang J, Guo Y, Chu H, Guan Y, Bi J, Wang B. Multiple functions of the RNA-binding protein HuR in cancer progression, treatment responses and prognosis. Vol. 14, International Journal of Molecular Sciences. 2013. p. 10015–41.

218. Uren PJ, Burns SC, Ruan J, Singh KK, Smith AD, Penalva LOF. Genomic analyses of the RNA-binding protein Hu antigen R (HuR) identify a complex network of target genes and novel characteristics of its binding sites. J Biol Chem. 2011;286(43):37063–6.

219. Fan XC, Steitz JA. Overexpression of HuR, a nuclear-cytoplasmic shuttling protein, increases the in

vivo stability of ARE-containing mRNAs. EMBO J. 1998;17(12):3448–60.

220. Meisner NC, Hintersteiner M, Seifert JM, Bauer R, Benoit RM, Widmer A, Schindler T, Uhl V, Lang M, Gstach H, Auer M. Terminal Adenosyl Transferase Activity of Posttranscriptional Regulator HuR Revealed by Confocal On-Bead Screening. J Mol Biol. 2009;386(2):435–50.

221. Brennan CM, Steitz JA. HuR and mRNA stability. Vol. 58, Cellular and Molecular Life Sciences. 2001. p. 266–77.

222. Joseph BP, Weber V, Knüpfer L, Giorgetti A, Alfonso-Prieto M, Krauß S, Carloni P, Rossetti G. Low Molecular Weight Inhibitors Targeting the RNA-Binding Protein HuR. Int J Mol Sci. 2023;24(17).

223. Zhang F, Cai Z, Lv H, Li W, Liang M, Wei X, Zhou F. Multiple functions of HuR in urinary tumors. Vol. 145, Journal of Cancer Research and Clinical Oncology. 2019. p. 11–8.

224. Peng W, Furuuchi N, Aslanukova L, Huang YH, Brown SZ, Jiang W, Addya S, Vishwakarma V, Peters E, Brody JR, Dixon DA, Sawicki JA. Elevated HuR in Pancreas Promotes a Pancreatitis-Like Inflammatory Microenvironment That Facilitates Tumor Development. Mol Cell Biol. 2018;38(3):e00427-17.

225. Zhu Z, Wang B, Bi J, Zhang C, Guo Y, Chu H, Liang X, Zhong C, Wang J. Cytoplasmic HuR expression correlates with P-gp, HER-2 positivity, and poor outcome in breast cancer. Tumor Biol. 2013;34(4):2299–308.

226. Koljonen V, Böhling T, Haglund C, Ristimäki A. Expression of HuR in Merkel cell carcinoma and in normal skin. J Cutan Pathol. 2008;35(1):10–4.

227. Denkert C, Koch I, Von Keyserlingk N, Noske A, Niesporek S, Dietel M, Weichert W. Expression of the ELAV-like protein HuR in human colon cancer: Association with tumor stage and cyclooxygenase-2. Mod Pathol. 2006;19(9):1261–9.

228. Mrena J, Wiksten JP, Thiel A, Kokkola A, Pohjola L, Lundin J, Nordling S, Ristimäki A, Haglund C. Cyclooxygenase-2 is an independent prognostic factor in gastric cancer and its expression is regulated by the messenger RNA stability factor HuR. Clin Cancer Res. 2005;11(20):7362–8.

229. Wang J, Zhao W, Guo Y, Zhang B, Xie Q, Xiang D, Gao J, Wang B, Chen Z. The expression of rna-binding protein hur in non-small cell lung cancer correlates with vascular endothelial growth factor-C expression and lymph node metastasis. Oncology. 2009;76(6):420–9.

230. Wang J, Wang B, Bi J, Zhang C. Cytoplasmic HuR expression correlates with angiogenesis, lymphangiogenesis, and poor outcome in lung cancer. Med Oncol. 2011;28(SUPPL. 1):577–85.

231. Denkert C, Weichert W, Winzer KJ, Müller BM, Noske A, Niesporek S, Kristiansen G, Guski H, Dietel M, Hauptmann S. Expression of the ELAV-like protein HuR is associated with higher tumor grade and increased cyclooxygenase-2 expression in human breast carcinoma. Clin Cancer Res. 2004;10(16):5580–6.

232. Denkert C, Weichert W, Pest S, Koch I, Licht D, Köbel M, Reles A, Sehouli J, Dietel M, Hauptmann S. Overexpression of the Embryonic-Lethal Abnormal Vision-like Protein HuR in Ovarian Carcinoma Is a Prognostic Factor and Is Associated with Increased Cyclooxygenase 2 Expression. Cancer Res. 2004;64(1):189–95.

233. Danilin S, Sourbier C, Thomas L, Lindner V, Rothhut S, Dormoy V, Helwig JJ, Jacqmin D, Lang H, Massfelder T. Role of the RNA-binding protein HuR in human renal cell carcinoma. Carcinogenesis. 2010;31(6):1018–26.

234. Kim GY, Lim SJ, Kim YW. Expression of HuR, COX-2, and survivin in lung cancers; Cytoplasmic HuR stabilizes cyclooxygenase-2 in squamous cell carcinomas. Mod Pathol. 2011;24(10):1336–47.

235. Mrena J, Wiksten JP, Kokkola A, Nordling S, Ristimäki A, Haglund C. COX-2 is associated with proliferation and apoptosis markers and serves as an independent prognostic factor in gastric cancer. Tumor Biol. 2010;31(1):1–7.

236. Stoppoloni D, Cardillo I, Verdina A, Vincenzi B, Menegozzo S, Santini M, Sacchi A, Baldi A,

Galati R. Expression of the embryonic lethal abnormal vision-like protein HuR in human mesothelioma: Association with cyclooxygenase-2 and prognosis. Cancer. 2008;113(10):2761–9.

237. Miyata Y, Watanabe SI, Sagara Y, Mitsunari K, Matsuo T, Ohba K, Sakai H. High Expression of HuR in Cytoplasm, but Not Nuclei, Is Associated with Malignant Aggressiveness and Prognosis in Bladder Cancer. PLoS One. 2013;8(3):e59095.

238. Dalmau J, Furneaux HM, Cordon-Cardo C, Posner JB. The expression of the Hu (paraneoplastic encephalomyelitis/sensory neuronopathy) antigen in human normal and tumor tissues. Am J Pathol. 1992;141(4):881–6.

239. King PH, Dropcho EJ. Expression of Hel-N1 and Hel-N2 in small-cell lung carcinoma. Ann Neurol. 1996;39(5):679–81.

240. King PH. Differential expression of the neuroendocrine genes Hel-NI and HuD in small-cell lung carcinoma: Evidence for down-regulation of HuD in the variant phenotype. Int J Cancer. 1997;74(4):378–82.

241. Prislei S, Martinelli E, Mariani M, Raspaglio G, Sieber S, Ferrandina G, Shahabi S, Scambia G, Ferlini C. MiR-200c and HuR in ovarian cancer. BMC Cancer. 2013;13:1–14.

242. Raspaglio G, De Maria I, Filippetti F, Martinelli E, Zannoni GF, Prislei S, Ferrandina G, Shahabi S, Scambia G, Ferlini C. HuR regulates β-tubulin isotype expression in ovarian cancer. Cancer Res. 2010;70(14):5891–900.

243. Gong F, Dong D, Zhang T, Xu W. Long non-coding RNA FENDRR attenuates the stemness of non-small cell lung cancer cells via decreasing multidrug resistance gene 1 (MDR1) expression through competitively binding with RNA binding protein HuR. Eur J Pharmacol. 2019;853:345–52.

244. To KKW, Leung WW, Ng SSM. Exploiting a novel miR-519c-HuR-ABCG2 regulatory pathway to overcome chemoresistance in colorectal cancer. Exp Cell Res. 2015;338(2):222–31.

245. Rasband WS. ImageJ. U S Natl Institutes Heal Bethesda, Maryland, USA, 1997-2018 [Internet]. Available from: https://imagej.nih.gov/ij/

246. Ko J, Park H, Heo L, Seok C. GalaxyWEB server for protein structure prediction and refinement. Nucleic Acids Res. 2012;40(W1):W294–7.

247. Laskowski RA, MacArthur MW, Thornton JM. PROCHECK : validation of protein-structure coordinates. In 2012.

248. Benkert P, Biasini M, Schwede T. Toward the estimation of the absolute quality of individual protein structure models. Bioinformatics. 2011;27(3):343–50.

249. Wiederstein M, Sippl MJ. ProSA-web: Interactive web service for the recognition of errors in three-dimensional structures of proteins. Nucleic Acids Res. 2007;35(SUPPL.2):W407–10.

250. Berman HM, Battistuz T, Bhat TN, Bluhm WF, Bourne PE, Burkhardt K, Feng Z, Gilliland GL, Iype L, Jain S, Fagan P, Marvin J, Padilla D, Ravichandran V, Schneider B, Thanki N, Weissig H, Westbrook JD, Zardecki C. The protein data bank. Acta Crystallogr Sect D Biol Crystallogr. 2002;58(6I):899–907.

251. Sayers EW, Bolton EE, Brister JR, Canese K, Chan J, Comeau DC, Connor R, Funk K, Kelly C, Kim S, Madej T, Marchler-Bauer A, Lanczycki C, Lathrop S, Lu Z, Thibaud-Nissen F, Murphy T, Phan L, Skripchenko Y, Tse T, Wang J, Williams R, Trawick BW, Pruitt KD, Sherry ST. Database resources of the national center for biotechnology information. Nucleic Acids Res. 2022;50(D1):D20–6.

252. Arnott S, Campbell-Smith PJ, Chandrasekaran R. In Handbook of Biochemistry and Molecular Biology. 3rd ed. Fasman GP, editor. Vol. II. Cleveland: CRC Press; 1976. 411–422 p.

253. Van Zundert GCP, Rodrigues JPGLM, Trellet M, Schmitz C, Kastritis PL, Karaca E, Melquiond ASJ, Van Dijk M, De Vries SJ, Bonvin AMJJ. The HADDOCK2.2 Web Server: User-Friendly Integrative Modeling of Biomolecular Complexes. J Mol Biol. 2016;428(4):720–5.

254. PyMOL | pymol.org [Internet]. [cited 2023 Nov 11]. Available from: https://pymol.org/2/

255. Pettersen EF, Goddard TD, Huang CC, Meng EC, Couch GS, Croll TI, Morris JH, Ferrin TE. UCSF ChimeraX: Structure visualization for researchers, educators, and developers. Protein Sci. 2021;30(1):70–82.

256. Song Y, Dimaio F, Wang RYR, Kim D, Miles C, Brunette T, Thompson J, Baker D. High-resolution comparative modeling with RosettaCM. Structure. 2013;21(10):1735–42.

257. Sievers F, Wilm A, Dineen D, Gibson TJ, Karplus K, Li W, Lopez R, McWilliam H, Remmert M, Söding J, Thompson JD, Higgins DG. Fast, scalable generation of high-quality protein multiple sequence alignments using Clustal Omega. Mol Syst Biol. 2011;7(1):539.

258. Gruber AR, Lorenz R, Bernhart SH, Neuböck R, Hofacker IL. The Vienna RNA websuite. Nucleic Acids Res. 2008;36(SUPPL_2):W70–4.

259. Zhang Y, Wang J, Xiao Y. 3dRNA: 3D Structure Prediction from Linear to Circular RNAs. J Mol Biol. 2022;434(11):167452.

260. Fallmann J, Sedlyarov V, Tanzer A, Kovarik P, Hofacker IL. AREsite2: An enhanced database for the comprehensive investigation of AU/GU/U-rich elements. Nucleic Acids Res. 2016;44(D1):D90–5.

261. Hamilton G, Rath B. A short update on cancer chemoresistance. Wiener Medizinische Wochenschrift. 2014;164(21–22):456–60.

262. McCarroll JA, Naim S, Sharbeen G, Russia N, Lee J, Kavallaris M, Goldstein D, Phillips PA. Role of pancreatic stellate cells in chemoresistance in pancreatic cancer. Front Physiol. 2014;5:86505.

263. Wang X, He S, Gu Y, Wang Q, Chu X, Jin M, Xu L, Wu Q, Zhou Q, Wang B, Zhang Y, Wang H, Zheng L. Fatty acid receptor GPR120 promotes breast cancer chemoresistance by upregulating ABC transporters expression and fatty acid synthesis. EBioMedicine. 2019;40:251–62.

264. Sakiyama M, Matsuo H, Takada Y, Nakamura T, Nakayama A, Takada T, Kitajiri SI, Wakai K, Suzuki H, Shinomiya N. Ethnic differences in ATP-binding cassette transporter, sub-family G, member 2 (ABCG2/BCRP): Genotype combinations and estimated functions. Drug Metab Pharmacokinet. 2014;29(6):490–2.

265. Xiao Q, Zhou Y, Lauschke VM. Ethnogeographic and inter-individual variability of human ABC transporters. Hum Genet. 2020;139(5):623–46.

266. Trock BJ, Leonessa F, Clarke R. Multidrug resistance in breast cancer: A meta-analysis of MDR1/gp170 expression and its possible functional significance. J Natl Cancer Inst. 1997;89(13):917–31.

267. Grogan TM, Spier CM, Salmon SE, Matzner M, Rybski J, Weinstein RS, Scheper RJ, Dalton WS. P-glycoprotein expression in human plasma cell myeloma: Correlation with prior chemotherapy. Blood. 1993;81(2):490–5.

268. Chan HSL, Grogan TM, Haddad G, DeBoer G, Ling V. P-glycoprotein expression: Critical determinant in the response to osteosarcoma chemotherapy. J Natl Cancer Inst. 1997;89(22):1706–15.

269. Lin JH, Yamazaki M. Role of P-glycoprotein in pharmacokinetics: Clinical implications. Vol. 42, Clinical Pharmacokinetics. 2003. p. 59–98.

270. Kim B, Fatayer H, Hanby AM, Horgan K, Perry SL, Valleley EMA, Verghese ET, Williams BJ, Thorne JL, Hughes TA. Neoadjuvant Chemotherapy Induces Expression Levels of Breast Cancer Resistance Protein That Predict Disease-Free Survival in Breast Cancer. PLoS One. 2013;8(5):e62766.

271. Zhang Z, Zhang W, Jin Y, Wang H, Gu F, Zhou J, Lao Z, Xu Z, Tang F, Zou L, Tang W, Lu R, Zou Q. Evaluating the response of neoadjuvant chemotherapy for treatment of breast cancer: Are tumor biomarkers and dynamic contrast enhanced MR images useful predictive tools? J Thorac Dis. 2014;6(6):785–94.

272. Rudas M, Filipits M, Taucher S, Stranzl T, Steger GG, Jakesz R, Pirker R, Pohl G. Expression of

MRP1, LRP and Pgp in breast carcinoma patients treated with preoperative chemotherapy. Breast Cancer Res Treat. 2003;81(2):149–57.

273. Wang J, Wang W, Cai H, Du B, Zhang L, Ma W, Hu Y, Feng S, Miao G. MACC1 facilitates chemoresistance and cancer stem cell-like properties of colon cancer cells through the PI3K/AKT signaling pathway. Mol Med Rep. 2017;16(6):8747–54.

274. Zhou H, Lin C, Zhang Y, Zhang X, Zhang C, Zhang P, Xie X, Ren Z. miR-506 enhances the sensitivity of human colorectal cancer cells to oxaliplatin by suppressing MDR1/P-gp expression. Cell Prolif. 2017;50(3):e12341.

275. Sikic BI. Natural and Acquired Resistance to Cancer Therapies. In: The Molecular Basis of Cancer: Fourth Edition. 2015. p. 651–60.

276. Sedláková I, Laco J, Caltová K, Červinka M, Tošner J, Řezáč A, Špaček J. Clinical significance of the resistance proteins LRP, Pgp, MRP1, MRP3, and MRP5 in epithelial ovarian cancer. Int J Gynecol Cancer. 2015;25(2):236–43.

277. Materna V, Pleger J, Hoffmann U, Lage H. RNA expression of MDR1/P-glycoprotein, DNA-topoisomerase I, and MRP2 in ovarian carcinoma patients: Correlation with chemotherapeutic response. Gynecol Oncol. 2004;94(1):152–60.

278. Yakirevich E, Sabo E, Naroditsky I, Sova Y, Lavie O, Resnick MB. Multidrug resistance-related phenotype and apoptosis-related protein expression in ovarian serous carcinomas. Gynecol Oncol. 2006;100(1):152–9.

279. Holzmayer TA, Hilsenbeck S, Von Hoff DD, Roninson IB. Clinical correlates of mdr1 (p-glycoprotein) gene expression in ovarian and small-cell lung carcinomas. J Natl Cancer Inst. 1992;84(19):1486–91.

280. Gu KS, Chen Y. Mechanism of P-glycoprotein expression in the SGC7901 human gastric adenocarcinoma cell line induced by cyclooxygenase-2. Asian Pacific J Cancer Prev. 2012;13(5).

281. Filipits M, Pohl G, Rudas M, Dietze O, Lax S, Grill R, Pirker R, Zielinski CC, Hausmaninger H, Kubista E, Samonigg H, Jakesz R. Clinical role of multidrug resistance protein 1 expression in chemotherapy resistance in early-stage breast cancer: The Austrian Breast and Colorectal Cancer Study Group. J Clin Oncol. 2005;23(6):1161–8.

282. Chang L, Hu Z, Zhou Z, Zhang H. Linc00518 Contributes to Multidrug Resistance Through Regulating the MiR-199a/MRP1 Axis in Breast Cancer. Cell Physiol Biochem. 2018;48(1):16–28.

283. Nakahara T, Sakaeda T, Nakamura T, Tamura T, Nishioka C, Aoyama N, Okamura N, Shirakawa T, Gotoh A, Kamigaki T, Ohno M, Kuroda Y, Matsuo M, Kasuga M, Okumura K. Chemosensitivity assessed by collagen gel droplet embedded culture drug sensitivity test, and MDR1, MRP1, and MRP2 mRNA expression in human colorectal adenocarcinomas. Pharm Res. 2004;21(3):406–12.

284. Nishioka C, Sakaeda T, Nakamura T, Moriya Y, Okamura N, Tamura T, Nakahara T, Aoyama N, Kamigaki T, Ohno M, Kuroda Y, Kasuga M, Okumura K. MDR1, MRP1 and MRP2 genotypes and in vitro chemosensitivity in Japanese patients with colorectal adenocarcinomas. Kobe J Med Sci. 2004;50(5–6):181–8.

285. Ji L, Wei Y, Jiang T, Wang S. Correlation of Nrf2, NQO1, MRP1, cmyc and p53 in colorectal cancer and their relationships to clinicopathologic features and survival. Int J Clin Exp Pathol. 2014;7(3):1124–31.

286. Xing Y, Wang ZH, Ma DH, Han Y. FTY720 enhances chemosensitivity of colon cancer cells to doxorubicin and etoposide via the modulation of P-glycoprotein and multidrug resistance protein 1. J Dig Dis. 2014;15(5):246–59.

287. He X, Ee PLR, Coon JS, Beck WT. Alternative splicing of the multidrug resistance protein 1/ATP binding cassette transporter subfamily gene in ovarian cancer creates functional spice variants and is associated with increased expression of the spiking factors PTB and SRp20. Clin Cancer Res. 2004;10(14):4652–60.

288. Wu H, Hait WN, Yang JM. Small interfering RNA-induced suppression of MDR1 (P-glycoprotein) restores sensitivity to multidrug-resistant cancer cells. Cancer Res. 2003;63(7):1515–9.

289. Lin-Lee YC, Tatebe S, Savaraj N, Ishikawa T, Tien Kuo M. Differential sensitivities of the MRP gene family and γ-glutamylcysteine synthetase to prooxidants in human colorectal carcinoma cell lines with different p53 status. Biochem Pharmacol. 2001;61(5).

290. Özvegy C, Litman T, Szakács G, Nagy Z, Bates S, Váradi A, Sarkadi B. Functional characterization of the human multidrug transporter, ABCG2, expressed in insect cells. Biochem Biophys Res Commun. 2001;285(1):111–7.

291. Britton KM, Eyre R, Harvey IJ, Stemke-Hale K, Browell D, Lennard TWJ, Meeson AP. Breast cancer, side population cells and ABCG2 expression. Cancer Lett. 2012;323(1):97–105.

292. Stein U, Lage H, Jordan A, Walther W, Bates SE, Litman T, Hohenberger P, Dietel M. Impact of BCRP/MXR, MRP1 and MDR1/P-glycoprotein on thermoresistant variants of atypical and classical multidrug resistant cancer cells. Int J Cancer. 2002;97(6):751–60.

293. Zhou S, Liao L, Chen C, Zeng W, Liu S, Su J, Zhao S, Chen M, Kuang Y, Chen X, Li J. CD147 mediates chemoresistance in breast cancer via ABCG2 by affecting its cellular localization and dimerization. Cancer Lett. 2013;337(2):285–92.

294. Hu L, Liang Y, Wu K, Wang C, Zhang T, Peng R, Zou F. Repressing PDCD4 activates JNK/ABCG2 pathway to induce chemoresistance to fluorouracil in colorectal cancer cells. Ann Transl Med. 2021;9(2):114.

295. Li X, Zou Z, Tang J, Zheng Y, Liu YU, Luo YAN, Liu Q, Wang Y. NOS1 upregulates ABCG2 expression contributing to DDP chemoresistance in ovarian cancer cells. Oncol Lett. 2019;17(2):1595–602.

296. Weroha SJ, Oberg AL, Ziegler KLA, Dakhilm SR, Rowland KM, Hartmann LC, Moore DF, Keeney GL, Peethambaram PP, Haluska P. Phase II trial of lapatinib and topotecan (LapTop) in patients with platinum-refractory/resistant ovarian and primary peritoneal carcinoma. Gynecol Oncol. 2011;122(1):116–20.

297. Ricci JW, Lovato DM, Severns V, Sklar LA, Larson RS. Novel ABCG2 Antagonists reverse topotecan-mediated chemotherapeutic resistance in ovarian carcinoma Xenografts. Mol Cancer Ther. 2016;15(12):2853–62.

298. Singh A, Wu H, Zhang P, Happel C, Ma J, Biswal S. Expression of ABCG2 (BCRP) is regulated by Nrf2 in cancer cells that confers side population and chemoresistance phenotype. Mol Cancer Ther. 2010;9(8).

299. de Boussac H, Orbán TI, Várady G, Tihanyi B, Bacquet C, Brózik A, Váradi A, Sarkadi B, Arányi T. Stimulus-induced expression of the ABCG2 multidrug transporter in HepG2 hepatocarcinoma model cells involves the ERK1/2 cascade and alternative promoters. Biochem Biophys Res Commun. 2012;426(2).

300. Hu C, Li H, Li J, Zhu Z, Yin S, Hao X, Yao M, Zheng S, Gu J. Analysis of ABCG2 expression and side population identifies intrinsic drug efflux in the HCC cell line MHCC-97L and its modulation by Akt signaling. Carcinogenesis. 2008;29(12).

301. Dharmapuri G, Doneti R, Philip GH, Kalle AM. Celecoxib sensitizes imatinib-resistant K562 cells to imatinib by inhibiting MRP1-5, ABCA2 and ABCG2 transporters via Wnt and Ras signaling pathways. Leuk Res. 2015;39(7).

302. Vollrath V, Wielandt AM, Iruretagoyena M, Chianale J. Role of Nrf2 in the regulation of the Mrp2 (ABCC2) gene. Biochem J. 2006;395(3).

303. Albermann N, Schmitz-Winnenthal FH, Z'graggen K, Volk C, Hoffmann MM, Haefeli WE, Weiss J. Expression of the drug transporters MDR1/ABCB1, MRP1/ABCC1, MRP2/ABCC2, BCRP/ABCG2, and PXR in peripheral blood mononuclear cells and their relationship with the expression in intestine and liver. Biochem Pharmacol. 2005;70(6).

304. Bark H, Xu HD, Kim SH, Yun J, Choi CH. P-glycoprotein down-regulates expression of breast

cancer resistance protein in a drug-free state. FEBS Lett. 2008;582(17):2595–600.

305. Cisternino S, Mercier C, Bourasset F, Roux F, Scherrmann JM. Expression, Up-Regulation, and Transport Activity of the Multidrug-Resistance Protein Abcg2 at the Mouse Blood-Brain Barrier. Cancer Res. 2004;64(9):3296–301.

306. Haber M, Marshall GM, Norris MD, Cheung B, Marshall GM, Norris MD. Expression of the Multidrug Resistance-associated Protein (MRP) Gene Correlates with Amplification and Overexpression of the N-myc Oncogene in Childhood Neuroblastoma. Cancer Res. 1994;54(19):5036–40.

307. Brock I, Hipfner DR, Nielsen BS, Jensen PB, Deeley RG, Cole SPC, Sehested M. Sequential Coexpression of the Multidrug Resistance Genes MRP and mdrl and Their Products in VP-16 (Etoposide)-selected H69 Small Cell Lung Cancer Cells. Cancer Res. 1995;55(3):459–62.

308. Friedrich RE, Punke C, Reymann A. Expression of multi-drug resistance genes (mdr1, mrp1, bcrp) in primary oral squamous cell carcinoma. Vol. 18, In Vivo. 2004. p. 133–48.

309. Choi CH, Kim HS, Rha HS, Jeong JH, Park YH, Min YD, Kee KH, Lim DY. Drug concentration-dependent expression of multidrug resistance-associated protein and P-glycoprotein in the doxorubicin-resistant acute myelogenous leukemia sublines. Mol Cells. 1999;9(3):314–9.

310. Brown JM, Giaccia AJ. The unique physiology of solid tumors: Opportunities (and problems) for cancer therapy. Cancer Res. 1998;58(7):1408–16.

311. Raguz S, Yagüe E. Resistance to chemotherapy: New treatments and novel insights into an old problem. Vol. 99, British Journal of Cancer. 2008. p. 387–91.

312. Semenza GL. Involvement of hypoxia-inducible factor 1 in human cancer. Intern Med. 2002;41(2):79–83.

313. Greijer AE, Van Der Wall E. The role of hypoxia inducible factor 1 (HIF-1) in hypoxia induced apoptosis. Vol. 57, Journal of Clinical Pathology. 2004. p. 1009–14.

314. Assidicky R, Tokat UM, Tarman IO, Saatci O, Ersan PG, Raza U, Ogul H, Riazalhosseini Y, Can T, Sahin O. Targeting HIF1-alpha/miR-326/ITGA5 axis potentiates chemotherapy response in triple-negative breast cancer. Breast Cancer Res Treat. 2022;193(2):331–48.

315. Generali D, Buffa FM, Berruti A, Brizzi MP, Campo L, Bonardi S, Bersiga A, Allevi G, Milani M, Aguggini S, Papotti M, Dogliotti L, Bottini A, Harris AL, Fox SB. Phosphorylated ERα, HIF-1α, and MAPK signaling as predictors of primary endocrine treatment response and resistance in patients with breast cancer. J Clin Oncol. 2009;27(2):227–34.

316. Generali D, Berruti A, Brizzi MP, Campo L, Bonardi S, Wigfield S, Bersiga A, Allevi G, Milani M, Aguggini S, Gandolfi V, Dogliotti L, Bottini A, Harris AL, Fox SB. Hypoxia-inducible factor-1α expression predicts a poor response to primary chemoendocrine therapy and disease-free survival in primary human breast cancer. Clin Cancer Res. 2006;12(15):4562–8.

317. Cutter NL, Walther T, Doyle KH, Frank R. Abstract 4525: Hypoxia signaling pathway plays a role in ovarian cancer chemoresistance. Cancer Res. 2017;77(13_Supplement):4525–4525.

318. Chen X, Liu M, Meng F, Sun B, Jin X, Jia C. The long noncoding RNA HIF1A-AS2 facilitates cisplatin resistance in bladder cancer. J Cell Biochem. 2019;120(1):243–52.

319. Danza K, Silvestris N, Simone G, Signorile M, Saragoni L, Brunetti O, Monti M, Mazzotta A, De Summa S, Mangia A, Tommasi S. Role of miR-27a, miR-181a and miR-20b in gastric cancer hypoxia-induced chemoresistance. Cancer Biol Ther. 2016;17(4):400–6.

320. Srikantan S, Gorospe M. HuR function in disease. Vol. 17, Frontiers in Bioscience. 2012. p. 189–205.

321. Abdelmohsen K, Gorospe M. Posttranscriptional regulation of cancer traits by HuR. Vol. 1, Wiley Interdisciplinary Reviews: RNA. 2010. p. 214–29.

322. Kim KY, Li SJ, Cha JD, Zhang X, Cha IH. Significance of molecular markers in survival prediction of oral squamous cell carcinoma. Head Neck. 2012;34(7):929–36.

323. Lal S, Burkhart RA, Beeharry N, Bhattacharjee V, Londin ER, Cozzitorto JA, Romeo C, Jimbo M, Norris ZA, Yeo CJ, Sawicki JA, Winter JM, Rigoutsos I, Yen TJ, Brody JR. HuR posttranscriptionally regulates WEE1: Implications for the DNA damage response in pancreatic cancer cells. Cancer Res. 2014;74(4):1128–40.

324. Cai J, Wang H, Jiao X, Huang R, Qin Q, Zhang J, Chen H, Feng D, Tian X, Wang H. The RNA-binding protein HuR confers oxaliplatin resistance of colorectal cancer by upregulating CdC6. Mol Cancer Ther. 2019;18(7):1243–54.

325. Goutas D, Pergaris A, Giaginis C, Theocharis S. HuR as Therapeutic Target in Cancer: What the Future Holds. Curr Med Chem. 2021;29(1):56–65.

326. Hostetter C, Licata LA, Witkiewicz A, Costantino CL, Yeo CJ, Brody JR, Keen JC. Cytoplasmic accumulation of the RNA binding protein HuR is central to tamoxifen resistance in estrogen receptor positive breast cancer cells. Cancer Biol Ther. 2008;7(9):1496–506.

327. Li W, Luo L, Shi W, Yin Y, Gao S. Ursolic acid reduces Adriamycin resistance of human ovarian cancer cells through promoting the HuR translocation from cytoplasm to nucleus. Environ Toxicol. 2021;36(2):267–75.

328. Blanco FF, Jimbo M, Wulfkuhle J, Gallagher I, Deng J, Enyenihi L, Meisner-Kober N, Londin E, Rigoutsos I, Sawicki JA, Risbud M V., Witkiewicz AK, McCue PA, Jiang W, Rui H, Yeo CJ, Petricoin E, Winter JM, Brody JR. The mRNA-binding protein HuR promotes hypoxia-induced chemoresistance through posttranscriptional regulation of the proto-oncogene PIM1 in pancreatic cancer cells. Oncogene. 2016;35(19):2529–41.

329. Goutas D, Goutas N, Theocharis S. Divulging the critical role of HuR in pancreatic cancer as a therapeutic target and a means to overcome chemoresistance. Vol. 13, Cancers. 2021. p. 4634.

330. Dhir T, Schultz CW, Jain A, Brown SZ, Haber A, Goetz A, Xi C, Su GH, Xu L, Posey J, Jiang W, Yeo CJ, Golan T, Pishvaian MJ, Brody JR. Abemaciclib is effective against pancreatic cancer cells and synergizes with HuR and YAP1 inhibition. Mol Cancer Res. 2019;17(10):2029–41.

331. Zhou H, Telonis AG, Jing Y, Xia NL, Biederman L, Jimbo M, Blanco F, Londin E, Brody JR, Rigoutsos I. GPRC5A is a potential oncogene in pancreatic ductal adenocarcinoma cells that is upregulated by gemcitabine with help from HuR. Cell Death Dis. 2016;7(7):e2294–e2294.

332. Romeo C, Weber MC, Zarei M, DeCicco D, Chand SN, Lobo AD, Winter JM, Sawicki JA, Sachs JN, Meisner-Kober N, Yeo CJ, Vadigepalli R, Tykocinski ML, Brody JR. HuR contributes to TRAIL resistance by restricting death receptor 4 expression in pancreatic cancer cells. Mol Cancer Res. 2016;14(7):599–611.

333. Jain A, Agostini LC, McCarthy GA, Chand SN, Ramirez AJ, Nevler A, Cozzitorto J, Schultz CW, Lowder CY, Smith KM, Waddell ID, Raitses-Gurevich M, Stossel C, Gorman YG, Atias D, Yeo CJ, Winter JM, Olive KP, Golan T, Pishvaian MJ, Ogilvie D, James DI, Jordan AM, Brody JR. Poly (ADP) ribose glycohydrolase can be effectively targeted in pancreatic cancer. Cancer Res. 2019;79(17):4491–502.

334. Chand SN, Zarei M, Schiewer MJ, Kamath AR, Romeo C, Lal S, Cozzitorto JA, Nevler A, Scolaro L, Londin E, Jiang W, Meisner-Kober N, Pishvaian MJ, Knudsen KE, Yeo CJ, Pascal JM, Winter JM, Brody JR. Posttranscriptional regulation of PARG mRNA by HuR facilitates DNA repair and resistance to PARP inhibitors. Cancer Res. 2017;77(18):5011–25.

335. Wei L, Zhang Q, Zhong C, Aubé J, Welch D, Wu X, Xu L. Abstract 1753: Functional inhibition of the RNA-binding protein HuR sensitizes triple-negative breast cancer to chemotherapy. Cancer Res. 2023;83(7_Supplement).

336. Badawi A, Biyanee A, Nasrullah U, Winslow S, Schmid T, Pfeilschifter J, Eberhardt W. Inhibition of IRES-dependent translation of caspase-2 by HuR confers chemotherapeutic drug resistance in colon carcinoma cells. Oncotarget. 2018;9(26):18367–85.

337. Lin GL, Ting HJ, Tseng TC, Juang V, Lo YL. Modulation of the mRNA-binding protein HuR as a novel reversal mechanism of epirubicin-triggered multidrug resistance in colorectal cancer cells. PLoS One. 2017;12(10):e0185625.

338. Ding Z, Yang L, Xie X, Xie F, Pan F, Li J, He J, Liang H. Expression and significance of hypoxia-inducible factor-1 alpha and MDR1/P-glycoprotein in human colon carcinoma tissue and cells. J Cancer Res Clin Oncol. 2010;136(11):1697–707.

339. Chen L, Feng P, Li S, Long D, Cheng J, Lu Y, Zhou D. Effect of hypoxia-inducible factor-1α silencing on the sensitivity of human brain glioma cells to doxorubicin and etoposide. Neurochem Res. 2009;34(5):984–90.

340. Liu L, Ning X, Sun L, Zhang H, Shi Y, Guo C, Han S, Liu J, Sun S, Han Z, Wu K, Fan D. Hypoxia-inducible factor-1α contributes to hypoxia-induced chemoresistance in gastric cancer. Cancer Sci. 2008;99(1):121–8.

341. Lv Y, Zhao S, Han J, Zheng L, Yang Z, Zhao L. Hypoxia-inducible factor-1α induces multidrug resistance protein in colon cancer. Onco Targets Ther. 2015;8:1941–8.

342. He X, Wang J, Wei W, Shi M, Xin B, Zhang T, Shen X. Hypoxia regulates ABCG2 activity through the activivation of ERK1/2/HIF-1α and contributes to chemoresistance in pancreatic cancer cells. Cancer Biol Ther. 2016;17(2):188–98.

343. Kalousi A, Mylonis I, Politou AS, Chachami G, Paraskeva E, Simos G. Casein kinase 1 regulates human hypoxia-inducible factor HIF-1. J Cell Sci. 2010;123(17):2976–86.

344. Tanimoto K, Yuichi M, Pereira T, Poellinger L. Mechanism of regulation of the hypoxia-inducible factor-1 alpha by the von Hippel-Lindau tumor suppressor protein. EMBO J. 2000;19(16):4298–309.

345. Talwar S, Jin J, Carroll B, Liu A, Gillespie MB, Palanisamy V. Caspase-mediated cleavage of RNA-binding protein HuR regulates c-myc protein expression after hypoxic stress. J Biol Chem. 2011;286(37):32333–43.

Supplementary Files

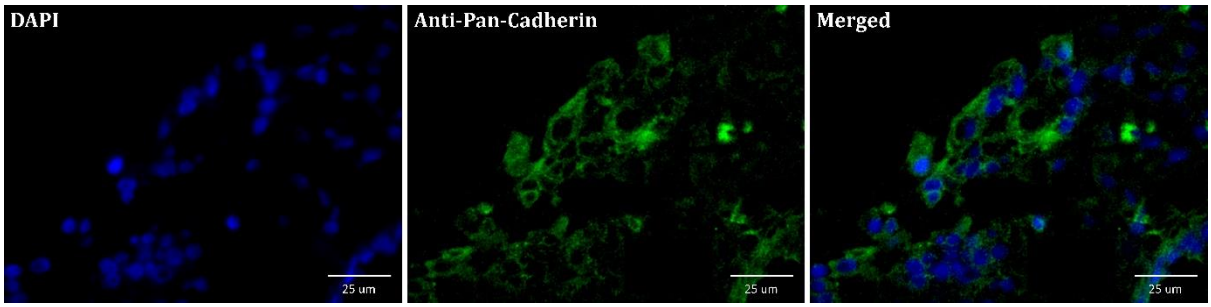

Supplementary figure 1: Immunofluorescence image of Pan-Cadherin expression to observe the cell quality in the tissue. The image shows expression of Pan-Cadherin (green) in tissues. The scale bar is 25 µm.

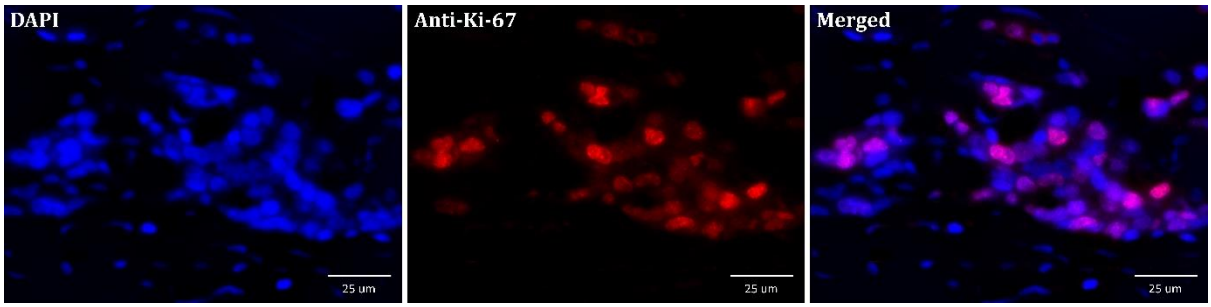

Supplementary figure 2: Immunofluorescence image of Ki-67 expression as a proliferation marker for the cancerous tissue. The image shows expression of Ki-67 (red) in tissues. The scale bar is 25 µm.

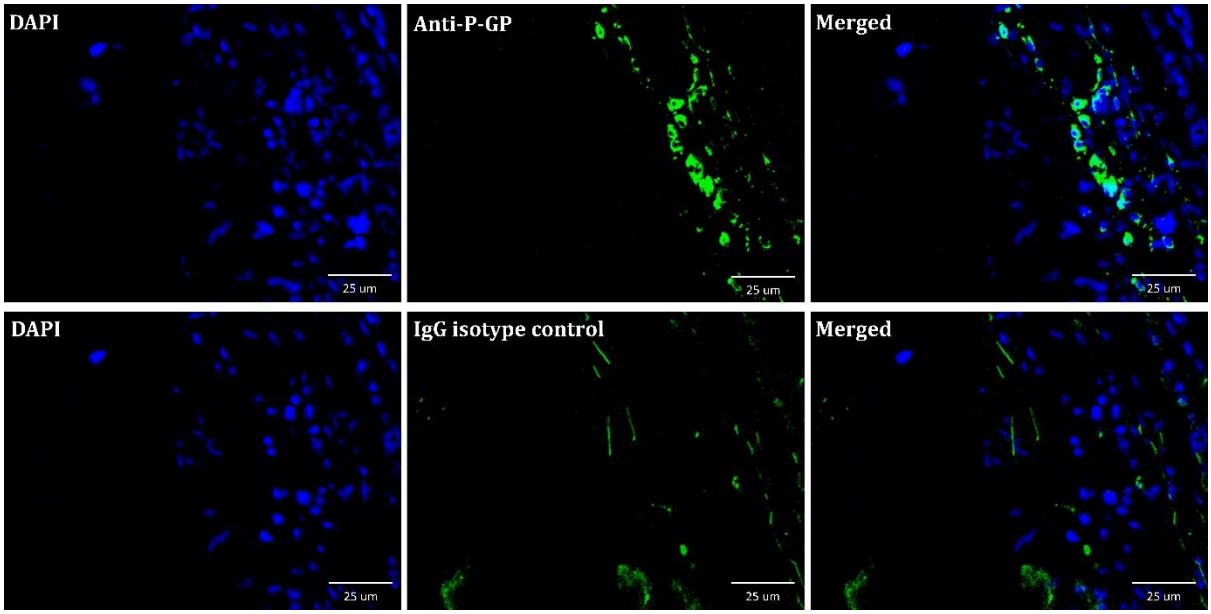

Supplementary figure 3: Immunofluorescence image of binding specificity validation for primary Ab Anti-P-GP. Same samples, but different sections were treated with Anti-P-GP (green) and IgG isotype control (green) to observe the non-specific binding of Anti-P-GP. The scale bar is 25 µm.

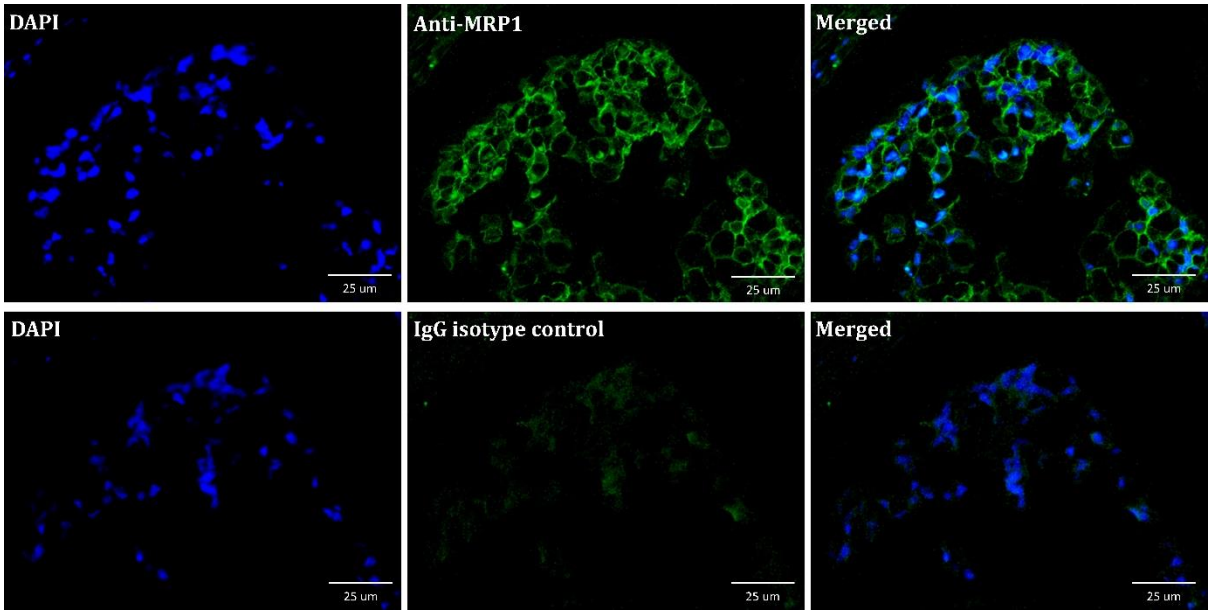

Supplementary figure 4: Immunofluorescence image of binding specificity validation for primary Ab Anti-MRP1. Same samples, but different sections were treated with Anti-MRP1 (green) and IgG isotype control (green) to observe the non-specific binding of Anti-MRP1. The scale bar is 25 µm.

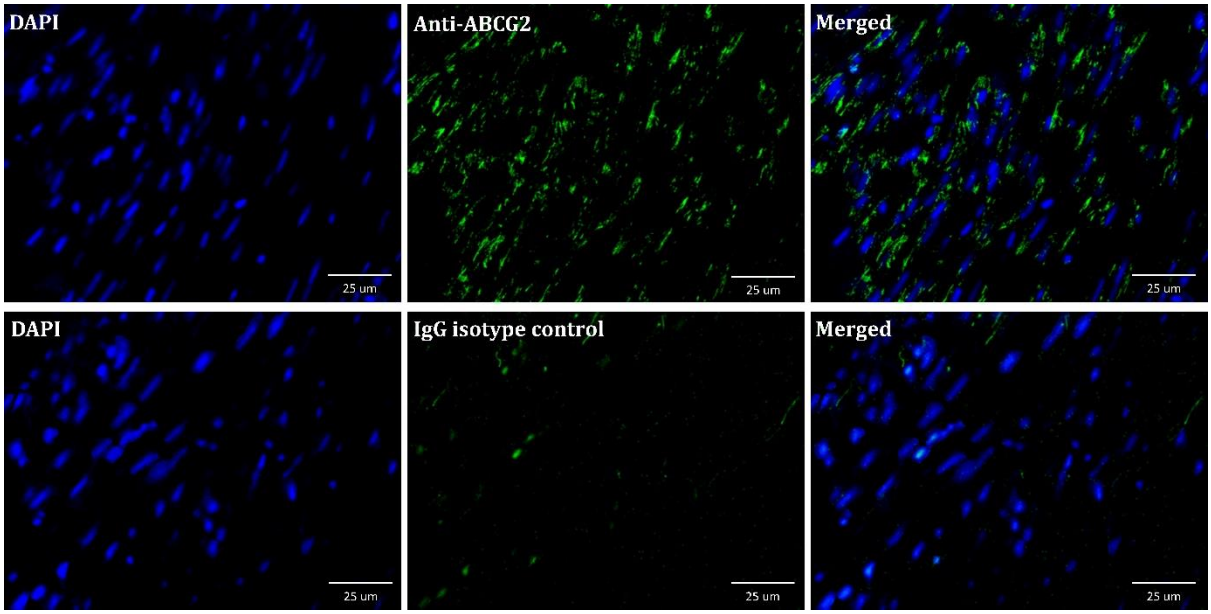

Supplementary figure 5: Immunofluorescence image of binding specificity validation for primary Ab Anti-ABCG2. Same samples, but different sections were treated with Anti- ABCG2 (green) and IgG isotype control (green) to observe the non-specific binding of Anti-ABCG2. The scale bar is 25 µm.

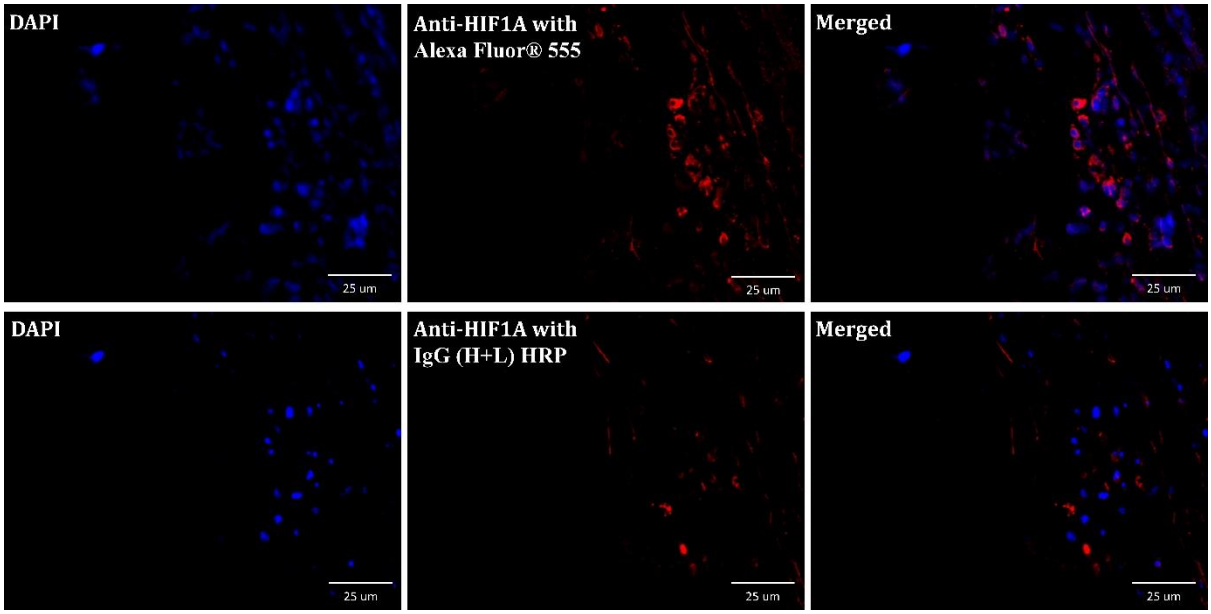

Supplementary figure 6: Immunofluorescence image of fluorescence activity validation for secondary Ab Alexa Fluor® 555. Same samples, but different sections were treated with Anti- HIF1A with Alexa Fluor® 555 (red) and Anti- HIF1A with IgG (H+L) HRP (red) to observe the fluorescence of Alexa Fluor® 555. The scale bar is 25 µm.

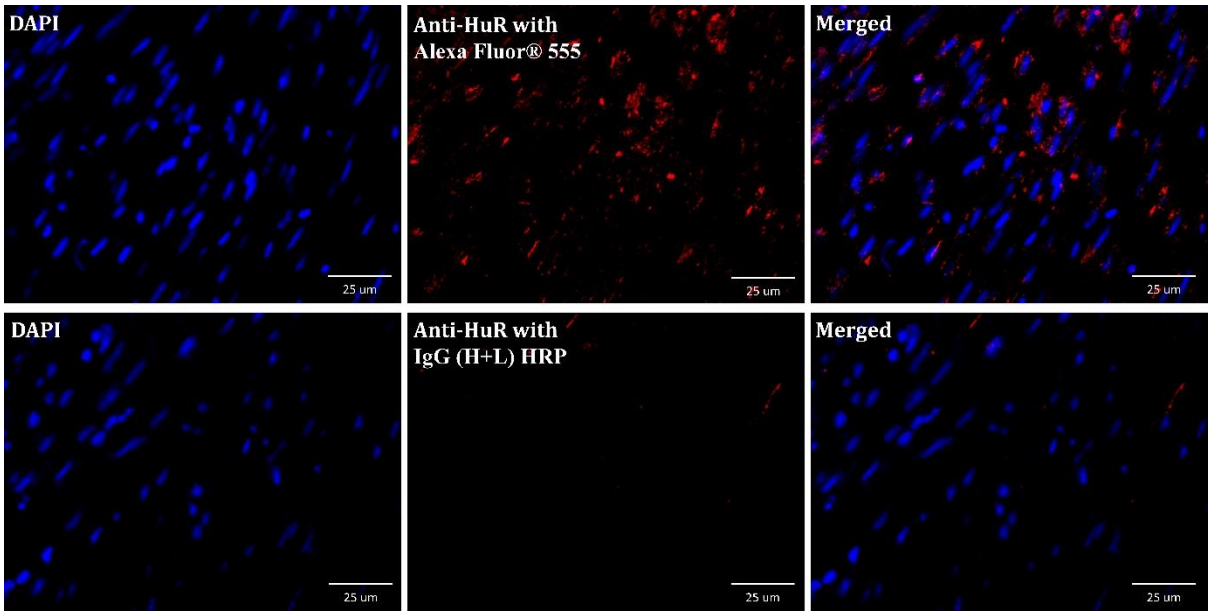

Supplementary figure 7: Immunofluorescence image of fluorescence activity validation for secondary Ab Alexa Fluor® 555. Same samples, but different sections were treated with Anti- HuR with Alexa Fluor® 555 (red) and Anti- HuR with IgG (H+L) HRP (red) to observe the fluorescence of Alexa Fluor® 555. The scale bar is 25 µm.

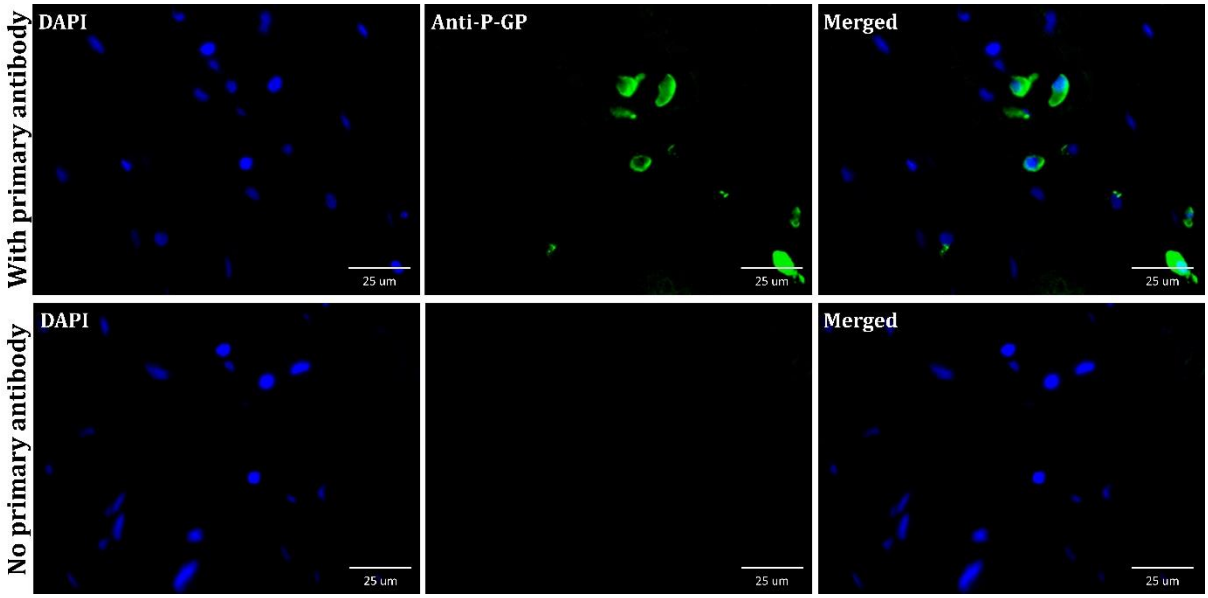

Supplementary figure 8: Immunofluorescence image of binding specificity validation for secondary Ab Alexa Fluor® 488. Same samples, but different sections were treated with (green) and without Anti-P-GP to observe the non-specific binding of Alexa Fluor® 488. The scale bar is 25 µm.

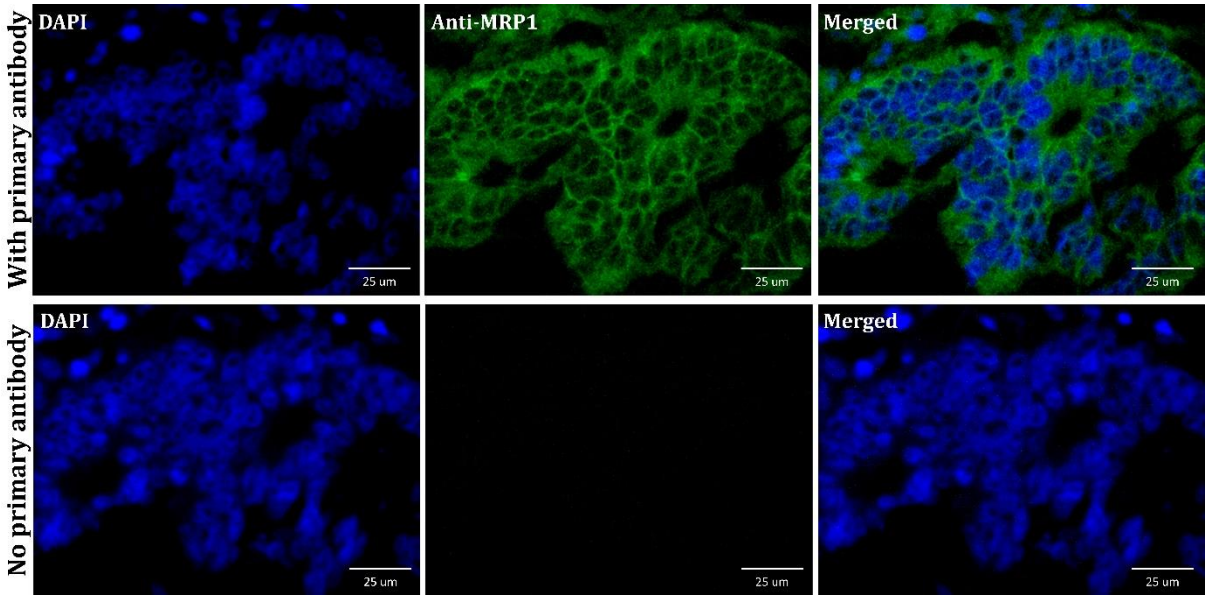

Supplementary figure 9: Immunofluorescence image of binding specificity validation for secondary Ab Alexa Fluor® 488. Same samples, but different sections were treated with (green) and without Anti-MRP1 to observe the non-specific binding of Alexa Fluor® 488. The scale bar is 25 µm.

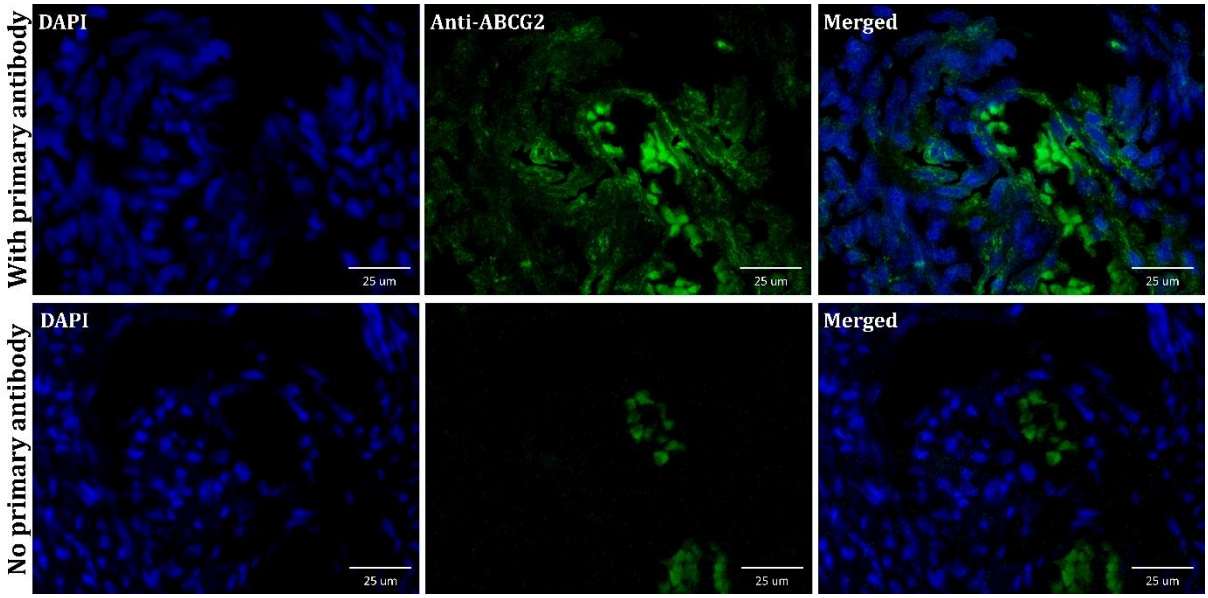

Supplementary figure 10: Immunofluorescence image of binding specificity validation for secondary Ab Alexa Fluor® 488. Same samples, but different sections were treated with (green) and without Anti-ABCG2 to observe the non-specific binding of Alexa Fluor® 488. The scale bar is 25 µm.

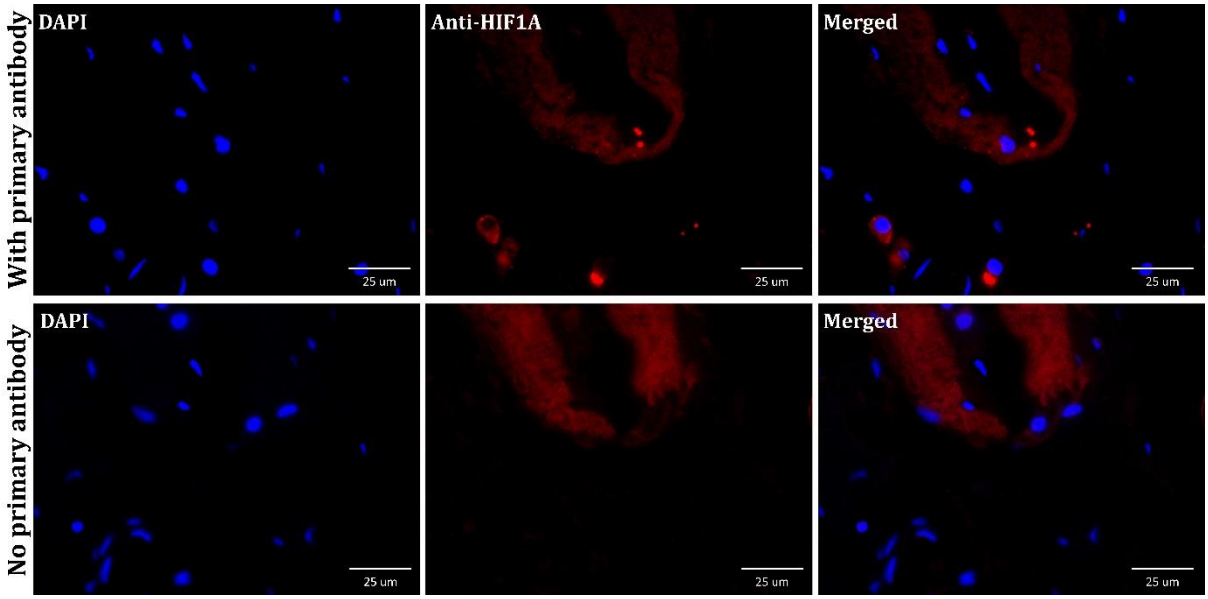

Supplementary figure 11: Immunofluorescence image of binding specificity validation for secondary Ab Alexa Fluor® 555. Same samples, but different sections were treated with (red) and without Anti-HIF1A to observe the non-specific binding of Alexa Fluor® 555. The scale bar is 25 µm.

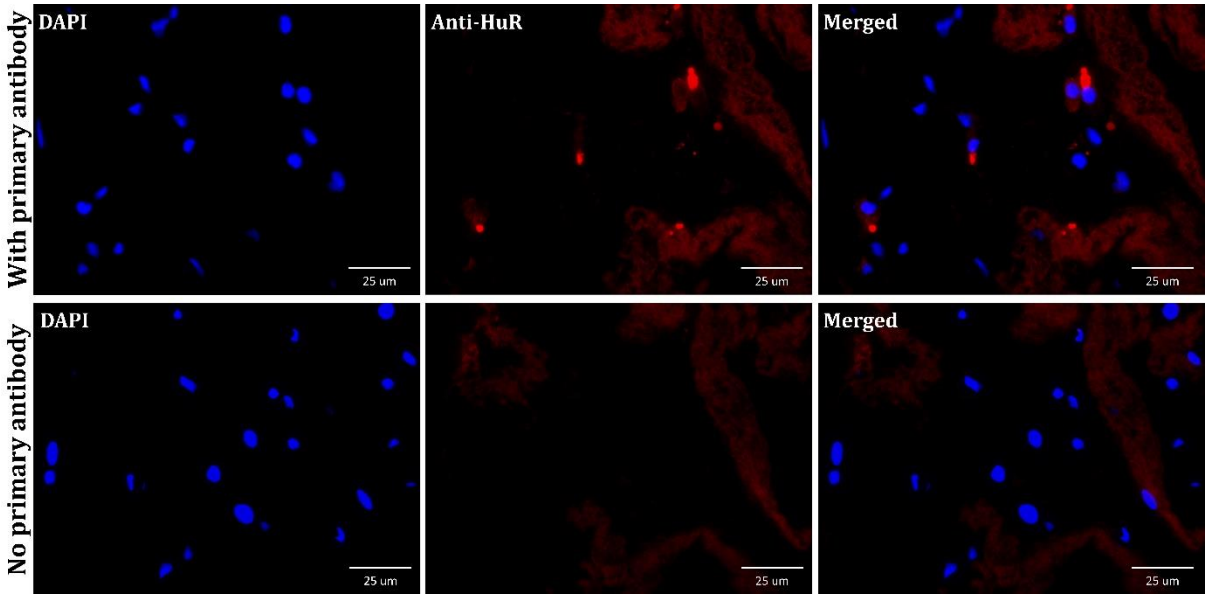

Supplementary figure 12: Immunofluorescence image of binding specificity validation for secondary Ab Alexa Fluor® 555. Same samples, but different sections were treated with (red) and without Anti-HuR to observe the non-specific binding of Alexa Fluor® 555. The scale bar is 25 µm.

Supplementary table 1: Normality tests for ABC transporters expression in breast cancer

Normality tests	P-GP (Chemoresistant)	P-GP (Control)	MRP1 (Chemoresistant)	MRP1 (Control)	ABCG2 (Chemoresistant)	ABCG2 (Control)
D'Agostino & Pearson test						
P value	0.0053	<0.0001	0.0411	0.0022	0.0006	0.0039
Passed normality test?	No	No	No	No	No	No
Anderson-Darling test						
P value	0.0212	<0.0001	0.2287	<0.0001	0.1042	<0.0001
Passed normality test?	No	No	Yes	No	Yes	No
Shapiro-Wilk test						
P value	0.0137	<0.0001	0.0945	<0.0001	0.0160	0.0002
Passed normality test?	No	No	Yes	No	No	No
Kolmogorov-Smirnov test						
P value	0.0040	<0.0001	>0.1000	<0.0001	>0.1000	0.0005
Passed normality test?	No	No	Yes	No	Yes	No

Supplementary table 2: Normality tests for ABC transporters expression in CRC

Normality tests	P-GP (Chemoresistant)	P-GP (Control)	MRP1 (Chemoresistant)	MRP1 (Control)	ABCG2 (Chemoresistant)	ABCG2 (Control)
D'Agostino & Pearson test						
P value	0.8135	<0.0001	0.0551	0.0893	0.6284	0.4443
Passed normality test?	Yes	No	Yes	Yes	Yes	Yes
Anderson-Darling test						
P value	0.8894	<0.0001	0.007	0.0258	0.9297	0.3195
Passed normality test?	Yes	No	No	No	Yes	Yes
Shapiro-Wilk test						
P value	0.8282	<0.0001	0.0046	0.0125	0.9665	0.2208
Passed normality test?	Yes	No	No	No	Yes	Yes
Kolmogorov-Smirnov test						
P value	>0.1000	0.0003	0.0791	0.0671	>0.1000	>0.1000
Passed normality test?	Yes	No	Yes	Yes	Yes	Yes

Supplementary table 3: Normality tests for ABC transporters expression in ovarian cancer

Normality tests	P-GP (Chemoresistant)	P-GP (Control)	MRP1 (Chemoresistant)	MRP1 (Control)	ABCG2 (Chemoresistant)	ABCG2 (Control)
D'Agostino & Pearson test						
P value	0.1846	0.5957	0.0005	0.12	0.3209	0.0239
Passed normality test?	Yes	Yes	No	Yes	Yes	No
Anderson-Darling test						
P value	0.4258	0.3173	0.0044	0.0925	0.4869	0.0418
Passed normality test?	Yes	Yes	No	Yes	Yes	No
Shapiro-Wilk test						
P value	0.4223	0.2673	0.0024	0.0988	0.5046	0.0256
Passed normality test?	Yes	Yes	No	Yes	Yes	No
Kolmogorov-Smirnov test						
P value	>0.1000	>0.1000	0.0132	>0.1000	>0.1000	>0.1000
Passed normality test?	Yes	Yes	No	Yes	Yes	Yes

Supplementary table 4: Normality tests for HIF1A expression in breast cancer

Normality tests	**Chemoresistant**	**Control**
D'Agostino & Pearson test		
P value	0.2515	<0.0001
Passed normality test?	Yes	No
Anderson-Darling test		
P value	0.0470	<0.0001
Passed normality test?	No	No
Shapiro-Wilk test		
P value	0.0325	<0.0001
Passed normality test?	No	No
Kolmogorov-Smirnov test		
P value	>0.1000	<0.0001
Passed normality test?	Yes	No

Supplementary table 5: Normality tests for HIF1A expression in CRC

Normality tests	**Chemoresistant**	**Control**
D'Agostino & Pearson test		
P value	0.0007	0.3856
Passed normality test?	No	Yes
Anderson-Darling test		
P value	0.0004	0.2237
Passed normality test?	No	Yes
Shapiro-Wilk test		
P value	0.0005	0.1870
Passed normality test?	No	Yes
Kolmogorov-Smirnov test		
P value	0.0112	>0.1000
Passed normality test?	No	Yes

Supplementary table 6: Normality tests for HIF1A expression in ovarian cancer

Normality tests	Chemoresistant	Control
D'Agostino & Pearson test		
P value	0.1610	0.1317
Passed normality test?	Yes	Yes
Anderson-Darling test		
P value	0.0822	0.1336
Passed normality test?	Yes	Yes
Shapiro-Wilk test		
P value	0.0673	0.1646
Passed normality test?	Yes	Yes
Kolmogorov-Smirnov test		
P value	>0.1000	0.0665
Passed normality test?	Yes	Yes

Supplementary table 7: Normality tests for HuR expression in breast cancer

Normality tests	Chemoresistant	Control
D'Agostino & Pearson test		
P value	<0.0001	<0.0001
Passed normality test?	No	No
Anderson-Darling test		
P value	0.0033	<0.0001
Passed normality test?	No	No
Shapiro-Wilk test		
P value	0.0002	<0.0001
Passed normality test?	No	No
Kolmogorov-Smirnov test		
P value	>0.1000	<0.0001
Passed normality test?	Yes	No

Supplementary table 8: Normality tests for HuR expression in CRC

Normality tests	Chemoresistant	Control
D'Agostino & Pearson test		
P value	0.0431	0.0304
Passed normality test?	No	No
Anderson-Darling test		
P value	0.0440	0.0962
Passed normality test?	No	Yes
Shapiro-Wilk test		
P value	0.0338	0.0460
Passed normality test?	No	No
Kolmogorov-Smirnov test		
P value	0.0251	>0.1000
Passed normality test?	No	Yes

Supplementary table 9: Normality tests for HuR expression in ovarian cancer

Normality tests	Chemoresistant	Control
D'Agostino & Pearson test		
P value	0.1699	0.6870
Passed normality test?	Yes	Yes
Anderson-Darling test		
P value	0.0765	0.7842
Passed normality test?	Yes	Yes
Shapiro-Wilk test		
P value	0.0920	0.7872
Passed normality test?	Yes	Yes
Kolmogorov-Smirnov test		
P value	0.0496	>0.1000
Passed normality test?	No	Yes

Supplementary table 10: All information on molecular docking of HIF1A protein and 'CGTG' sequence from the promoter region of ABC transporters DNA

AA region of HIF1A	HADDOCK score	Cluster size	RMSD from the overall lowest-energy structure	Van der Waals energy	Electrostatic energy	Desolvation energy	Restraints violation energy	Buried Surface Area	Z-Score
P-GP promoter region									
238--348	28.5 +/- 9.7	8	23.9 +/- 0.6	-69.8 +/- 7.2	-74.9 +/- 39.5	-3.4 +/- 2.5	1166.7 +/- 96.9	1717.0 +/- 83.9	-1.7
395-411	-59.0 +/- 0.5	121	39.7 +/- 1.2	-48.1 +/- 2.8	-78.0 +/- 8.5	-4.3 +/- 3.1	90.3 +/- 28.6	1299.2 +/- 121.6	-2.3
549-582	-28.2 +/- 10.7	9	87.5 +/- 0.1	-39.2 +/- 6.4	-153.1 +/- 45.1	-0.1 +/- 1.2	416.8 +/- 56.4	1298.9 +/- 152.9	-2.1
717-757	-75.8 +/- 10.2	16	86.4 +/- 0.3	-69.3 +/- 7.5	-294.9 +/- 50.2	4.3 +/- 4.2	481.1 +/- 32.0	2530.3 +/- 153.1	-1.7
775-826	-90.0 +/- 1.7	5	10.9 +/- 2.5	-73.2 +/- 11.1	-346.2 +/- 47.0	7.1 +/- 2.2	452.0 +/- 24.1	2115.4 +/- 303.8	-1.3
MRP1 promoter region									
238--348	11.7 +/- 9.0	7	38.3 +/- 0.6	-57.3 +/- 5.4	-237.6 +/- 37.8	5.5 +/- 4.4	1110.3 +/- 67.8	1457.7 +/- 97.8	-1.1
395-411	-65.0 +/- 2.6	108	72.6 +/- 0.5	-50.4 +/- 5.0	-99.7 +/- 9.2	-4.3 +/- 2.6	97.3 +/- 25.6	1365.1 +/- 47.8	-1.8
549-582	-44.8 +/- 4.3	8	4.9 +/- 2.8	-45.2 +/- 4.4	-167.6 +/- 36.4	-1.6 +/- 0.8	355.3 +/- 96.4	1355.9 +/- 220.7	-2.5
717-757	-85.4 +/- 1.5	15	88.4 +/- 0.3	-69.9 +/- 5.7	-320.7 +/- 12.6	-2.9 +/- 2.6	516.2 +/- 66.8	2234.9 +/- 230.7	-2.3
775-826	-85.4 +/- 1.5	15	88.4 +/- 0.3	-69.9 +/- 5.7	-320.7 +/- 12.6	-2.9 +/- 2.6	516.2 +/- 66.8	2234.9 +/- 230.7	-2.3
ABCG2 promoter region									
238--348	24.6 +/- 6.0	33	33.8 +/- 0.9	-67.5 +/- 9.0	-60.4 +/- 14.1	-8.4 +/- 3.4	1125.3 +/- 105.3	1652.7 +/- 140.2	-2
395-411	-58.2 +/- 1.8	118	50.5 +/- 0.7	-45.8 +/- 4.2	-84.8 +/- 12.1	-4.4 +/- 2.5	89.5 +/- 42.6	1267.1 +/- 67.7	-1.6
549-582	-47.8 +/- 4.3	12	89.3 +/- 0.1	-44.7 +/- 4.6	-207.3 +/- 20.0	-2.3 +/- 2.4	407.0 +/- 25.1	1363.0 +/- 97.7	-2.6
717-757	-82.8 +/- 28.3	8	60.3 +/- 0.3	-65.2 +/- 11.7	-342.0 +/- 87.9	-2.4 +/- 5.4	532.1 +/- 73.1	2199.8 +/- 160.1	-1.9
775-826	-88.7 +/- 11.3	77	1.7 +/- 1.1	-88.6 +/- 11.4	-211.1 +/- 25.2	-2.0 +/- 1.8	440.2 +/- 33.8	2227.7 +/- 163.7	-1.1

Supplementary table 11: Normality tests for ABC transporters and HIF1A co-expression in chemoresistant breast cancer

Normality tests	Co_P-GP+HIF1 (Chemoresistant)	Co_P-GP+HIF1A (Control)	Co_MRP1+HIF1A (Chemoresistant)	Co_MRP1+HIF1A (Control)	Co_ABCG2+HIF1 A (Chemoresistant)	Co_ABCG2+HIF1 A (Control)
D' Agostino & Pearson test						
P value	0.0278	<0.0001	0.0063	<0.0001	0.5625	<0.0001
Passed normality test?	No	No	No	No	Yes	No
Anderson-Darling test						
P value	0.0425	<0.0001	0.0006	<0.0001	0.4897	<0.0001
Passed normality test?	No	No	No	No	Yes	No
Shapiro-Wilk test						
P value	0.0271	<0.0001	0.0012	<0.0001	0.4086	<0.0001
Passed normality test?	No	No	No	No	Yes	No
Kolmogorov-Smirnov test						
P value	>0.1000	<0.0001	0.0027	<0.0001	>0.1000	<0.0001
Passed normality test?	Yes	No	No	No	Yes	No

Supplementary table 12: Normality tests for ABC transporters and HIF1A co-expression in chemoresistant CRC

Normality tests	Co_P-GP+HIF1 (Chemoresistant)	Co_P-GP+HIF1A (Control)	Co_MRP1+HIF1A (Chemoresistant)	Co_MRP1+HIF1A (Control)	Co_ABCG2+HIF1A (Chemoresistant)	Co_ABCG2+HIF1A (Control)
D' Agostino & Pearson test						
P value	0.0006	0.6269	0.0212	0.0773	0.6694	0.9025
Passed normality test?	No	Yes	No	Yes	Yes	Yes
Anderson-Darling test						
P value	<0.0001	0.0158	<0.0001	0.0207	0.6535	0.0975
Passed normality test?	No	No	No	No	Yes	Yes
Shapiro-Wilk test						
P value	0.0002	0.0144	0.0003	0.0185	0.5762	0.1019
Passed normality test?	No	No	No	No	Yes	Yes
Kolmogorov-Smirnov test						
P value	<0.0001	0.0124	<0.0001	0.0146	>0.1000	>0.1000
Passed normality test?	No	No	No	No	Yes	Yes

Supplementary table 13: Normality tests for ABC transporters and HIF1A co-expression in chemoresistant ovarian cancer

Normality tests	Co_P-GP+HIF1A (Chemoresistant)	Co_P-GP+HIF1A (Control)	Co_MRP1+HIF1A (Chemoresistant)	Co_MRP1+HIF1A (Control)	Co_ABCG2+HIF1A (Chemoresistant)	Co_ABCG2+HIF1A (Control)
D' Agostino & Pearson test						
P value	0.0618	0.2883	0.2271	0.8199	0.0042	0.4458
Passed normality test?	Yes	Yes	Yes	Yes	No	Yes
Anderson-Darling test						
P value	0.0042	0.0776	0.0264	0.5723	0.0384	0.2788
Passed normality test?	No	Yes	No	Yes	No	Yes
Shapiro-Wilk test						
P value	0.0046	0.0742	0.0222	0.6096	0.0248	0.2015
Passed normality test?	No	Yes	No	Yes	No	Yes
Kolmogorov-Smirnov test						
P value	0.0025	0.0684	0.0416	>0.1000	0.0536	>0.1000
Passed normality test?	No	Yes	No	Yes	Yes	Yes

Supplementary table 14: All information on molecular docking of HuR protein and AU-rich region from the 3'UTR of *P-GP* mRNA

AU-rich regions	HADDOCK score	Cluster size	RMSD from the overall lowest-energy structure	Van der Waals energy	Electrostatic energy	Desolvation energy	Restraints violation energy	Buried Surface Area	Z-Score
UUUGUUU	-45.8 +/- 2.9	65	0.4 +/- 0.3	-58.4 +/- 4.3	-251.6 +/- 12.3	11.7 +/- 1.2	512.2 +/- 51.2	1440.0 +/- 51.7	-2.5
AAAUUUUAUAA	-47.9 +/- 4.5	32	0.6 +/- 0.4	-65.9 +/- 5.4	-286.3 +/- 25.3	19.7 +/- 2.6	555.7 +/- 81.9	1700.0 +/- 64.3	-2.2
AUUUU	-27.3 +/- 4.0	32	0.2 +/- 0.1	-63.5 +/- 2.2	-255.9 +/- 10.4	13.0 +/- 0.5	744.5 +/- 26.7	1232.0 +/- 29.9	-2.2
AAAUUUUAU	-32.9 +/- 11.4	14	0.3 +/- 0.2	-57.3 +/- 2.9	-218.0 +/- 11.4	10.0 +/- 1.6	580.5 +/- 100.8	1412.6 +/- 46.3	-2.1
AUUUUAU	-35.1 +/- 6.5	11	0.6 +/- 0.5	-50.3 +/- 2.9	-295.4 +/- 38.4	13.6 +/- 3.9	607.1 +/- 91.8	1373.9 +/- 34.4	-1.9
AUUUA	-18.3 +/- 7.1	61	0.5 +/- 0.3	-56.8 +/- 8.8	-188.3 +/- 34.0	8.6 +/- 3.8	674.9 +/- 66.2	1303.0 +/- 79.1	-1.7
UUUUA	-10.3 +/- 1.9	49	0.5 +/- 0.3	-49.9 +/- 9.9	-203.7 +/- 28.6	9.1 +/- 2.9	711.9 +/- 48.0	1114.2 +/- 83.1	-1.7
GUUUG	-21.8 +/- 2.2	52	0.6 +/- 0.5	-48.3 +/- 6.8	-245.8 +/- 11.7	12.8 +/- 2.4	628.1 +/- 47.3	1145.2 +/- 108.1	-1.6
AAUUUUAUA	-24.5 +/- 5.0	40	5.2 +/- 0.1	-57.5 +/- 2.5	-194.7 +/- 35.5	14.5 +/- 2.2	573.1 +/- 90.7	1384.5 +/- 46.7	-1.5
AUAAAUUUUAUAA	-43.4 +/- 6.4	26	0.9 +/- 0.6	-69.0 +/- 11.2	-265.0 +/- 28.0	19.0 +/- 2.1	596.3 +/- 81.1	1769.0 +/- 113.4	-1.5
AUUUUAA	-25.3 +/- 2.1	44	3.6 +/- 0.1	-53.4 +/- 3.6	-240.9 +/- 27.1	14.2 +/- 3.7	620.8 +/- 65.0	1365.4 +/- 48.7	-1.5
UAAAUUUUAUA	-29.0 +/- 1.6	24	6.1 +/- 0.1	-62.8 +/- 6.6	-249.2 +/- 27.7	15.8 +/- 3.1	679.2 +/- 36.9	1552.6 +/- 78.9	-1.5
AUUAAA	-53.9 +/- 7.7	58	0.4 +/- 0.2	-68.4 +/- 2.4	-231.4 +/- 9.9	8.5 +/- 1.5	523.1 +/- 73.2	1465.3 +/- 32.3	-1.4
AAUUUUA	-18.9 +/- 5.6	23	0.5 +/- 0.4	-52.2 +/- 4.3	-226.2 +/- 14.5	9.9 +/- 2.4	686.5 +/- 75.1	1123.5 +/- 86.2	-1.3
UUUUU	-9.9 +/- 5.1	51	1.0 +/- 0.2	-48.7 +/- 4.1	-220.5 +/- 22.6	8.0 +/- 2.1	748.7 +/- 54.3	1092.2 +/- 38.5	-1.3
UUUUUAA	-28.8 +/- 2.5	51	1.7 +/- 0.1	-44.8 +/- 7.8	-254.3 +/- 33.6	12.4 +/- 1.3	544.7 +/- 61.9	1332.7 +/- 98.5	-1.2
AAUAAA	-9.9 +/- 1.9	28	2.2 +/- 0.0	-54.6 +/- 2.6	-179.1 +/- 3.4	8.7 +/- 1.8	718.2 +/- 19.0	1066.2 +/- 21.4	-0.9

Supplementary table 15: All information on molecular docking of HuR protein and AU-rich region from the 3'UTR of *MRP1* mRNA

AU-rich regions	HADDOCK score	Cluster size	RMSD from the overall lowest-energy structure	Van der Waals energy	Electrostatic energy	Desolvation energy	Restraints violation energy	Buried Surface Area	Z-Score
UUAUUUUUU	-52.6 +/- 11.5	65	0.7 +/- 0.5	-60.4 +/- 7.6	-311.2 +/- 14.0	16.2 +/- 2.5	538.3 +/- 79.6	1646.7 +/- 109.5	-2.5
UUUUUUUUUAA	-69.0 +/- 4.0	17	3.3 +/- 0.0	-95.0 +/- 11.7	-223.0 +/- 14.0	23.4 +/- 1.7	472.1 +/- 56.4	1988.3 +/- 82.3	-2.3
UUUUUUUUUUUAA	-58.5 +/- 4.5	9	6.4 +/- 0.1	-79.8 +/- 6.8	-284.1 +/- 31.2	22.6 +/- 2.8	555.4 +/- 48.6	1930.9 +/- 133.0	-2.3
UAUAUUUAUUU	-63.7 +/- 4.2	15	0.6 +/- 0.4	-73.7 +/- 5.1	-274.0 +/- 19.7	17.4 +/- 3.6	474.9 +/- 26.0	1887.5 +/- 123.7	-2.2
UUUUUUA	-35.1 +/- 3.6	66	0.6 +/- 0.3	-51.1 +/- 9.3	-267.1 +/- 30.1	15.5 +/- 1.3	539.6 +/- 64.3	1450.2 +/- 85.6	-2.2
AUUUU	5.1 +/- 7.9	5	0.3 +/- 0.2	-55.3 +/- 7.3	-110.5 +/- 12.4	8.8 +/- 2.1	737.5 +/- 97.1	1174.5 +/- 73.1	-2.1
UAUUUUU	-34.4 +/- 6.2	75	0.4 +/- 0.3	-56.1 +/- 8.5	-265.4 +/- 23.8	13.6 +/- 0.9	611.8 +/- 72.8	1467.1 +/- 92.0	-2.1
UUUUUUUUUUUUA	-67.2 +/- 7.0	8	0.5 +/- 0.3	-77.7 +/- 1.9	-347.5 +/- 30.9	28.4 +/- 3.4	515.4 +/- 107.0	1961.0 +/- 37.1	-2.1
UUUUUUU	-35.1 +/- 1.7	62	0.8 +/- 0.1	-55.6 +/- 6.7	-273.4 +/- 11.1	13.3 +/- 1.4	618.7 +/- 74.2	1456.6 +/- 18.9	-2
UUUUUUUAA	-62.5 +/- 6.2	45	0.4 +/- 0.2	-71.2 +/- 7.8	-288.8 +/- 17.0	18.5 +/- 1.1	480.2 +/- 113.5	1842.1 +/- 38.9	-1.9
UUUUUUUUA	-54.0 +/- 5.2	16	0.8 +/- 0.6	-69.5 +/- 7.3	-286.5 +/- 29.9	14.8 +/- 2.2	580.0 +/- 64.1	1733.4 +/- 37.7	-1.9
AUUUUUU	-36.3 +/- 7.3	84	0.7 +/- 0.4	-49.8 +/- 2.8	-276.6 +/- 21.2	15.7 +/- 1.1	531.5 +/- 87.4	1366.8 +/- 58.2	-1.8
AUUUUUUUUUU	-47.3 +/- 7.3	17	5.9 +/- 0.1	-80.9 +/- 8.7	-196.9 +/- 43.7	15.6 +/- 3.3	573.5 +/- 51.9	1692.8 +/- 128.5	-1.8
UAUUUAU	-29.9 +/- 1.5	65	0.3 +/- 0.2	-48.8 +/- 4.4	-248.0 +/- 36.8	12.7 +/- 2.7	557.2 +/- 49.6	1293.6 +/- 53.9	-1.8
UUUUA	-20.8 +/- 5.0	34	0.3 +/- 0.2	-62.8 +/- 7.2	-181.0 +/- 23.4	8.9 +/- 3.7	693.7 +/- 60.9	1302.3 +/- 40.5	-1.8
UUUUU	-23.1 +/- 5.0	40	0.5 +/- 0.5	-52.2 +/- 4.8	-206.7 +/- 11.4	8.8 +/- 2.9	616.4 +/- 54.2	1238.0 +/- 125.4	-1.7
UUUUUAA	-47.4 +/- 1.7	71	0.9 +/- 0.5	-57.8 +/- 5.4	-258.9 +/- 17.1	12.8 +/- 1.4	493.7 +/- 85.8	1507.4 +/- 21.1	-1.7
UUUUUUUUUUA	-54.8 +/- 13.8	4	0.7 +/- 0.4	-72.6 +/- 3.4	-309.5 +/- 44.3	23.6 +/- 2.1	561.0 +/- 104.0	1830.9 +/- 53.7	-1.7
UUUUUUUUUUU	-55.2 +/- 10.2	14	6.1 +/- 0.1	-63.3 +/- 8.9	-323.3 +/- 21.9	20.5 +/- 3.5	521.9 +/- 119.3	1789.0 +/- 53.0	-1.7
AUAUAUUUAUUUU	-42.8 +/- 7.4	5	3.8 +/- 0.1	-67.3 +/- 5.9	-250.9 +/- 26.5	16.1 +/- 1.9	585.5 +/- 63.6	1702.8 +/- 79.2	-1.5

AU-rich regions	**HADDOCK score**	**Cluster size**	**RMSD from the overall lowest-energy structure**	**Van der Waals energy**	**Electrostatic energy**	**Desolvation energy**	**Restraints violation energy**	**Buried Surface Area**	**Z-Score**
AUUUA	-14.2 +/- 10.2	46	0.3 +/- 0.2	-44.3 +/- 3.5	-240.3 +/- 18.5	12.2 +/- 1.5	659.7 +/- 51.4	1131.8 +/- 36.1	-1.4
AUUUUUUUU	-10.2 +/- 3.1	39	4.5 +/- 0.2	-67.6 +/- 5.6	-48.0 +/- 6.9	5.3 +/- 5.3	617.5 +/- 80.0	1480.5 +/- 108.9	-1.4
AUAUUUAUU	-37.6 +/- 9.7	35	0.6 +/- 0.3	-57.6 +/- 4.6	-275.0 +/- 31.9	16.3 +/- 2.9	586.7 +/- 90.6	1523.4 +/- 120.4	-1.2
AUUUUUUUUUUUU	-42.0 +/- 2.8	14	7.3 +/- 0.4	-61.8 +/- 4.9	-283.1 +/- 82.0	20.2 +/- 4.9	563.0 +/- 70.1	1747.1 +/- 90.0	-1.2
GUUUG	-1.4 +/- 9.6	34	1.1 +/- 0.7	-45.1 +/- 6.6	-150.0 +/- 32.8	4.9 +/- 1.5	688.0 +/- 72.9	982.5 +/- 103.9	-1.2
UUUUUUUUU	-34.8 +/- 10.8	6	4.5 +/- 0.1	-76.6 +/- 5.1	-227.2 +/- 22.7	21.0 +/- 1.0	662.2 +/- 60.1	1761.6 +/- 28.5	-1.2

Supplementary table 16: All information on molecular docking of HuR protein and AU-rich region from the 3'UTR of *ABCG2* TV1 mRNA

AU-rich regions	HADDOCK score	Cluster size	RMSD from the overall lowest-energy structure	Van der Waals energy	Electrostatic energy	Desolvation energy	Restraints violation energy	Buried Surface Area	Z-Score
UUAUUUAAU	-62.2 +/- 5.0	31	0.4 +/- 0.2	-82.7 +/- 4.8	-268.1 +/- 21.1	11.9 +/- 1.8	622.5 +/- 54.3	2060.8 +/- 54.6	-2.5
UAAUUUAUU	-73.0 +/- 5.2	36	0.4 +/- 0.2	-79.8 +/- 2.3	-306.3 +/- 13.8	16.1 +/- 1.2	519.7 +/- 62.6	1863.5 +/- 32.0	-2.4
UUUUUUU	-32.2 +/- 6.5	34	0.5 +/- 0.3	-54.3 +/- 3.6	-241.7 +/- 30.6	13.5 +/- 1.6	569.4 +/- 84.6	1361.0 +/- 57.3	-2.3
AUAUUUUUA	-56.3 +/- 1.2	86	0.5 +/- 0.3	-65.9 +/- 3.1	-255.3 +/- 11.8	13.0 +/- 0.5	475.9 +/- 28.6	1581.8 +/- 56.3	-2.1
UAUUUAA	-35.9 +/- 1.0	41	0.8 +/- 0.6	-55.7 +/- 9.1	-262.5 +/- 31.8	13.1 +/- 1.0	591.8 +/- 105.6	1513.0 +/- 97.8	-2.1
AUUAUUUAAUA	-52.0 +/- 6.2	10	0.8 +/- 0.5	-60.5 +/- 8.1	-270.5 +/- 34.3	10.4 +/- 3.6	520.7 +/- 83.3	1637.5 +/- 69.4	-2
UUAAUUUUAUU	-66.9 +/- 5.4	74	0.5 +/- 0.3	-68.3 +/- 6.7	-251.7 +/- 28.8	10.6 +/- 2.4	412.4 +/- 57.0	1679.5 +/- 40.8	-2
UUUAAUUUUAUUU	-82.0 +/- 8.3	54	0.5 +/- 0.3	-81.6 +/- 4.6	-286.6 +/- 20.6	16.7 +/- 2.3	402.6 +/- 87.8	1957.5 +/- 28.1	-2
UUUUAUUUUUUUA	-51.5 +/- 6.8	14	0.5 +/- 0.3	-66.1 +/- 6.4	-305.2 +/- 20.0	18.3 +/- 2.7	573.4 +/- 129.8	1806.6 +/- 63.8	-2
UUAUUUUUUUA	-37.4 +/- 4.5	4	3.1 +/- 0.1	-64.3 +/- 4.0	-274.7 +/- 6.7	12.3 +/- 0.9	695.7 +/- 57.3	1399.5 +/- 39.6	-1.8
UUUAUUUUUUU	-38.3 +/- 9.2	16	4.6 +/- 0.1	-63.1 +/- 7.0	-244.6 +/- 21.5	9.6 +/- 1.6	640.9 +/- 63.3	1632.1 +/- 64.2	-1.8
UUUGUUU	-24.3 +/- 10.7	6	0.5 +/- 0.3	-42.6 +/- 5.1	-357.4 +/- 45.5	12.0 +/- 1.8	777.6 +/- 38.1	1150.4 +/- 43.5	-1.8
UUUUUAA	-47.3 +/- 6.5	65	1.0 +/- 0.6	-64.8 +/- 4.3	-237.9 +/- 23.3	12.7 +/- 1.6	524.4 +/- 61.4	1608.1 +/- 75.9	-1.8
UUUUUUA	-47.9 +/- 3.0	55	2.1 +/- 0.2	-62.6 +/- 11.6	-264.5 +/- 18.6	15.8 +/- 1.6	519.1 +/- 92.2	1556.4 +/- 76.5	-1.8
AUUUUAU	-31.2 +/- 5.3	99	0.6 +/- 0.4	-57.0 +/- 1.2	-201.7 +/- 13.1	14.9 +/- 3.3	512.9 +/- 85.3	1383.8 +/- 47.1	-1.7
GUUUG	-23.8 +/- 2.4	39	0.3 +/- 0.2	-55.0 +/- 3.4	-207.8 +/- 15.4	14.9 +/- 1.8	579.3 +/- 28.9	1142.0 +/- 35.0	-1.7
UUUUUUAAA	-28.7 +/- 4.0	20	1.8 +/- 0.3	-66.0 +/- 4.3	-213.2 +/- 26.1	22.4 +/- 3.1	575.4 +/- 96.5	1719.7 +/- 57.3	-1.7
AAUAAA	-29.4 +/- 18.0	7	0.3 +/- 0.2	-48.8 +/- 5.0	-292.6 +/- 13.9	9.7 +/- 1.1	681.8 +/- 142.5	1181.6 +/- 37.0	-1.6
AUUUUUU	-9.3 +/- 1.2	25	2.3 +/- 0.1	-45.0 +/- 6.0	-238.1 +/- 49.5	12.1 +/- 1.8	711.7 +/- 49.9	1085.4 +/- 43.4	-1.6
UUUUA	-11.9 +/- 2.6	62	0.6 +/- 0.4	-42.1 +/- 6.5	-171.8 +/- 10.6	5.8 +/- 1.3	588.1 +/- 55.7	1049.6 +/- 99.7	-1.6

AU-rich regions	HADDOCK score	Cluster size	RMSD from the overall lowest-energy structure	Van der Waals energy	Electrostatic energy	Desolvation energy	Restraints violation energy	Buried Surface Area	Z-Score
AAUUUAU	-34.6 +/- 5.3	46	1.4 +/- 0.9	-63.3 +/- 4.4	-222.6 +/- 30.0	16.3 +/- 2.1	569.6 +/- 50.2	1403.9 +/- 83.6	-1.5
AUUAAA	-29.6 +/- 1.4	54	1.4 +/- 0.3	-52.2 +/- 5.0	-206.2 +/- 20.8	11.6 +/- 2.4	522.6 +/- 37.0	1336.9 +/- 84.5	-1.5
UAUUUUUAU	-59.3 +/- 10.5	49	0.9 +/- 0.7	-67.2 +/- 3.6	-267.9 +/- 22.9	11.3 +/- 2.0	501.1 +/- 90.9	1589.0 +/- 116.6	-1.5
UUUUU	-10.0 +/- 4.9	51	0.7 +/- 0.4	-40.5 +/- 9.2	-192.5 +/- 29.1	9.3 +/- 2.0	597.3 +/- 51.0	1014.4 +/- 61.3	-1.5
UUUUUAU	-40.3 +/- 4.0	58	3.0 +/- 0.2	-64.8 +/- 5.4	-198.2 +/- 27.1	12.5 +/- 3.0	516.6 +/- 18.9	1508.0 +/- 58.8	-1.5
AAUUUUA	-23.0 +/- 5.5	89	0.5 +/- 0.3	-55.0 +/- 3.3	-199.6 +/- 34.9	16.5 +/- 1.4	553.5 +/- 31.5	1316.5 +/- 49.5	-1.4
AUUUA	-15.3 +/- 4.3	51	0.7 +/- 0.5	-55.8 +/- 4.2	-174.4 +/- 35.1	9.0 +/- 4.2	663.8 +/- 34.0	1238.3 +/- 76.2	-1.4
AUUUUUUUA	-24.4 +/- 4.4	29	1.5 +/- 0.5	-56.9 +/- 11.4	-234.3 +/- 27.1	11.4 +/- 4.0	679.1 +/- 76.2	1318.0 +/- 117.1	-1.4
UAUUUUUUU	-24.7 +/- 2.8	18	2.9 +/- 0.2	-51.4 +/- 10.4	-270.8 +/- 44.1	13.2 +/- 2.8	676.6 +/- 67.5	1305.7 +/- 105.3	-1.4
AAUUUUAUU	-41.0 +/- 3.0	45	1.6 +/- 0.6	-61.8 +/- 7.5	-196.2 +/- 54.7	12.7 +/- 2.9	473.1 +/- 67.0	1545.1 +/- 10.9	-1.3
AUUUU	-7.5 +/- 5.3	48	0.7 +/- 0.5	-48.6 +/- 7.1	-208.5 +/- 24.4	9.1 +/- 2.6	737.8 +/- 76.8	983.4 +/- 108.7	-1.3
UAAUUUUAUUU	-51.1 +/- 4.7	6	0.6 +/- 0.4	-61.0 +/- 2.9	-293.2 +/- 21.0	14.9 +/- 1.0	535.9 +/- 53.0	1631.3 +/- 43.1	-1.3
UUAAUUUUAUUUU	-61.2 +/- 5.1	52	0.6 +/- 0.5	-70.7 +/- 2.8	-263.7 +/- 17.8	16.3 +/- 2.3	459.5 +/- 42.8	1806.3 +/- 55.4	-1.3
AAUUUAA	-15.3 +/- 2.1	15	1.9 +/- 0.1	-43.9 +/- 1.9	-259.2 +/- 14.5	13.5 +/- 0.7	668.9 +/- 58.3	1222.2 +/- 36.3	-1.2
UAAUUUUAU	-45.7 +/- 5.1	72	0.8 +/- 0.5	-56.5 +/- 6.9	-277.4 +/- 15.7	13.4 +/- 3.2	527.6 +/- 92.2	1552.4 +/- 79.6	-1.2
UAUAUUUUUAU	-47.6 +/- 2.9	6	6.4 +/- 0.3	-56.9 +/- 7.5	-296.0 +/- 39.9	17.8 +/- 4.6	507.4 +/- 81.6	1694.7 +/- 141.5	-1.2
UAUUUUU	-6.4 +/- 9.9	20	2.0 +/- 0.0	-44.0 +/- 6.9	-204.0 +/- 17.1	6.1 +/- 2.7	723.5 +/- 100.0	1091.0 +/- 64.0	-1.2
UUAUUUUUU	-14.9 +/- 2.0	62	2.6 +/- 0.0	-43.8 +/- 8.4	-251.2 +/- 13.3	9.0 +/- 0.5	702.1 +/- 68.7	1162.4 +/- 62.3	-1.2
AUUUUUA	-35.1 +/- 0.7	69	4.3 +/- 0.1	-60.8 +/- 3.0	-217.2 +/- 17.2	14.3 +/- 1.6	548.2 +/- 51.8	1476.5 +/- 39.1	-1.1

Supplementary table 17: All information on molecular docking of HuR protein and AU-rich region from the 3'UTR of *ABCG2* TV2 mRNA

AU-rich regions	HADDOCK score	Cluster size	RMSD from the overall lowest-energy structure	Van der Waals energy	Electrostatic energy	Desolvation energy	Restraints violation energy	Buried Surface Area	Z-Score
UUAUUUUUUUA	-46.3 +/- 6.1	29	0.4 +/- 0.2	-66.4 +/- 3.8	-289.0 +/- 17.4	7.3 +/- 1.6	706.2 +/- 43.9	1411.1 +/- 51.3	-2.6
AAUUUUA	-37.4 +/- 3.6	92	0.4 +/- 0.2	-55.9 +/- 0.7	-235.1 +/- 48.3	12.6 +/- 1.7	528.6 +/- 60.9	1454.1 +/- 40.3	-2.3
UAUUUUU	-34.1 +/- 1.2	34	0.5 +/- 0.3	-64.0 +/- 3.4	-213.6 +/- 39.9	8.5 +/- 2.3	641.1 +/- 85.1	1352.3 +/- 36.4	-2.3
UUUGUUU	-57.7 +/- 5.5	47	0.4 +/- 0.3	-65.3 +/- 3.0	-291.8 +/- 25.2	12.2 +/- 3.0	537.0 +/- 54.4	1528.1 +/- 21.0	-2.3
UAUUUAA	-42.5 +/- 3.4	26	0.5 +/- 0.3	-62.0 +/- 3.8	-284.4 +/- 22.3	12.8 +/- 2.1	635.4 +/- 49.7	1546.1 +/- 113.4	-2.2
AUUUUAU	-26.1 +/- 4.6	79	0.8 +/- 0.5	-57.9 +/- 3.5	-197.0 +/- 47.4	14.9 +/- 2.2	562.5 +/- 76.8	1415.3 +/- 72.2	-2.1
UUUUU	-16.2 +/- 2.4	61	3.9 +/- 0.0	-52.8 +/- 2.3	-204.2 +/- 16.4	15.3 +/- 1.0	621.8 +/- 42.8	1143.5 +/- 46.5	-2.1
UUUUUUA	-43.3 +/- 2.7	64	0.3 +/- 0.2	-66.6 +/- 5.8	-236.7 +/- 20.5	17.8 +/- 1.9	528.0 +/- 74.8	1429.3 +/- 52.7	-2.1
UUUUUUAAA	-58.7 +/- 7.9	52	0.7 +/- 0.5	-63.1 +/- 1.2	-292.0 +/- 28.6	10.9 +/- 2.0	519.0 +/- 98.8	1569.5 +/- 47.6	-2.1
UUUUUUU	-32.7 +/- 4.9	56	3.1 +/- 0.1	-56.5 +/- 3.4	-262.9 +/- 39.7	6.8 +/- 1.7	695.7 +/- 71.7	1360.2 +/- 39.3	-2
AUUUUUA	-37.8 +/- 6.8	84	0.6 +/- 0.5	-51.5 +/- 5.0	-250.7 +/- 33.4	12.2 +/- 2.4	515.8 +/- 69.4	1424.6 +/- 63.7	-1.9
GUUUG	-20.7 +/- 5.3	21	0.4 +/- 0.3	-52.5 +/- 2.2	-200.5 +/- 24.9	16.3 +/- 0.9	556.3 +/- 48.2	1096.2 +/- 53.6	-1.9
UAUUUUUAU	-40.4 +/- 6.5	58	0.4 +/- 0.2	-77.2 +/- 1.0	-198.4 +/- 6.3	16.5 +/- 0.4	599.3 +/- 70.8	1636.4 +/- 44.4	-1.9
AUUUUUUUA	-34.5 +/- 7.1	9	3.7 +/- 0.0	-70.2 +/- 2.1	-235.6 +/- 21.5	10.0 +/- 2.8	728.6 +/- 65.2	1432.1 +/- 61.0	-1.8
UAAUUUUAUUU	-49.3 +/- 0.8	72	5.5 +/- 0.0	-66.7 +/- 4.0	-201.7 +/- 27.6	9.3 +/- 1.3	484.3 +/- 37.6	1739.8 +/- 45.7	-1.8
UAUAUUUUUAU	-46.7 +/- 10.6	7	0.6 +/- 0.4	-68.8 +/- 4.7	-270.2 +/- 26.1	19.8 +/- 1.3	563.3 +/- 79.5	1689.5 +/- 32.7	-1.8
UAUUUUUUU	-35.4 +/- 7.7	7	2.9 +/- 0.1	-63.9 +/- 6.2	-232.2 +/- 7.4	7.3 +/- 0.9	675.9 +/- 79.8	1407.7 +/- 57.9	-1.8
UUUUUAA	-30.8 +/- 3.1	76	0.6 +/- 0.4	-53.3 +/- 4.9	-238.4 +/- 9.3	11.5 +/- 2.7	587.8 +/- 31.3	1359.1 +/- 28.0	-1.8
AUUUU	-8.2 +/- 2.4	90	1.4 +/- 0.8	-48.9 +/- 4.8	-193.8 +/- 6.9	9.3 +/- 2.0	701.6 +/- 81.3	1053.8 +/- 45.5	-1.7

AU-rich regions	HADDOCK score	Cluster size	RMSD from the overall lowest-energy structure	Van der Waals energy	Electrostatic energy	Desolvation energy	Restraints violation energy	Buried Surface Area	Z-Score
AUUUUUU	-16.5 +/- 13.4	7	0.4 +/- 0.3	-57.8 +/- 4.3	-202.3 +/- 10.3	8.4 +/- 1.4	734.2 +/- 106.5	1229.4 +/- 55.6	-1.7
UUAAUUUUAUU	-48.8 +/- 0.6	71	3.5 +/- 0.1	-63.6 +/- 1.7	-229.7 +/- 13.1	10.3 +/- 1.3	503.9 +/- 26.4	1691.8 +/- 25.1	-1.7
UUUAAUUUUAUUU	-57.2 +/- 5.4	22	0.6 +/- 0.4	-64.6 +/- 5.1	-345.6 +/- 39.4	26.4 +/- 2.1	501.6 +/- 52.2	1699.3 +/- 49.3	-1.7
AAUUUAU	-28.4 +/- 3.9	82	1.2 +/- 0.4	-54.3 +/- 5.2	-196.5 +/- 23.2	12.1 +/- 2.7	532.1 +/- 83.3	1351.1 +/- 127.5	-1.6
AUAUUUUUA	-30.4 +/- 4.3	55	0.3 +/- 0.2	-75.1 +/- 4.0	-186.2 +/- 10.8	20.7 +/- 2.0	612.4 +/- 42.5	1734.1 +/- 46.2	-1.6
AUUAUUUAAUA	-68.0 +/- 13.5	8	1.1 +/- 0.7	-65.2 +/- 1.9	-372.0 +/- 44.3	21.3 +/- 2.6	502.6 +/- 77.3	1886.4 +/- 76.2	-1.6
UUUUAUUUUUUUA	-53.0 +/- 6.4	7	0.4 +/- 0.2	-78.4 +/- 5.4	-277.5 +/- 8.1	17.3 +/- 0.4	636.7 +/- 44.0	1878.7 +/- 36.6	-1.6
UUUUUAU	-26.6 +/- 3.6	48	3.1 +/- 0.1	-61.5 +/- 4.7	-171.1 +/- 17.2	13.8 +/- 1.9	553.5 +/- 39.8	1384.6 +/- 30.5	-1.6
AAUUUAA	-28.9 +/- 2.3	26	1.1 +/- 0.7	-52.6 +/- 5.1	-241.8 +/- 31.6	14.9 +/- 3.7	571.3 +/- 40.3	1362.1 +/- 108.7	-1.5
UAAUUUUAU	-42.1 +/- 7.2	41	0.7 +/- 0.5	-54.9 +/- 7.9	-250.3 +/- 23.3	14.8 +/- 1.1	480.3 +/- 118.7	1510.2 +/- 62.2	-1.5
UUAUUUUUU	-31.8 +/- 7.5	13	0.6 +/- 0.4	-60.0 +/- 5.8	-232.2 +/- 67.3	9.3 +/- 3.6	653.5 +/- 42.6	1400.9 +/- 137.9	-1.5
AAUAAA	-44.2 +/- 2.8	120	0.4 +/- 0.3	-71.2 +/- 3.3	-166.5 +/- 35.0	7.6 +/- 2.7	527.9 +/- 70.8	1527.0 +/- 28.4	-1.4
UUAAUUUUAUUUU	-49.2 +/- 5.8	27	6.0 +/- 0.0	-72.3 +/- 3.4	-280.0 +/- 11.8	19.8 +/- 0.6	593.2 +/- 36.0	1847.4 +/- 65.0	-1.4
UUAUUUAAU	-61.4 +/- 7.2	29	0.9 +/- 0.5	-62.2 +/- 1.9	-345.1 +/- 23.5	14.7 +/- 3.4	551.0 +/- 91.7	1656.4 +/- 85.5	-1.4
AUUAAA	-26.5 +/- 4.3	13	2.9 +/- 0.1	-49.5 +/- 8.3	-210.2 +/- 13.3	10.4 +/- 1.3	546.1 +/- 28.9	1330.9 +/- 80.8	-1.3
AUUUA	-17.6 +/- 3.1	49	2.6 +/- 0.0	-46.3 +/- 5.0	-250.9 +/- 21.9	10.4 +/- 1.6	685.3 +/- 52.9	1144.5 +/- 33.3	-1.3
UAAUUUAUU	-44.3 +/- 5.6	24	4.6 +/- 0.1	-64.7 +/- 6.3	-204.1 +/- 27.7	12.5 +/- 0.8	486.4 +/- 63.9	1542.0 +/- 113.9	-1.3
UUUAUUUUUUU	-38.5 +/- 6.5	49	3.2 +/- 0.1	-64.3 +/- 3.2	-216.9 +/- 36.8	13.9 +/- 3.3	552.3 +/- 81.1	1632.7 +/- 78.7	-1.2
AAUUUUAUU	-34.3 +/- 6.9	6	3.8 +/- 0.2	-61.9 +/- 1.7	-230.7 +/- 19.9	16.3 +/- 2.1	574.4 +/- 32.0	1633.1 +/- 34.7	-1.1
UUUUA	0.3 +/- 5.0	22	0.5 +/- 0.5	-48.0 +/- 0.5	-144.4 +/- 11.0	9.4 +/- 2.6	677.3 +/- 51.2	1072.9 +/- 49.8	-1

Supplementary table 18: All information on molecular docking of HuR protein and AU-rich region from the 3'UTR of *ABCG2* TV3 mRNA

AU-rich regions	HADDOCK score	Cluster size	RMSD from the overall lowest-energy structure	Van der Waals energy	Electrostatic energy	Desolvation energy	Restraints violation energy	Buried Surface Area	Z-Score
AUUUUUUUA	-36.7 +/- 4.9	15	0.6 +/- 0.4	-49.5 +/- 4.9	-311.9 +/- 18.4	13.1 +/- 1.1	621.1 +/- 36.6	1342.9 +/- 65.0	-2.7
UUUUAUUUUUUUA	-64.5 +/- 4.4	41	0.6 +/- 0.6	-74.3 +/- 2.1	-320.9 +/- 46.0	15.1 +/- 2.8	588.4 +/- 75.4	1757.2 +/- 14.1	-2.6
AAUUUUA	-40.8 +/- 11.4	59	1.0 +/- 0.6	-57.8 +/- 8.7	-261.1 +/- 37.2	13.5 +/- 2.6	557.6 +/- 116.5	1411.5 +/- 137.9	-2.4
UAUUUUUUU	-33.1 +/- 11.2	13	0.4 +/- 0.3	-58.4 +/- 3.6	-281.5 +/- 14.5	15.0 +/- 1.2	667.0 +/- 87.8	1477.1 +/- 64.4	-2.4
UUAAUUUUAUUUU	-73.5 +/- 7.1	8	0.7 +/- 0.4	-78.8 +/- 4.3	-338.5 +/- 16.6	27.7 +/- 0.9	452.5 +/- 76.5	2092.0 +/- 84.1	-2.4
UUAAUUUUAUU	-46.0 +/- 7.7	37	6.2 +/- 0.1	-71.8 +/- 7.0	-204.4 +/- 20.1	10.1 +/- 1.8	565.3 +/- 27.5	1678.2 +/- 58.1	-2.3
UUUAUUUUUUU	-46.3 +/- 5.9	28	0.3 +/- 0.2	-69.4 +/- 3.1	-276.7 +/- 23.1	12.8 +/- 1.0	656.2 +/- 37.6	1670.1 +/- 53.0	-2.3
UUUUUAA	-27.3 +/- 4.5	22	0.5 +/- 0.3	-59.9 +/- 6.3	-290.9 +/- 15.4	9.2 +/- 1.2	815.4 +/- 33.9	1273.9 +/- 38.3	-2.2
AUUUUUU	-34.7 +/- 2.7	25	0.3 +/- 0.2	-58.7 +/- 4.5	-265.8 +/- 34.4	14.9 +/- 0.8	622.5 +/- 40.9	1372.9 +/- 76.1	-2.1
GUUUG	-12.2 +/- 3.5	54	2.0 +/- 0.0	-39.3 +/- 3.7	-245.1 +/- 13.9	7.7 +/- 1.5	683.8 +/- 80.0	1031.3 +/- 32.2	-2.1
UAAUUUUAU	-53.0 +/- 5.5	46	0.6 +/- 0.4	-56.5 +/- 7.1	-358.0 +/- 39.5	18.6 +/- 4.2	564.9 +/- 65.3	1747.0 +/- 86.4	-2.1
AUUAUUUAAUA	-52.2 +/- 4.8	6	0.5 +/- 0.3	-58.3 +/- 4.2	-338.9 +/- 8.5	13.8 +/- 2.5	600.2 +/- 68.8	1598.2 +/- 41.0	-2
UAAUUUUAUUU	-46.0 +/- 21.3	4	0.7 +/- 0.6	-63.8 +/- 9.9	-272.6 +/- 29.9	19.3 +/- 1.6	530.0 +/- 76.9	1822.4 +/- 242.5	-2
UUUGUUU	-40.8 +/- 3.3	81	0.6 +/- 0.4	-55.4 +/- 6.1	-286.6 +/- 13.9	16.3 +/- 1.7	555.2 +/- 59.3	1385.6 +/- 50.9	-2
UUUUUUA	-34.6 +/- 9.1	41	0.5 +/- 0.5	-50.4 +/- 6.1	-276.2 +/- 13.3	9.0 +/- 0.4	619.6 +/- 74.4	1209.5 +/- 59.9	-2
UUAUUUUUUUA	-41.6 +/- 5.3	9	3.4 +/- 0.0	-67.4 +/- 5.9	-244.2 +/- 24.4	13.3 +/- 1.9	613.3 +/- 68.0	1492.9 +/- 48.0	-1.9
UUUUU	-16.9 +/- 4.4	48	0.3 +/- 0.2	-51.7 +/- 1.4	-223.1 +/- 9.5	5.8 +/- 1.0	735.8 +/- 27.1	999.8 +/- 47.0	-1.9
AAUUUAU	-39.1 +/- 8.1	18	0.9 +/- 0.7	-62.1 +/- 2.5	-213.8 +/- 49.2	18.0 +/- 1.0	478.1 +/- 42.1	1608.3 +/- 52.7	-1.8
AUUUUAU	-35.2 +/- 5.4	37	0.8 +/- 0.5	-60.9 +/- 1.8	-241.8 +/- 20.0	12.8 +/- 1.7	612.5 +/- 72.5	1407.5 +/- 39.4	-1.8

AU-rich regions	HADDOCK score	Cluster size	RMSD from the overall lowest-	Van der Waals energy	Electrostatic energy	Desolvation energy	Restraints violation	Buried Surface Area	Z-Score
AUUUUUA	-39.7 +/- 7.1	85	0.9 +/- 0.6	-55.4 +/- 7.8	-261.1 +/- 18.1	18.4 +/- 1.6	495.4 +/- 60.8	1455.2 +/- 111.7	-1.8
UAAUUUAUU	-55.1 +/- 8.9	37	0.4 +/- 0.2	-60.2 +/- 5.1	-318.9 +/- 8.3	14.7 +/- 2.4	542.4 +/- 65.2	1701.2 +/- 39.3	-1.8
UUUUUUU	-21.1 +/- 3.8	30	2.5 +/- 0.4	-53.5 +/- 6.5	-213.3 +/- 27.6	8.5 +/- 2.0	665.1 +/- 92.3	1227.3 +/- 62.5	-1.8
AAUAAA	-32.7 +/- 5.1	12	0.2 +/- 0.1	-57.3 +/- 1.3	-289.1 +/- 19.6	10.0 +/- 1.7	723.7 +/- 36.1	1237.6 +/- 24.1	-1.7
AAUUUAA	-20.8 +/- 4.3	67	3.3 +/- 0.1	-53.0 +/- 3.9	-199.7 +/- 35.3	13.4 +/- 3.6	588.1 +/- 82.3	1301.1 +/- 52.1	-1.7
AUUAAA	-20.6 +/- 5.8	22	0.4 +/- 0.2	-55.6 +/- 4.4	-211.3 +/- 19.1	15.1 +/- 1.7	621.8 +/- 68.5	1279.0 +/- 92.6	-1.7
UUAUUUUUU	-39.5 +/- 4.2	18	0.5 +/- 0.4	-52.5 +/- 2.3	-345.6 +/- 24.8	11.9 +/- 3.7	702.4 +/- 53.2	1352.9 +/- 65.8	-1.7
UUUAAUUUUAUUU	-58.2 +/- 1.5	61	2.2 +/- 0.1	-73.1 +/- 2.4	-258.1 +/- 16.4	15.2 +/- 1.5	513.3 +/- 53.0	1768.0 +/- 85.8	-1.7
UUUUUAU	-36.7 +/- 3.0	74	1.7 +/- 0.1	-65.1 +/- 3.0	-212.2 +/- 15.1	12.3 +/- 1.7	585.1 +/- 61.6	1393.6 +/- 41.2	-1.7
AAUUUUAUU	-44.1 +/- 9.6	20	0.6 +/- 0.4	-68.1 +/- 7.5	-270.9 +/- 37.5	17.3 +/- 3.7	608.8 +/- 24.1	1723.8 +/- 84.4	-1.5
AUAUUUUUA	-47.5 +/- 8.9	62	0.5 +/- 0.3	-64.5 +/- 3.3	-264.7 +/- 25.3	15.1 +/- 0.8	549.4 +/- 88.5	1616.3 +/- 52.5	-1.5
AUUUU	-5.6 +/- 10.4	70	0.4 +/- 0.2	-46.5 +/- 2.2	-151.5 +/- 16.0	9.6 +/- 1.1	615.8 +/- 72.7	1039.0 +/- 45.8	-1.5
UAUAUUUUUAU	-52.3 +/- 5.1	46	0.8 +/- 0.6	-60.3 +/- 5.4	-262.9 +/- 30.6	13.3 +/- 1.6	472.4 +/- 47.9	1616.1 +/- 83.8	-1.5
UAUUUAA	-33.9 +/- 9.2	7	0.7 +/- 0.6	-56.7 +/- 3.8	-272.0 +/- 42.2	18.1 +/- 5.7	591.0 +/- 36.5	1388.2 +/- 84.2	-1.5
UAUUUUUAU	-45.7 +/- 2.2	80	2.1 +/- 0.2	-61.5 +/- 2.8	-244.0 +/- 36.0	14.6 +/- 1.4	499.4 +/- 70.2	1557.7 +/- 28.8	-1.5
UUAUUUAAU	-40.2 +/- 13.5	6	0.4 +/- 0.2	-76.5 +/- 5.7	-226.2 +/- 19.4	18.4 +/- 2.2	631.3 +/- 50.3	1738.8 +/- 100.3	-1.5
UAUUUUU	-20.0 +/- 4.2	10	2.1 +/- 0.1	-53.7 +/- 7.8	-218.6 +/- 18.2	7.6 +/- 2.4	698.6 +/- 103.3	1243.3 +/- 68.2	-1.4
UUUUA	-5.7 +/- 3.0	77	2.5 +/- 0.1	-48.3 +/- 3.3	-156.0 +/- 28.2	7.0 +/- 1.3	668.7 +/- 37.7	1082.2 +/- 70.3	-1.3
AUUUA	-11.7 +/- 2.5	66	2.6 +/- 0.1	-58.5 +/- 7.5	-134.3 +/- 12.4	11.4 +/- 1.6	622.9 +/- 32.2	1223.3 +/- 78.9	-1.2
UUUUUUAAA	-24.2 +/- 6.2	14	3.7 +/- 0.1	-48.6 +/- 5.3	-301.1 +/- 58.8	19.4 +/- 4.3	652.8 +/- 81.8	1298.9 +/- 148.7	-1

Supplementary table 19: Normality tests for ABC transporters and HuR co-expression in chemoresistant breast cancer

Normality tests	Co_P-GP+HuR (Chemoresistant)	Co_P-GP+HuR (Control)	Co_MRP1+HuR (Chemoresistant)	Co_MRP1+HuR (Control)	Co_ABCG2+HuR (Chemoresistant)	Co_ABCG2+HuR (Control)
D' Agostino & Pearson test						
P value	0.0193	<0.0001	0.0662	<0.0001	0.1116	<0.0001
Passed normality test?	No	No	Yes	No	Yes	No
Anderson-Darling test						
P value	0.051	<0.0001	<0.0001	<0.0001	0.056	<0.0001
Passed normality test?	Yes	No	No	No	Yes	No
Shapiro-Wilk test						
P value	0.0629	<0.0001	<0.0001	<0.0001	0.0312	<0.0001
Passed normality test?	Yes	No	No	No	No	No
Kolmogorov-Smirnov test						
P value	0.045	<0.0001	<0.0001	<0.0001	>0.1000	<0.0001
Passed normality test?	No	No	No	No	Yes	No

Supplementary table 20: Normality tests for ABC transporters and HuR co-expression in chemoresistant CRC

Normality tests	Co_P-GP+HuR (Chemoresistant)	Co_P-GP+HuR (Control)	Co_MRP1+HuR (Chemoresistant)	Co_MRP1+HuR (Control)	Co_ABCG2+HuR (Chemoresistant)	Co_ABCG2+HuR (Control)
D' Agostino & Pearson test						
P value	<0.0001	0.015	0.0032	0.1731	0.442	0.0039
Passed normality test?	No	No	No	Yes	Yes	No
Anderson-Darling test						
P value	<0.0001	0.003	<0.0001	0.0137	0.6245	0.1264
Passed normality test?	No	No	No	No	Yes	Yes
Shapiro-Wilk test						
P value	<0.0001	0.0051	0.0001	0.0125	0.4753	0.0331
Passed normality test?	No	No	No	No	Yes	No
Kolmogorov-Smirnov test						
P value	0.0009	0.001	0.0036	0.032	>0.1000	>0.1000
Passed normality test?	No	No	No	No	Yes	Yes

Supplementary table 21: Normality tests for ABC transporters and HuR co-expression in chemoresistant ovarian cancer

Normality tests	Co_P-GP+HuR (Chemoresistant)	Co_P-GP+HuR (Control)	Co_MRP1+HuR (Chemoresistant)	Co_MRP1+HuR (Control)	Co_ABCG2+HuR (Chemoresistant)	Co_ABCG2+HuR (Control)
D' Agostino & Pearson test						
P value	0.4178	0.4455	0.0171	NA	<0.0001	0.3393
Passed normality test?	Yes	Yes	No	NA	No	Yes
Anderson-Darling test						
P value	0.0747	0.045	0.0028	NA	0.0005	0.11
Passed normality test?	Yes	No	No	NA	No	Yes
Shapiro-Wilk test						
P value	0.0727	0.0392	0.0022	0.3748	0.0004	0.1397
Passed normality test?	Yes	No	No	Yes	No	Yes
Kolmogorov-Smirnov test						
P value	0.0475	0.0571	0.004	>0.1000	0.0008	>0.1000
Passed normality test?	No	Yes	No	Yes	No	Yes